POLITECNICO DI MILANO

Facoltà di Ingegneria Industriale

Dipartimento di Ingegneria Aerospaziale

Q-Band design of a platelet orthomode transducer for cosmological applications

Relatore : Prof. Carlo Capsoni
Corelatore : Dott. Cristian Franceschet
Controrelatore : Prof. Marco Bersanelli

Autore
Giacomo Trevisan
matricola : 740526

A.A. 2011/2012

Acknowledgments

Vorrei ringraziare tutte le persone che mi hanno permesso di portare avanti e svolgere questa tesi poco convenzionale, in particolare i professori dei dipartimenti di Ingegneria aerospaziale e di elettronica e informazione del politecnico di Milano, e il gruppo di cosmologia della facolta di Fisica dell'Universita degli studi di Milano.
Tra questi sono specialmente grato al professor Bersanelli, che si è subito interessato al mio desiderio da studente di ingegneria di confrontarmi con il campo scientifico della cosmologia; al professor Bernelli che fin dalla mia esperienza all'estero mi ha discretamente incoraggiato a prendere iniziativa sul mio percorso formativo ed ha accettato la proposta di una tesi in collaborazione con una universita diversa dal politecnico; al professor Capsoni che mi ha accolto come suo tesista a lavoro iniziato.
Un ringraziamento particolare va poi alle persone con le quali il confronto costruttivo è stato fondamentale e a chi ha seguito da vicino il mio lavoro: Cristian, Gianbattista, Enrico e Francesco.

Abstract

This thesis proposes the electromagnetic design of an orthomode transducer (OMT) based on waveguide transmission, oriented to be realized with the platelet technique, that is, the overlap of thin sheets processed individually in order to compose the desired guided path.
The band of frequencies identified for this study is the Q, centred on 40 GHz. Obtained with COMSOL the initial design of a compact OMT with good performance in terms of transmission, isolation and cross polarization, this was later adapted to be achieved without degradation of performance using traditional milling on multiple sheets, considering the constraints and limitations of this technology.
The results are satisfactory and show that this type of construction technique can be promising in view of planar arrays of orthomode transducers and feedhorns, towards which points much technological effort for the future generation of cosmic radiation and polarization detectors.

Keywords: orthomode transducer, platelet, Q-Band, polarisation, cosmic microwave background

Sommario

Questo lavoro di tesi propone il progetto elettromagnetico di un trasduttore ortomodo (OMT) e basato sulla trasmissione in guida d'onda, orientato ad essere realizzato con la tecnica platelet, cioè la sovrapposizione di lamine sottili lavorate singolarmente in modo da comporre il percorso in guida desiderato.
La banda di frequenze individuata per questo studio è la Q, centrata sui 40 GHz. Ottenuto tramite il supporto software di COMSOL il design iniziale di un OMT compatto con buone prestazioni in termini di trasmissione, isolamento e polarizzazione incrociata è stato in un secondo momento riadattato per essere realizzato senza degradazione delle prestazioni tramite fresatura tradizionale su più lamine, considerando quindi vincoli e limiti di questa tecnologia.
I risultati ottenuti sono soddisfacenti e mostrano che questo tipo di tecnica costruttiva può essere promettente in vista di schiere planari di trasduttori ortomodo e illuminatori, verso le quali sembrano orientati gli sforzi progettuali per i rilevatori di radiazione e polarizzazione cosmica di futura generazione.

Parole chiave: trasduttore ortomodo, platelet, Banda Q, polarizzazione, radiazione cosmica di fondo

Introduction

Space has been for years one of my major interests, which lead my academic career to aerospace and then space engineering. This same motivation got me search for collaborations with the scientific world, to support whose researches many space missions are intended. In the field of astronomy, more than in others, a strict collaboration between science and engineering is necessary to achieve scientific goals and engineering innovations.
An emblematic example can be found in the branch of physics called Radio Astronomy .
Its birth can be dated back to 1930, when Jansky, an engineer of the Bell telephones laboratories noticed a radio signal source interfering with transatlantic voice transmission, with a period of a sidereal day, ca. 23 hours and 56 minutes, i.e. some 4 minutes shorter than the solar one.
Investigating it with a large directive antenna, he eventually recognized in the Milky Way its origin and detected the centre of our galaxy in the direction of the Sagittarius constellation, where the source has its absolute peak.
It was again an engineer, Reber, who first got a sky survey in the radio frequency range, using a self-built 9 m parabolic antenna in his own backyard in 1937.
But it was only with the end of the Second World War that the scientific interest on the radio field grew: in 1964 two young physicists, Arno Penzias and Robert Wilson, serendipitously discovered the Cosmic Microwave Background radiation (CMB), predicted by George Gamow in 1948, in accordance with the model of an expanding universe proposed by Lemaitre throughout the 1920s, and supported by observation evidences of the increasing distance between the Earth and extra-galactic Nebulae throughout the 1920s.
From then on the CMB represents the principal object of study in modern cosmology, as it hides a big deal of information on the early phases of the universe, which would allow a better knowledge of its large scale structure and evolution: CMB is in fact the oldest observable radiation

source, generated about 380.000 years after the Big Bang, when the expanding universe cooled down to a temperature low enough to allow separation of the primordial plasma in stable matter and radiation.
In the last decades, important progress has been made thanks to a rapid increment in sensitivity and reliability of scientific payloads on space missions.
My collaboration with the group of cosmology of the University of Milan started in this frame.
In this work I propose a compact design of an Orthomode Trasducer (OMT), a passive element of a radiometric chain assembly. This OMT is conceived to be realized with a well promising technology (platelet), that allows production of large arrays of receivers, prerequisite for future scientific instruments for the observation of the CMB polarization.
Chapter 1 reviews some details about CMB and its importance in observational cosmology, focusing on its properties such as its polarization.
Chapter 2 discusses the principle of electromagnetic waves and their guided transmission, whereas a brief introduction to OMTs state of the art with a focus on the platelet technology is exposed in Chapter 3.
The design procedure leading to the eventual prototype of OMT in Q-band, that is the aim of this work, is reported in Chapter 4.
Chapter 5 concludes this thesis with a critical analysis of obtained results and further proposed improvements of this work.
Finally the mechanical drawings for a future fabrication and verification of the OMT are attached to the appendix.

Contents

List of Figures

List of Tables

Chapter 1

CMB and modern cosmology

1.1 The Cosmic Microwave Background

Cosmology is the science investigating the universe at its largest scales, to understand its structure, its origins and evolution.
Among the cosmological models proposed during the last century, the most reliable is the one called Warm Big Bang, which appears to be more consistent with the scientific findings of the recent past decades.
This model explains explains the evolution of the universe up to the present time starting from a singularity point of the space-time, when all matter and energy were condensed in a dense state with a theoretically unlimited energy level. The sudden explosion called hot big bang started the expansion process which is still going on, and the progressive cooling lead the universe toward the large scale structure we observe nowadays, about 13.7 billions years after.
Four main evidences confirm this theory: expansions, nucleosynthesis of light elements, large scale structures and the cosmic microwave background.

There are significant evidences of the expansion of the universe. It was Edwin Hubble in 1917 who first measured the redshift of some galaxies to study their motion, and proposed a proportional relation between the distance of two bodies and their recessional velocity, through the Hubble constant H_0, which is nowadays precisely known.

According to this model, there was a short period of about 17 minutes (from 3 minutes to 20 minutes after the start of expansion, called nucleosynthesis era) in which the mean energy of the universe allowed the formation of stable nuclei, after which nuclear fusion was prevented until the birth of the first stars. In this short period, only light ele-

ments could be produced, and their abundance in the universe has been predicted from this model, with good accordance to observations.

The standard Hot Big Bang model also provides a framework in which to understand the collapse of matter to form galaxies and other large-scale structures observed in the Universe today, after the energy of the universe had sufficiently decreased to let gravitational forces between the particles become effective, to let any density peak become a gravitational attraction center.

Finally, one of the principal evidences is the cosmic microwave background radiation (CMB): it is the remnant of the first radiation permeating the universe, and is therefore a sort of photography of the universe as it was ca.380.000 years after the big bang.
By that time, temperature had dropped sufficiently for electrons and protons to combine into hydrogen atoms. From then onwards, radiation was effectively unable to interact with the background gas (so one speaks of radiation-matter decoupling era); it has propagated freely ever since, while constantly losing energy because its wavelength is stretched by the expansion of the Universe. Originally, the radiation temperature was about 3000 degrees Kelvin, whereas today it has fallen to only 3K.
The photons of the CMB permeates the whole universe according with the cosmological principle, but appear to be emitted by a cosmic background spherical surface with center on the observing point (Earth) and a radius of about 13 billions light years, i.e. the distance they have travelled ever since.
The existence of the CMB is necessary in the scenario of a hot big bang: it was first predicted in 1948 by George Gamow and observed in 1964 by Arno Penzias and Robert Woodrow Wilson, after a 20 year long study, for which they gained the Nobel price in 1978.
For what said, the CMB is one of the most powerful means to improve our knowledge of the universe and its history, so that it has been the center of modern cosmological researches up to now.
According to observations and measurements, it shows a spectrum very close to that of a perfect black body, shown in Figure 1.2(fonte NASA[6]),whose most precise measure was taken by the FIRAS instrument on the COBE satellite in 1989.
The black body spectrum of the CMB is a consequence of the thermic equilibrium of the universe before the decoupling, when the universe was ionized: after that, the expansion didn't modify its shape, but has decreased its temperature proportionally to its redshift.
We can write:

$$T = 1 + z;$$

where z is the scaling factor of the wavelength of photons, due to the expansion, and defined as:

$$z = \frac{\Delta\lambda}{\lambda_e};$$

in which $\Delta\lambda$ is the wavelength difference between the measured one and the emitted one, λ_e.
Temperature is up to now the cosmological parameter known with higher accuracy: the CMB is emitting at a temperature of 2.725 ± 0.002K, with a high level of isotropy at large scales.
Nonetheless, temperature anisotropies have been discovered by the DMR instrument aboard on COBE, more accurately studied by WMAP (Figure 1.1) and is being even more precisely mapped by the Planck satellite, launched in 2009 by a combined ESA/NASA project with a strong Italian participation.
There exist many types of anisotropy in a microwave scan of the Sky as seen from an Earth Orbit.
To get information on the CMB, the measurements must be cleaned from all other microwave sources, such as the Milky Way.
After that, a first level of CMB anisotropy is present at a level of $\Delta T/T \sim 10^{-3}$, appearing as a dipole type distribution: this is not an intrinsic temperature anisotropy, but is due to the motion of the local group of galaxies w.r.t. the CMB.
The first intrinsic anisotropies can be observed at a level of After that, a first level of CMB anisotropy is present at a level of $\Delta T/T \sim 10^{-5}$, on angular scales down to 5′.
These anisotropies represent the footprint of the density fluctuations of the primordial universe, which, after the rapid expansion period called inflation, were brought to cosmic scales and were responsible of the birth of the structure of the universe as we observe it today.
The analytical description method used is the series expansion in spheric harmonics:

$$\frac{\Delta T}{T}(\theta, \phi) = \sum_{l,m} a_{l,m} \mathbf{Y}_l^m(\theta, \phi). \tag{1.1}$$

Assuming a Gaussian distribution of the fluctuations, all informations can be described by the autocorrelation function, $\mathbf{C}(\theta)$:

$$\mathbf{C}(\theta) = \frac{1}{4\pi} \sum_l \mathbf{C}_l \mathbf{P}_l(\cos\theta). \tag{1.2}$$

where the coefficients

$$\mathbf{C}_l = \langle |a_{l,m}|^2 \rangle = \frac{1}{2l+1} \sum_{-l}^{l} |a_{l,m}|^2. \tag{1.3}$$

are used to construct the Angular Power Spectrum, which indicates the intensity of the different harmonics associated to a multi-pole order $l = \pi/\theta$, and therefore with an angular scale θ.
Results of different instruments and satellites in terms of Angular Power Spectrum are illustrated in Figure 1.2. The study on the temperature anisotropies allows the measurement of most of the principal cosmologic parameters, including the Hubble constant H_0, the total energy density in the universe and the specific energy associated to the cosmologic constant Ω_0.
Altogether, not all the cosmological parameters can be evaluated from the temperature anisotropies: some of them have similar effects on the CMB, so that they cannot be isolated and uniquely defined.
This problem can be solved by another important characteristic of the CMB, i.e. its polarization.
As it will be explained in Chapter 2, polarization indicates the direction of the electric field associated to the propagation of an electromagnetic wave.
The superposition of different modes of propagation (which can be polarized in different directions) of radio signals of the CMB, lets part of the polarizations compensate and vanish, so that not all the emitted intensity is polarized along the dominant direction.
The CMB emission can be split in a non polarized (randomly polarized) and a completely polarized components, where the magnitude of the polarized signal is very weak, corresponding to some μK, i.e. a tenth of the pure temperature anisotropy.Figure 1.1 shows as white lines the polarized signals measured by WMAP.
An accurate measure of the CMB polarization requires therefore highly sensitive instruments.
Polarization anisotropy is assumed to be caused on the CMB radiation through Thomson scattering during the recombination era: only quadrupole anisotrpies can generate after Thomson scattering a polarized radiation, and there exist only three geometrically differing quadrupole anisotropies, corresponding to $l = 2$ and $m = 0, 1, 2$ in the series expansion (respectively scalar, vectorial and tensorial quadrupoles); these are associated with density and vorticity fluctuation on the primordial universe, and to gravitational waves due to the inflationary expansion, as illustrated in Figure 1.3.

The pattern of polarization which arises from these perturbations and their modulation can be separated in two different patterns, with handedness properties similar to the electric and magnetic fields, respectively; therefore they have been called E-modes and B-modes.
A deep introduction on these two modes is not the aim of this work, so only their main properties will be briefly referred.
E-modes are caused by scalar and tensorial perturbations and their pattern shows no handedness; for this reason E-mode pattern is correlated with temperature anisotropies. Scalar are energetically dominant, and their first evidences of such modes were collected and measured by WMAP and DASI.
B-modes represent the handed pattern of polarization, which is mainly consequences of the tensorial perturbations: gravitational waves are believed to bring along E- and B-modes in similar amounts, but at a lower level of energy.
As with temperature anisotropies, polarization can be described in terms of spherical harmonics, to obtain equivalent temperature angular power spectra for E- and B-modes, as shown in Figure 1.4.
As previously said, the study of CMB polarization pattern is a key step to improve the our knowledge of cosmological parameters, to verify cosmological models and get a better description of the universe, hoping to get some important information about the so called dark energy and matter.
Moreover, polarization is the only mean to get information and evidences of the inflation era and try to understand what happened from the first fractions of seconds after the Big Bang to the decoupling era, about 380.000 years later.

1.2 How to measure CMB radiation

There are two types of receiving instruments in use to detect the radiation coming from the CMB: bolometers, very broad band thermal receivers, and radiometer chains, both connected to corrugated feed horns on the front end, and to the acquisition electronic system at the back end.
The peculiarity of thermic sensors is their sensibility to very low energy signals at low frequencies. In fact, the quantic effects on which other instruments at infrared and optical frequencies rely (such as photoconductors), can't be efficiently adopted in the millimetre and submillimeter

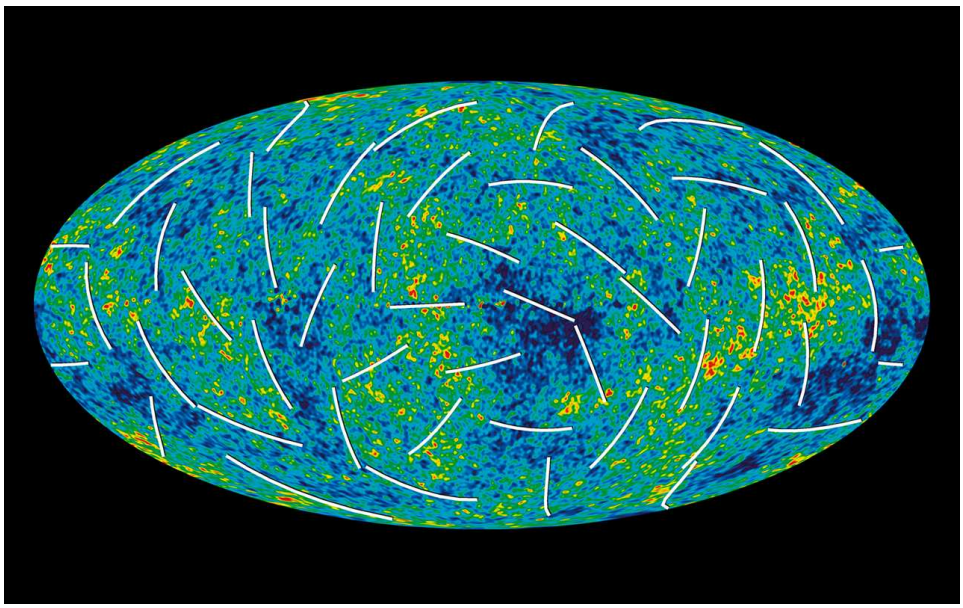

Figure 1.1: CMB observations made by WMAP[5]; white lines indicate the directions of polarization of the primordial light. A better esteem of polarization patterns could reveal particulars of the first fractions of second after the Big Bang.

bands.
In thermic sensors, the great amount of photons collected at the receiver, infers a variation in its temperature, which in turn alters its electric resistance which can be revealed through potential measurements.
As a matter of fact, the first bolometers at the end of the XIX century were similar to Wheatstone bridges, in which two adjacent arms were substituted with thin platinum stripes. Since then bolometers have been supplied with cryogenic cycles and new materials, to provide work temperatures near the absolute thermal zero, thus granting high sensibility to low energy signals.

Bolometers are very efficient at millimetric and submillimetric wavelengths, and are usually made of opportunely altered semiconductors. A scheme of a simple bolometer is reported in Figure 1.5. On the left the thermic circuit is shown, consisting in an element which warms by absorbing the to measure radiation (Power Q). The sensible element is in weak thermic contact (conductance G) with a thermostat at temperature T_0, and kept at $T > T_0$, in absence of radiation, by dissipation of Joule Power P.
On the right is the electric feeding system: the bias current is forced to flow with a load resistance RL serial to the bolometer, and a low noise

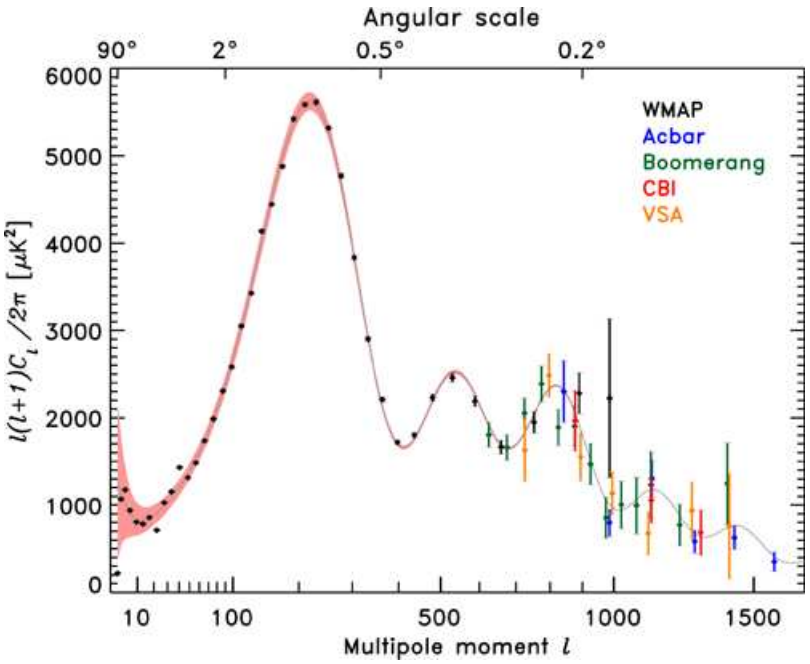

Figure 1.2: CMB Power Spectrum esteem obtained with the indicated instruments. On the x-axis the multipole moment l indicates the order of spherical harmonics with whom data are compared; small l relates with large angular scale and viceversa

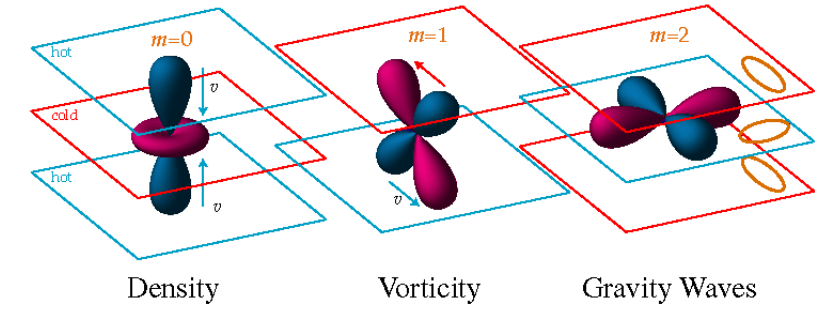

Figure 1.3: Representation of the three quadrupole pertubations and their causes.

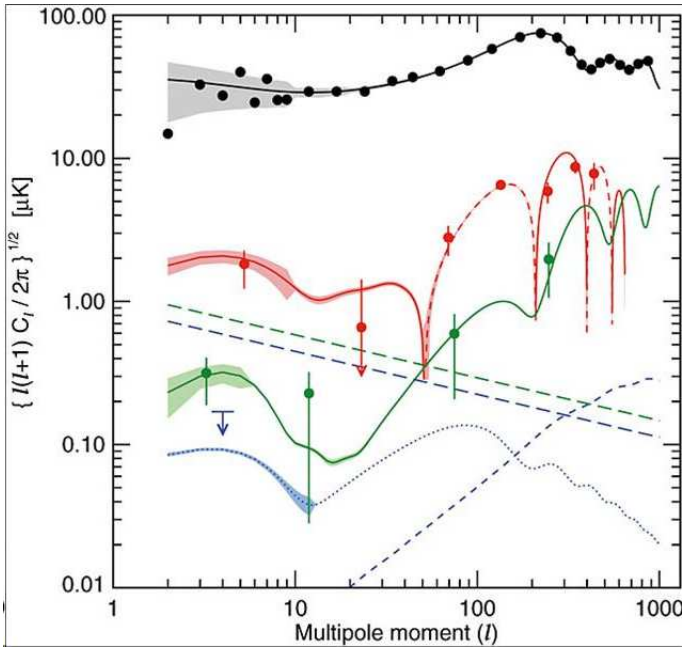

Figure 1.4: Temperature and polarization modes power spectra with their measure uncertainties.

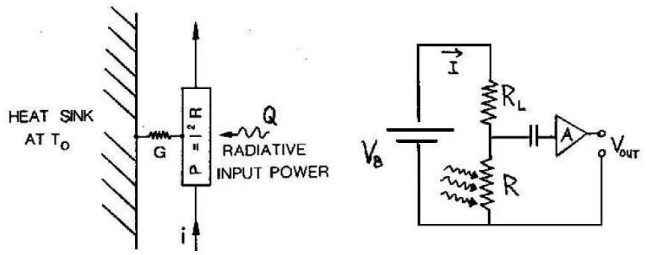

Figure 1.5: Bolometer: thermic and electric feeding circuits.[15]

battery provides the bias voltage VB. A low noise amplifier amplifies the modulated radiation signal.
However, common bolometers would allow a detection of the mere temperature level of photons, and not of the electromagnetic waves, thus being transparent to polarization.
In the last years, technological researches have led to new polarization sensitive bolometric instruments (PSBs), on which nowadays are based a large part of last and next generation CMB polarization oriented projects, especially at submillimetric and quasi-optical wavelength (100 - 1000 GHz), as their design is not significantly frequency dependant, dimensions apart.

The second type of sensor is the one on which this work is based.

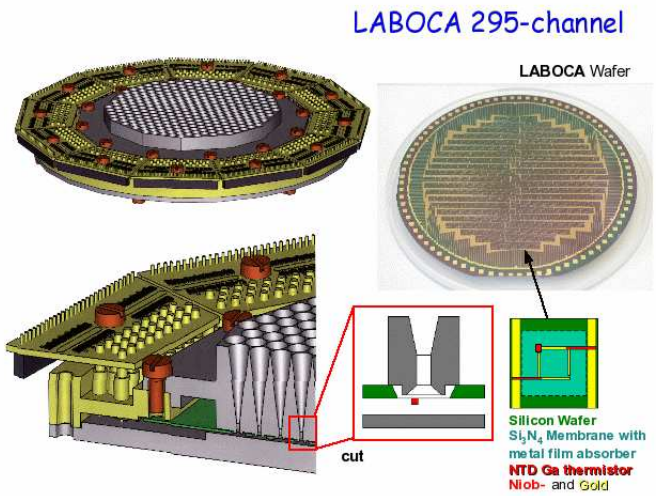

Figure 1.6: A CAD representation of the bolometric array of LABOCA telescope: on the right bottom a single bolometer overview.

Radiometers are coherent receivers, i.e. they are sensible to magnitude and phase of an incident electromagnetic field: for this reason, such instruments are intrinsically spectroscopical, thus allowing to get a precise spectrum analysis in the sensor frequency range.
The Low Frequency Instrument mounted on Planck is based on this second type of receivers; Figure 1.7 presents the radiometer chain assembly of the LFI, say all the elements from the feed horn antennas to the data acquisition system.
As can be seen, each RCA comprises two radiometers carrying the two orthogonal polarizations. The RCA is constituted by a front-end module (FEM) and a back-end module (BEM), linked with waveguide lines interfacing with 3 V-Grooves.

Following the scheme in Figure 1.7a each FEM includes a corrugated

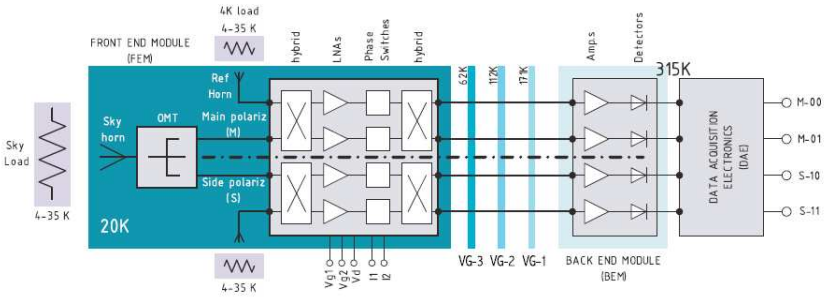

(a)

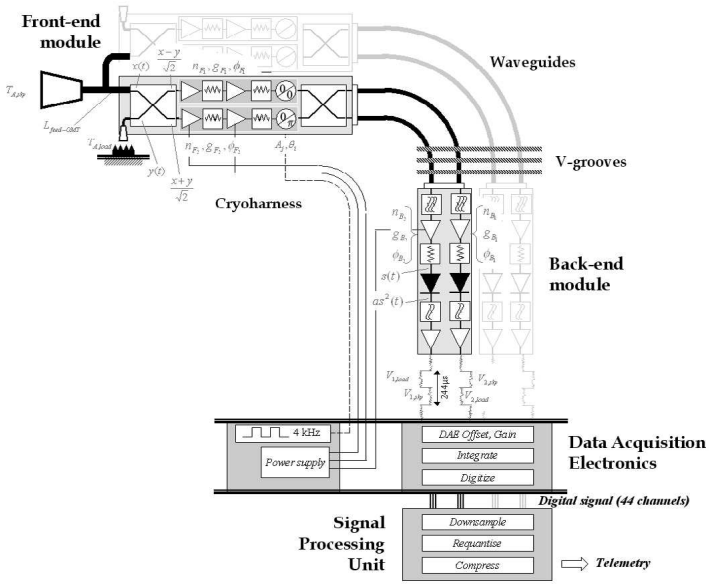

(b)

Figure 1.7: Two schematics of the LFI system displaying the main components of the two RCAs connected wit a horn. (a)Thermal interfaces [13]; (b) details of the operations on signals and of power supply units.[14]

feed horn (Sky horn), an orthomode transducer (OMT), which divides the incoming radiation into two orthogonally linear polarized waves (M and S), a front-end unit composed by hybrids, a Low Noise Amplifiers (LNAs) and a phase switches. Hybrids are 4 port devices, coupling two input signals and equally destributin teir power at te output ports, as remarked in Figure 1.7b: one input port receives a polarized signal from the Sky($x(t)$) via the feed horn and OMT, the other lets a reference load

signal in ($y(t)$), having the same mean temperature level of the Sky (4K to 35K).
These signals are then amplified by the cryogenic low-noise amplifiers (LNAs) characterised by noise voltage, gain, and phase ($nF1$, $gF1$, $fF1$ and $nF2$, $gF2$, $fF2$). One of the two signals then runs through a switch that shifts the phase between 0 and π at a frequency of 4096 Hz. A second phase switch is mounted for symmetry and redundancy on the other radiometer leg, but it does not introduce any switching phase shift. The signals are then recombined by a second π hybrid coupler, thus producing an output, which is a sequence of signals proportional to x(t) and y(t) alternating at twice the phase switch frequency.The whole FEM operates at 20 K.
A set of four waveguides connect the FEM to the back-end module (BEM), passing through the V-Grooves which are the main thermal shields from the cold payload to the warmer on board electronics . At the BEM, the RF signals are further amplified in the two legs of the radiometers by room temperature amplifiers, filtered and then detected by square-law detector diodes.

1.3 Improving polarization patterns

As previously observed, these two types of instruments are already mounted and in use in many missions and telescopes directly designed to observe and study the CMB. As a matter of fact, however, a precise measure of the polarization pattern has not yet been carried out, because of the higher order performances required especially to study the B-modes, and not even the Planck mission will provide it with satisfactory accuracy.
To this aim, there are different design aspects to be improved, along with the direct optimization of the design of sensors:

The intrusivity of the front-end optics over the polarization has to be as much as possible compensated: solutions limiting the leakage of the temperature anisotropies and of E-modes in the B-modes' spectrum are researched; some solutions have already been presented both for off-axis (with Mizuguchi-Dragoni correction) and on-axis systems [7].

Performances of polarization modulators must be optimized: Polarization modulation allows for clean separation of the polarized light

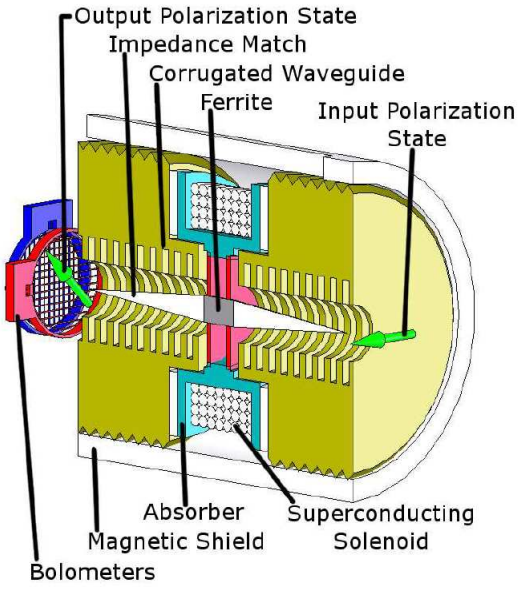

Figure 1.8: A Faraday Rotation Modulator (FRM) pixel, cross-sectional view (FRM) pixel. Polarized light enters from the right, is rotated by 45° and then analysed (decomposed into orthogonal polarization components, which are detected individually by the polarization-sensitive bolometers, or PSBs). For each FRM pixel, the PSBs are contained within a corrugated feedhorn, cooled to 0.25 K, located approximately 20 cm from the FRM, which is placed in a corrugated waveguide at the interface between two corrugated feedhorns, placed back-to-back and cooled to 4 K [16]

.

from a source and the non polarized background. This is likely to be an important element in systems designed to search for the B-mode polarization as the non polarized contribution from the CMB is much larger than the faint signature of inflation. Many types of polarization modulators exist at different TRL levels, most of which are used combined to bolometric detectors [16]. An example of a Faraday Rotator Modulator is shown in Figure 1.8.
Altogether, this component is not proved to be necessary, and in particular is generally avoided in radiometric chains of coherent detectors, as can be inferred again looking at Figure 1.7.

Existing millimetre-wave detectors already operate close to photon background limit, the sensitivity can be improved using arrays of sensors, through comparative compensation of noise and the use of interferometry on EM waves: arrays of hundreds to thousands pixels would suit the goal, but their dimensions must be at the same time minimized,

especially in the design of orbiting instruments whose bulk is limited by the fairing capabilities of the launchers.
The concept design of such arrays is likely to be based on elementary

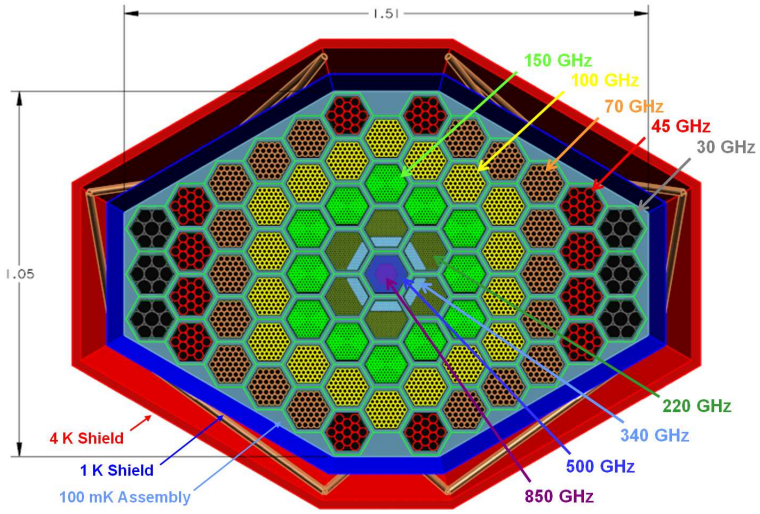

Figure 1.9: A solution for EPIC focal plane: a composition of equal hexagons hosting a number of detectors increasing with work frequency, as their dimensions are supposed to decrease, for a total of 11094 detectors. [17]

.

cells hosting a limited number of pixel of the front end module.
All the major Space societies are investing much on this task for future projects:in Figure 1.9 is shown the focal plane of a future US mission, EPIC (Experimental Probe of Inflationary Cosmology), which will investigate the CMB polarization in a wide frequency range (30 to 850 GHz) using bolometric detectors.

The very low temperatures associated to CMB forces instruments work environment to be cooled to cryogenic temperatures, to minimize noise temperature and improve the sensitivity.
An example of cryo-cooling system is shown in Figure 1.10
As can be inferred from these requirements, bolometers seem to represent the best solution in terms of small dimensions and sensitivity to radiation, and are the preferred choice at high frequency.
All the same, to let a bolometric detector be polarization sensitive, some devices have to be designed, and a first waveguide path (including feed horns, frequency filters and polarization modulators) is likely to be necessary, as it was in the Planck HFI.
There is a broad interest also in the radiometric chains using OMTs as

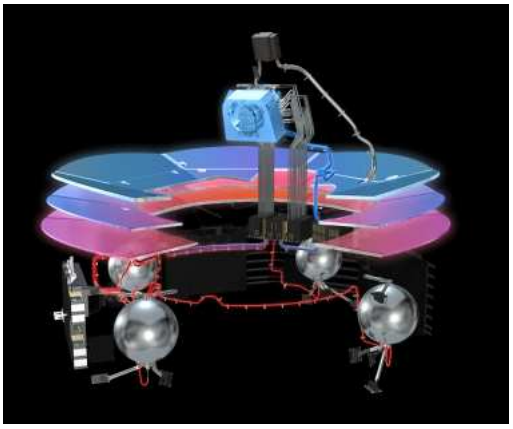

Figure 1.10: Illustration of the active cooling system on board the Planck spacecraft, with the components of the 0.1 K cooler highlighted. Also the three V-grooves of the passive cooling system are coloured, representing their progressively lower temperature from bottom to top. Three high pressure tanks filled with ^4He and one high pressure tank filled with ^3He are housed in the service module (four highlighted silver spheres in this view).ref:ESA/AOES Medialab

polarization discriminator, of which different designs and fabrication techniques exist, to introduce which is intended section 3.

1.3.1 Influence of scientific payloads on space missions

Even though there exist many ground based telescopes studying deep space and CMB, spacecrafts constitute the most promising systems to improve cosmological models.
Mounting on a spacecraft a highly scientific payload like a telescope for CMB measurements entails many constraints on the space mission and its subsystems.
Scanning the whole sky requires an effective scanning strategy, and a consequent trajectory of the pointing direction of the payload, which should be performed through a correct attitude control. The mass and the position of the scientific instruments and their supporting subsystems further affect the ADCS through the performances requirements on the actuators, as well as the support structure.
Thermal control system is also very important on a satellite, since the space environment presents both thermal sources (the Sun and all radiating objects) and sinks (deep space at an average temperature of

2.7 K); on scientific satellites thermal control is particularly important, since high thermal stability and cryogenic temperatures are typically demanded by a space telescope during its whole operative life.

Chapter 2

Guided electromagnetic field propagation

2.1 Maxwell's equations and constitutive laws

Electromagnetic phenomena are all those involving electric and magnetic fields propagating through vacuum or a dielectric medium.
All of these physical phenomena were mathematically unified and described in an elegant equation system by Maxwell at the end of XIX century. Maxwell's equations were presented in their modern and rigorous form in 1887 by Heaviside, whose efforts solved some of the mathematical complexities in Maxwell's theory, introduced vector notation and provided a foundation to practical applications of guided waves and transmission lines. Maxwell's equations are accurate at any frequency and in any transmission system of any complexity, though some simplifications can be taken in the different frequency bands.
Let us briefly introduce the electromagnetic spectrum through Figure 2.1. A classification of the different bands of frequency is useful, as the power and thus the effects of EM radiation are very different from a wavelength band to another.
A first natural division refers to that part of adiation which we perceive through our eyes as visible light: we speak of optical band from about 400 THz to 790 THz (wavelengths from 750 nm to about 390 nm), and of suboptical and superoptical respectively at lower and higher frequencies.
Since power is directely proportional to frequency through the Planck's constant, the upper part of superoptical radiation band is also called ionizing radiation, as its wave energy exceeds the first ionizing energy

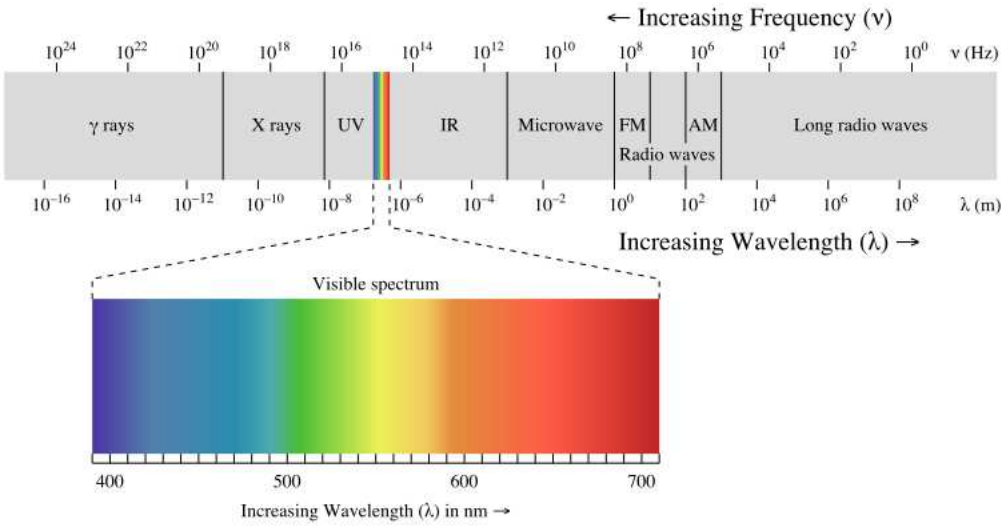

Figure 2.1: Electromagnetic Spectrum

of big atoms (ca 10eV) and comprises far ultraviolet, X-Ray and γ-Ray radiations.
In the optical band, waves have legths generally far smaller than the objects they interact with, and do not carry great amounts of energy. This allows a simplification in Maxwell's theory, leading to the classic geometric optic rules.
At very low frequencies (the long radio waves band), analogue dimensional considerations lead to the lumped element description which is usual in circuit theory: in this case the wavelength is usually far greater than the characteristic dimensions of circuit components and cables.
A wide part of the suboptical spectrum is the radio wave band, which conventionally goes from 3 KHz to 300GHz (wavelengths from 100km to 1mm).
The lower part of the radio field is widely exploited for data transmission and communication, so that the use of the different frequencies (channels) is restricted and regulated by international agreements; the upper part, from 30 GHz to 300GHz, is known as EHF(Extremely High Frequencies) or millimetric band, for it comprises wavelengths from 1cm to 1mm.
At frequencies above 300 Ghz it is usual to speak of Infrared and theraherz radiation.
The millimetric and far infrared bands, together with the UHF (Ultra High Frequency, from 300MHz to 3GHz) and SHF (Super High Fre-

quency, 3-30GHz) waves, are grouped in the microwave radiation band, thus comprising wavelengths from 1 mm to 1 meter.
In microwave engineering it is usual to handle with transmission line components and instruments with dimensions similar to the length of the waves they should transmit: a lumped decription similar to the standard circuit theory is often not valid in this field, since phase of a voltage or current might change significantly over the physical extent of a device.
For this reason, one must often approach a microwave problem with Maxwell's equations and their solutions, in which great mathematical complexity may arise.
the most general formulation of these equations is integral, over domains of volume V and closed boundary surface S, on which a closed contour C can be traced:

$$\oint_C \vec{E} \cdot d\vec{l} = -\frac{\partial}{\partial t}\int_S \vec{B} \cdot d\vec{s} - \int_S \vec{M} \cdot d\vec{s}; \tag{2.1}$$

$$\oint_C \vec{H} \cdot d\vec{l} = \frac{\partial}{\partial t}\int_S \vec{D} \cdot d\vec{s} + \int_S \vec{J} \cdot d\vec{s} = \frac{\partial}{\partial t}\int_S \vec{D} \cdot d\vec{s} + \vec{I}; \tag{2.2}$$

$$\oint_S \vec{D} \cdot d\vec{s} = \int_V \rho dv = Q; \tag{2.3}$$

$$\oint_S \vec{B} \cdot d\vec{s} = 0; \tag{2.4}$$

The quantities in these equations are defined as follows:
$\vec{E}(x, y, z, t)$ is the electric field intensity, in V/m.
$\vec{H}(x, y, z, t)$ is the magnetic field intensity, in A/m.
$\vec{D}(x, y, z, t)$ is the electric flux density, in $Coul/m^2$.
$\vec{B}(x, y, z, t)$ is the magnetic flux density, in Wb/m^2.
$\vec{M}(x, y, z, t)$ is the (fictitious) magnetic current density, in V/m^2.
$\vec{J}(x, y, z, t)$ is the electric current density, in A/m^2, and $\vec{I}$ the total electric current flow through the surface S, in A.

ρ is the electric charge density, in C/m^3,and consequently Q represents the total charge in the closed volume V, in C.
The sources of electromagnetic fields are the electric charges, since electric current density $\vec{J}$ is really the flow of charge and magnetic current $\vec{M}$ is a fictitious mathematical convenience, whose real source is always an electric current loop or some similar type of magnetic dipole.

In free space, the electric and magnetic field intensities are simply related as follows:

$$\vec{B} = \mu_0 \vec{H}; \tag{2.5}$$

$$\vec{D} = \epsilon_0 \vec{E}; \tag{2.6}$$

where $\mu_0 = 4\pi \times 10^{-7} henry/m$ is the permeability of free space, and $\epsilon_0 = 8.854 \times 10^{-12} farad/m$ is the permittivity of free-space.
It is often the case that magnetic and electric currents flow through different dielectric objects, on which depend the birth of electring dipoles, thus altering the constitutive relations, whose most general expression is the following:

$$\vec{D} = \epsilon_0 \vec{E} + \vec{P}_e \tag{2.7}$$

$$\vec{B} = \mu_0 \vec{H} + \vec{P}_m. \tag{2.8}$$

For linear electric and magnetic materials, the polarization vectors ,$\vec{P}_e$ and $\vec{P}_m$, depend linearly from $\vec{E}$ and $\vec{B}$, respectively, and allow the effects of dielectric materials to be put together defining the coefficient matrices of permittivity ($\bar{\bar{\epsilon}}$) and of permeability ($\bar{\bar{\mu}}$):

$$\vec{D} = \bar{\bar{\epsilon}}\vec{E} = \begin{bmatrix} \epsilon_{xx} & \epsilon_{xy} & \epsilon_{xz} \\ \epsilon_{yx} & \epsilon_{yy} & \epsilon_{yz} \\ \epsilon_{zx} & \epsilon_{zy} & \epsilon_{zz} \end{bmatrix} \vec{E} \tag{2.9}$$

$$\vec{B} = \bar{\bar{\mu}}\vec{H} = \begin{bmatrix} \mu_{xx} & \mu_{xy} & \mu_{xz} \\ \mu_{yx} & \mu_{yy} & \mu_{yz} \\ \mu_{zx} & \mu_{zy} & \mu_{zz} \end{bmatrix} \vec{H} \tag{2.10}$$

These matrices are in general full for arbitrary material; for isotropic matererials permittivity and permeability matrices can be condensed to real scalar coefficients (ϵ and μ).
In turn, $\vec{J}$ directely dependent on $\vec{E}$ by the electrical conductivity σ, which is in general a real matrix, and is a source of power loss through the medium. The higher is σ, the better electromagnetic fields are transmitted; a conductor with $\sigma = \infty$ is called perfect.
Maxwell's equations can be written in differential time-varying form as follows :

$$\nabla \times \vec{E} = -\frac{\partial \vec{B}}{\partial t} - \vec{M}; \tag{2.11}$$

$$\nabla \times \vec{H} = \frac{\partial \vec{D}}{\partial t} + \vec{J} = \frac{\partial \vec{D}}{\partial t} + \sigma \vec{E}; \tag{2.12}$$

$$\nabla \cdot \vec{D} = \rho; \tag{2.13}$$

$$\nabla \cdot \vec{B} = 0; \tag{2.14}$$

It is simple to switch from a formulation to the other applying the Stokes' theorem to (2.11) and (2.12), and the divergence theorme to (2.13) and (2.14).
These equations are useful to solve time dependent problems, but a frequency dependant formulation is often preferable to analyze spectral properties: transforming the (2.11)(2.12)(2.13)(2.14) in frequency domain, through vector phasors notation, yelds, for isotropic materials:

$$\nabla \times \vec{E} = -j\omega\vec{B} - \vec{M} = -j\omega\mu\vec{H} - \vec{M}; \tag{2.15}$$

$$\nabla \times \vec{H} = j\omega\vec{D} + \vec{J} = j\omega\epsilon\vec{E} + \vec{J}; \tag{2.16}$$

$$\nabla \cdot \vec{D} = \rho; \tag{2.17}$$

$$\nabla \cdot \vec{B} = 0; \tag{2.18}$$

The differential form is less general in that it applyies only over differentiable domains, otherwise some particular boundary conditions should be used to describe the dicontinuities.

Boundary Conditions

To solve these differential equations, a typical approach is to consider a certain source-free domain and then apply boundary conditions to solve for coefficients. We will present different boundary conditions for specific cases.

Fields at a general material interface

If we consider the interface between two bodies, as shown in Figure 2.2, with electric charge density ρ_s at the interface, the integral form of the last two Maxwell's equations ((2.3),(2.4)) applied to an infinitesimal volume around the interface lead to the sequent boundary conditions for the normal direction:

$$\hat{n} \cdot (\vec{D}_2 - \vec{D}_1) = \rho_s, \tag{2.19}$$

$$\hat{n} \cdot (\vec{D}_2 - \vec{D}_1) = 0. \tag{2.20}$$

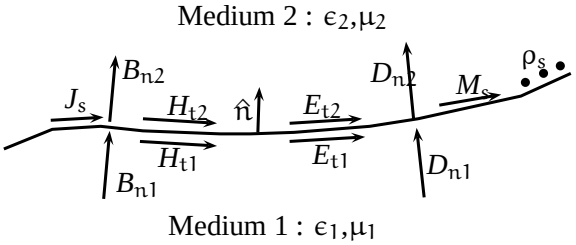

Figure 2.2: Interface between two media with electric charge density

For the tangential components, we refer to the phasor form of (2.1) and (2.2) and in a similar way we obtain:

$$(\vec{E}_2 - \vec{E}_1) \times \hat{n} = \vec{M}_s, \tag{2.21}$$

$$(\vec{H}_2 - \vec{H}_1) \times \hat{n} = \vec{J}_s. \tag{2.22}$$

These are the most general conditions at an arbitrary interface, which state the continuity of the normal fields components across the interface and the equality of the tangential components of $\vec{E}$ and $\vec{H}$, if $\rho_s = 0$.
Since Maxwell's equations are not all independet of each other, these condition are reduntant, too.

Electric Wall boundary

An interesting case in microwave problems is the presence of good conductors (like metals) at boundaries, which can be considered lossless and are thus often approximable with perfect conductors ($\sigma \to \infty$).
In these cases equations (2.19) to (2.22) reduce to:

$$\hat{n} \cdot \vec{D} = \rho_s, \tag{2.23}$$

$$\hat{n} \cdot \vec{B} = 0. \tag{2.24}$$

$$\hat{n} \times \vec{E} = 0, \tag{2.25}$$

$$\hat{n} \times \vec{H} = \vec{J}_s. \tag{2.26}$$

Such a boundary shorts out the tangential components of $\vec{E}$, which must vanish on the surface of the conductor, and is thus called electric wall.
This case is similar to the voltage and current at the end of a short-circuited transmission line.

Magnetic Wall Boundary

The dual of the preceeding case is a boundary where the tangential components of $\vec{H}$ is zero, and is called magnetic boundary.
This is an ideal condition that may be approximated by a corrugated surface or in certain planar transmission problems, and is mathematically convenient as it simplificates the equations.
Magnetic boundary is analogous to the voltage and current at the end of an open-circuited transmission line, and follows these conditions:

$$\hat{n} \cdot \vec{D} = 0, \tag{2.27}$$

$$\hat{n} \cdot \vec{B} = 0. \tag{2.28}$$

$$\hat{n} \times \vec{E} = -\vec{M}_s, \tag{2.29}$$

$$\hat{n} \times \vec{H} = 0. \tag{2.30}$$

Wave equation

From the two curl Maxwell's equations, (2.15) and(2.16), we can find independent equations describing the propagation of $\vec{E}$ and $\vec{H}$ in a general lossy material:

$$\nabla^2\vec{E} + \omega^2\mu\epsilon\left(1 - j\frac{\sigma}{\omega\epsilon}\right) + \sigma\vec{E} = 0, \tag{2.31}$$

$$\nabla^2\vec{H} + \omega^2\mu\epsilon\left(1 - j\frac{\sigma}{\omega\epsilon}\right) + \sigma\vec{H} = 0. \tag{2.32}$$

We call complex wavenumber γ the common parameter

$$j\omega\sqrt{\mu\epsilon}\sqrt{1 - j\frac{\sigma}{\omega\epsilon}} = \alpha + j\beta = \gamma,$$

Note that the form of such equations gives for single-frequency waves an harmonic solution for the propagating fields, with γ being the complex constant of propagation. For lossless materials $\alpha = Re(\gamma) = 0$ and the wave propagates without amplitude decrease, otherwise the waves are exponentially damped, with a velocity depending on its value.
The ratio of $\vec{E}$ and $\vec{H}$ fields is called wave impedance η, which is for plane waves the intrinsic impedance of the propagation medium,

$$\eta = \frac{j\omega\mu}{\gamma} \tag{2.33}$$

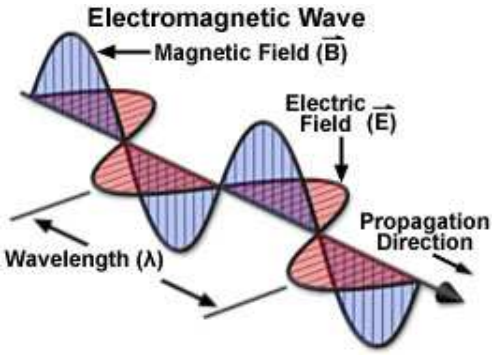

Figure 2.3: Schematic of a propagating EM plane wave

An important aspect of propagating plane waves is the orthogonality between the field vectors $\vec{E}$, $\vec{H}$ and the propagation direction ($\vec{E} \perp \vec{H} \perp \hat{k}$), as shown in Figure 2.3; all the characteristic of a travelling wave can be obtained from Maxwell's equations, comprised the propagation speed in the medium v_p, which equals the speed of light and was the first evidence of the electromagnetic nature of light.
For completeness, we report the speed of light in free space:

$$c = v_p = \frac{1}{\sqrt{\mu_0 \epsilon_0}} = 2.998 \times 10^8 m/s;$$

and the cheracteristic impedance of vacuum to plane waves:

$$\eta_0 = \sqrt{\frac{\mu_0}{\epsilon_0}} = 377\Omega.$$

For rigorous dimonstrations we refer to literature [1][2][3].

Polarization

A general plane wave has non-zero components only in the plane orthogonal to the direction of propagation.
The property which characterizes the direction of $\vec{E}$ vector along time in its plane is called polarization.
It is usual to project $\vec{E}$ on the two orthogonal axes of the complex plane, and classify the polarization types through a lossless material after the phase properties along time of the two component vectors, as shown in Figure 2.4 and next briefly explained.

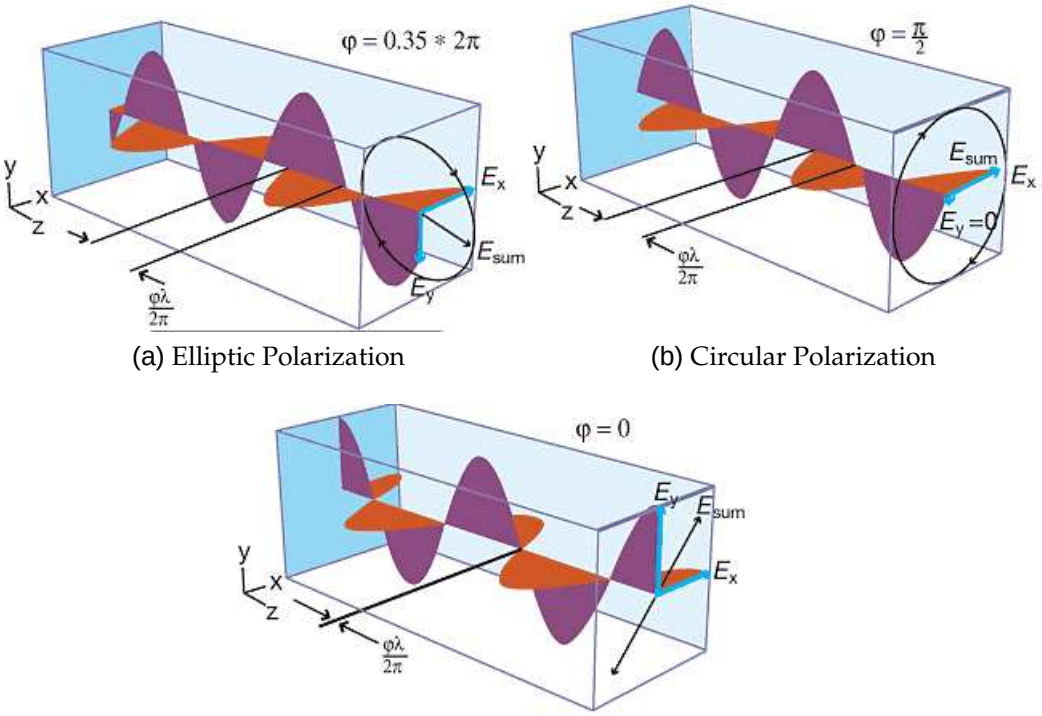

(a) Elliptic Polarization

(b) Circular Polarization

(c) Linear Polarization

Figure 2.4: Polarization types

Elliptical Polarization

Refering to Figure 2.4a, we notice that a plane wave whose electric field projections (E_x and E_y) oscillate with constant non zero phase shift generates an electric field vector following an elliptic trajectory in its plane. This type of polarization is thus called elliptic.

Circular Polarization

A particular case of elliptic polarization occurs if the phase shift between E_x and E_y is $\frac{\pi}{2}$. The trajectory followed by $\vec{E}$ is circular, as shown in Figure 2.4b and the wave is referred to as circularly polarized.

Linear Polarization

A last remarkable case is the one in which the two field projections have a zero phase difference. In this case, reported in Figure 2.4c, we speak of linear polarization, as the electric field vector direction remains fixed and its trajectory is a segment.

A single tone wave is thus characterized by one of these three polarization conditions.
In general a signal occupies a frequency band and the total power is the sum of the spectral power over the bandwidth; at each frequency involved, the EM field can show different polarizations.
One can define a mean polarization summing up the power associated to each angular direction in the XY plane (perpendicular to the direction of propagation, Z) and normalizing it through the total power.
If this power ratio is unity, the signal has the same polarization at all frequencies and is thus defined *totally polarized*.
If a random polarization occurs, the mean polarized power tends to zero, since at each angular direction it is very probable to have two inversely polarized signals whose net power contribution is the difference of the single powers. Such a signal is thus named *non-polarized*.
These two are the extreme cases of polarization, which are very unlikely to occur in reality. Every intermediate case, in which a finite power ratio between zero and unity can be found, is then referred to as *partially polarized* signal.

2.2 Waveguides

As observed introducing the boundary conditions, the propagation of EM fields is influenced and modified when interacting with a material different than free space.
The possibility of using conductor materials to transfer electromagnetic waves with low losses through a desired path is at the basis of waveguide transmission.
We will now briefly introduce some considerations on the mathematical approach to waveguide solutions, without purporting to exhaust the argument.
Let us consider throughout the analisys a domain without internal internal electrical sources and a propagation mean without losses: with respect to the preceeding general relations it means $\rho = 0$, $J = 0$ and

$\sigma = 0$.
Another typical guess in guided propagation is the electric wall boundary condition, since the walls of a waveguide are usually good conductors with very small skin depth.
The wave equations are:

$$\nabla^2\vec{E} + k^2\vec{E} = 0, \text{where} k = \omega\sqrt{\mu\epsilon}. \tag{2.34}$$

The walls influence propagation through the propagation constant γ, which is in the rule different from k.
We will search for field solutions with the form:

$$\vec{E}(x, y, z) = \vec{E}(x, y)e^{-\gamma z}; \tag{2.35}$$

that is to say fields with three spatial varying in the propagation direction (longitudinal axis z of the waveguide) only through the constant γ. Dividing the Laplace operator in a tangential (index t, refering to the xy plane) and a longitudinal (z) components, and considering the properties of exponentials, we can write:

$$\nabla^2 = \nabla_t^2 + \frac{\partial^2}{\partial z^2} = \nabla_t^2 + \gamma^2; \tag{2.36}$$

We obtain the equations of guided waves:

$$\nabla_t^2\vec{E} + (k^2 + \gamma^2)\vec{E} = \nabla_t^2\vec{E} + k_c^2\vec{E}\vec{0}; \tag{2.37}$$

and, with the same procedure:

$$\nabla_t^2\vec{H} + k_c^2\vec{H} = \vec{0}; \tag{2.38}$$

where k_c depends from the boundary conditions and can be expressed similarly to k, defining a characteristic pulsation ω_c, which is called cutoffpulsation.

$$k_c = \omega_c\sqrt{\mu\epsilon}; \tag{2.39}$$

$\vec{E}$ and $\vec{H}$ are 3D vectors, but through the Faraday-Lenz equation and the Ampère law, it can be demonstrated (citeLezioniMicroonde) that only the longitudinal components, E_z and H_z, are independent.

$$E_x = -\frac{1}{\gamma^2 + k^2}\left(\gamma\partial_x E_z + j\omega\mu\partial_y H_z\right); \tag{2.40}$$

$$E_y = \frac{1}{\gamma^2 + k^2}\left(-\gamma\partial_x E_z + j\omega\mu\partial_y H_z\right); \tag{2.41}$$

$$H_x = \frac{1}{\gamma^2 + k^2} \left(-\gamma \partial_x H_z + j\omega\epsilon \partial_y E_z\right); \tag{2.42}$$

$$H_y = -\frac{1}{\gamma^2 + k^2} \left(\gamma \partial_x H_z + j\omega\epsilon \partial_y E_z\right); \tag{2.43}$$

The linearity of Maxwell's equations allows a modal decomposition of the generale solution of propagating fields, i.e. the description of a general solution with the superposition of particular (and simple) solutions, called modes.
We can distingish three types of mode:

- **TM modes** are those in which $H_z = 0$ and $E_z \neq 0$;
- **TE modes** occur when $H_z \neq 0$ and $E_z = 0$;
- **TEM modes** have both $H_z = 0$ and $E_z = 0$.

The last type cannot propagate in single conductor guides, since can lead to non zero field solutions only if $\gamma = k$ and therefore $k_c = 0$, a non physical condition for such waveguides. TE and TM modes can propagate through a guide only at frequencies above the cutoff frequency ($f_c = \omega_c/2\pi$).
Below this value, in fact, the propagation factor

$$\gamma = \sqrt{k_c^2 - k^2} = \sqrt{\mu\epsilon}\sqrt{\omega_c^2 - \omega^2} \tag{2.44}$$

is a real number, and the fields undergo a negative exponential attenuation. Introducing the conceipt of *modal impedance* for TM and TE modes as

$$Z_{0TM} = \frac{E_x}{H_y} = \frac{-E_y}{H_x} = \frac{\gamma}{j\omega\epsilon} \tag{2.45}$$

and

$$Z_{0TE} = \frac{E_x}{H_y} = \frac{-E_y}{H_x} = \frac{j\omega\epsilon}{\gamma} \tag{2.46}$$

we can observe that for real γ this impedance is imaginary and is thus purely capacitive. This means that the attenuation below the cutoff is not due to power dissipation, but to the accumulation and reflection: the mode doesn't propagate at all.
We propose the analytical solution of TM and TE modes in a simple and rectangular waveguide, refering to Figure 2.5.

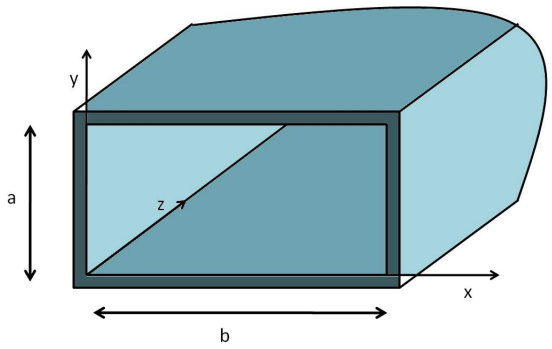

Figure 2.5: Schematic of a rectangular waveguide.

TM modes in rectangular waveguides

In TM modes we consider $H_z = 0$, so the electric field $\vec{E}(x, y)$ is the unknown: using the separation of variables, we write

$$\vec{E}(x, y) = X(x)Y(x) \quad \text{and} \quad k_c^2 = k_x^2 + k_y^2, \tag{2.47}$$

and obtain for both components an harmonic solution.

$$X(x) = A\cos(k_x x) + B\sin(k_x x) Y(y) = C\cos(k_y y) + D\sin(k_y y). \tag{2.48}$$

The boundary condition is the annihilation of the electric field on the conductor guide (electric boundary condition), that is

$$\vec{E}(0, y) = \vec{E}(a, y) = \vec{E}(x, 0) = \vec{E}(x, b) = \vec{0}; \tag{2.49}$$

which lead to the solution of the TM modal shapes

$$E_z(x, y) = BD\sin(\frac{n\pi}{a}x)\sin(\frac{m\pi}{b}y) \tag{2.50}$$

where n, m are integer non zero indices, and define the cutoff frequency of each mode TM_{nm}, recalling that

$$k_c = \sqrt{k_x^2 + k_y^2} = \sqrt{\left(\frac{n\pi}{a}\right)^2 + \left(\frac{m\pi}{b}\right)^2}; \tag{2.51}$$

The first TM mode frequency is found at $n = m = 1$.

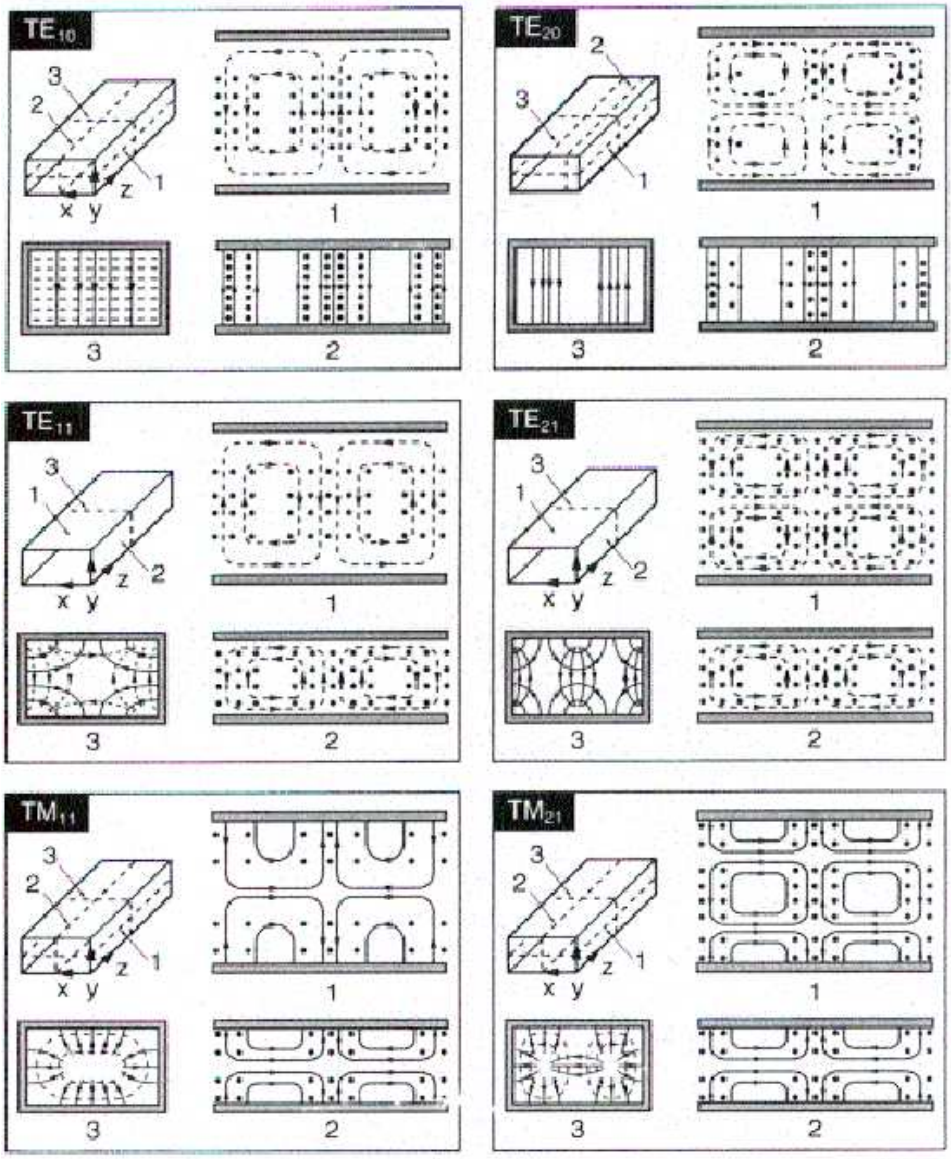

Figure 2.6: representation of the first TE and TM modes in a rectangular waveguide.

TE modes in rectangular waveguides

TE modes can be analyzed from the guided wave equation w.r.t. the magnetic field, since here $E_z = 0$.
As in TM modes, separation of variables is used and combined with the boundary conditions.
In this case, to eliminate the electric field vector on the guide, we must put to zero(from equations 2.40 2.41 with $E_z = 0$) the derivative of $\vec{H}$ in the normal direction to the conductor surface:

$$\frac{\partial H}{\partial n}|_{0,y} = \frac{\partial H}{\partial n}|_{a,y} = \frac{\partial H}{\partial n}|_{x,0} = \frac{\partial H}{\partial n}|_{x,b} = 0; \tag{2.52}$$

and find the modal shapes of the associated to H_z:

$$H_z(x,y) = BDcos(\frac{n\pi}{a}x)cos(\frac{m\pi}{b}y) \tag{2.53}$$

where we can see that the parameters k_x and k_y are the same as in TM modes.
Physical TE modes exist even when one index equals zero; thus, the principal mode for a rectangular waveguide is the TE_{10}, since it shows the lower cutoff frequency.
Figure 2.6 illustrate the field distributions of the first TE and TM modes in rectangular waveguides.

Modes in circular waveguides

The analitical method to describe the propagation modes in circular waveguides with radius R (Figure 2.7 is similar to that presented for rectangular ones: it starts with the guided wave equations (which must be expressed in cylindrical cohordinates), and applies the perfect electric conductor boundary, but requires a field representation through Bessel functions.
For a complete tractation of these modes we refer to microwave handbooks like [1], [2] and [3].
The mode cutoff parameters are:

$$TEmodes \quad k_c = \frac{f'_{p,q}}{R}$$

$$TMmodes \quad k_c = \frac{f_{p,q}}{R}$$

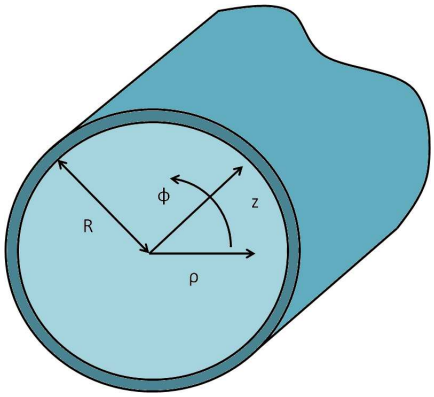

Figure 2.7: Schematic of a circular waveguide

Table 2.1: Bessel function parameters.

p	f_{p1}	f_{p2}	f_{p3}	p	f'_{p1}	f'_{p2}	f'_{p3}
0	2.405	5.520	8.654	0	3.832	7.016	10.174
1	3.832	7.016	10.174	1	1.841	5.331	8.536
2	5.135	8.417	11.620	2	3.054	6.706	9.970

with integer indices p, q ($q \neq 0$), where f and f' are tabulated in literature. Table 2.1 lists the first parameters of both, while Figure2.8 shows the shapes of the first TE and TM modes in circular waveguides; there can be seen that the lowest value of k_c is related to the TE_{11}.

A characteristic of the modes (in any type of waveguide) is their reciprocal orthogonality. This means that they don't share EM power and can be treated separately. This allows to introduce a circuital representation for waveguide modes: each mode can be seen as a transmission line with a particular line impedance (the modal impedance).

Moreover, in uniform waveguides the propagating field is well approximated by the first (dominant) mode, and is thus possible to carry out a preliminary single mode design of a waveguide path with a transmission line analogy.

Reflection and Scattering parameters

Let us briefly introduce transmission lines theory principal ideas, which can be seen as an extension of circuit theory, when phase variations over the line becomes non neglectable, so the lumped circuit

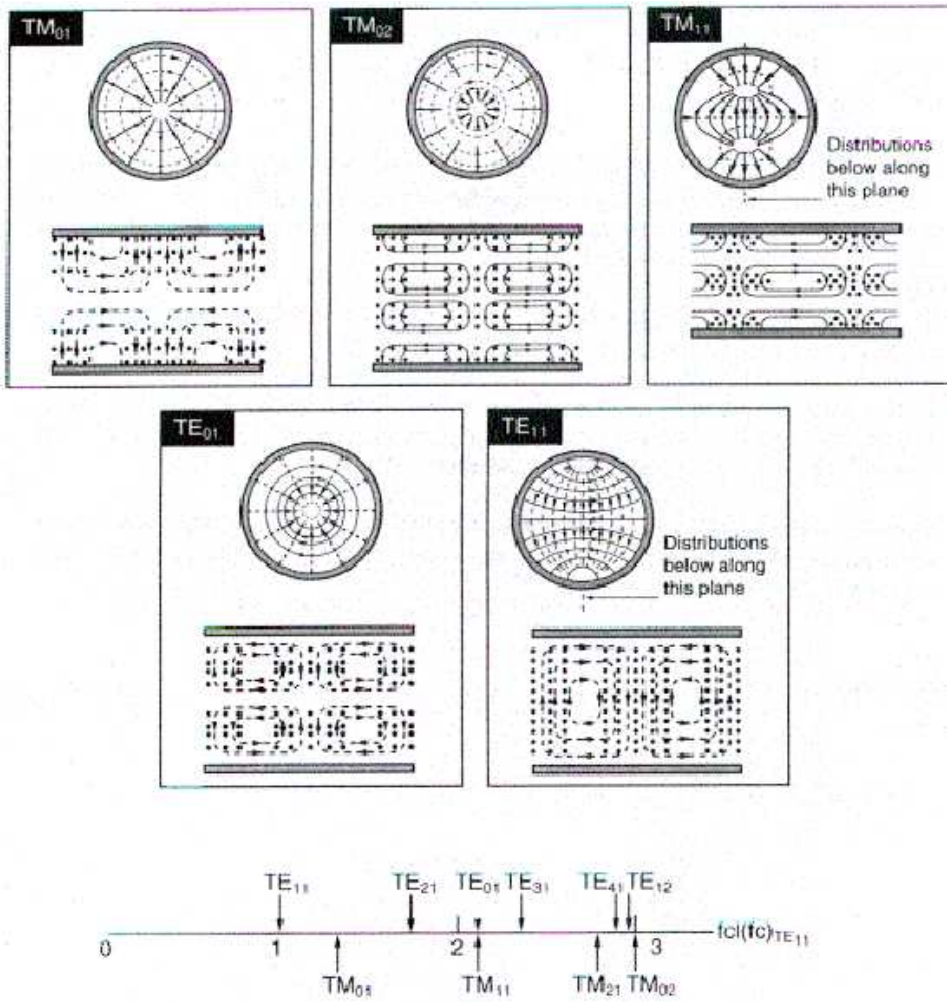

Figure 2.8: representation of the first TE and TM modes in a cylindrical waveguide.

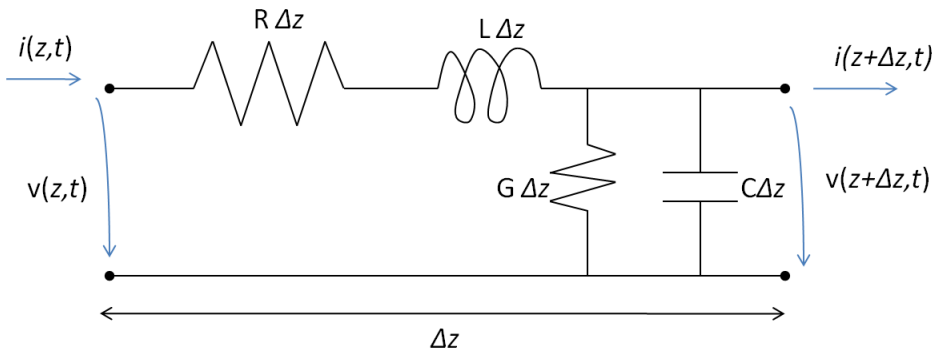

Figure 2.9: Lumped approximation of a finite length transmission line.

elements cannot be adopted.
A lumped description can be recovered considering small length Δz, in which analogue elements can be defined per unit length. Thus we will have:

- R = series resistance per unit length, in Ω/m;
- C = shunt capacitance per unit length, in F/m;
- L = series inductance per unit length, in S/m;
- G = shunt conductance per unit length, in H/m;

A finite length transmission line can be viewed as shown in Figure2.9; using Kirchoff's laws we can solve for voltage and current and find equation which are a particular form of Maxwell's curl equations:

$$\frac{dV(z)}{dz} = -(R + j\omega L)I(z) \tag{2.54}$$

$$\frac{dI(z)}{dz} = -(G + j\omega C)V(z). \tag{2.55}$$

The characteristic line impedance can be defined as:

$$Z_0 = \frac{R + j\omega L}{\gamma} = \frac{V_0^+}{I_0^+} = \frac{-V_0^-}{I_0^-}. \tag{2.56}$$

where V_0 and I_0 are the amplitudes of the travelling voltage and current. We can trace a correspondence between the characteristic impedance of a waveguide, defined previously, and that of a transmission line, i.e. between the electric quantities (V,I) and the electromagnetic fields (E,H).

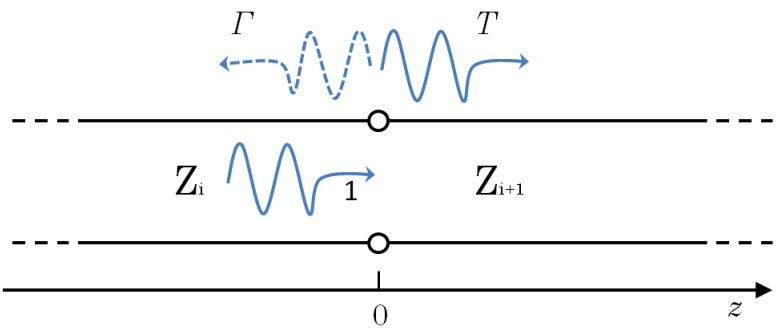

Figure 2.10: Schematic of the wave reflection across a discontinuity.

A significant parameter to describe the propagation through a line is the reflection parameter $\Gamma(z)$. The general solution of the wave equations describes wave travelling in both positive and negative z directions, the latter of those have a physical interpretation only as reflected wave component.
Reflection can occur in a microwave network if an impedance discontinuity is present, due for instance to a local geometrical discontinuity, is present, as shown in figure 2.10.
In each section point of a transmission line (and thus of a waveguide) we can define a ratio between transmitted and reflected waves,Γ, through which we can get many physical properties of the mode field, and the Transmission parameter T [3]:

$$\Gamma(z) = \frac{V_{ref}}{V_{inc}} e^{j2\gamma\Delta z} = \frac{Z_{i+1} - Z_i}{Z_{i+1} + Z_i} \tag{2.57}$$

$$T = 1 + \Gamma(z) = \frac{2Z_{i+1}}{Z_{i+1} + Z_i} \tag{2.58}$$

Since in general the point of interest is the efficiency of power transmission from the input to the output sections, which we name *ports*, these parameters are usually defined on the ports of a device, which are two (in simple transmission lines) or more, dependuing on the complexity of the network.
This allows for a black box description of any network with n ports: let a_i and b_j be respectively the incoming power at the $i-th$ port and the outgoing power at the $j-th$ port, we can relate transmission T and reflection Γ to the transfer functions matrix of the device, called scattering matrix **S**.

$$\begin{Bmatrix} a_1 \\ a_2 \\ \vdots \\ a_i \\ \vdots \\ a_n \end{Bmatrix} = \begin{pmatrix} S_{11} & S_{12} & & S_{1j} & & S_{1n} \\ S_{21} & S_{22} & & S_{2j} & & S_{2n} \\ & & \ddots & & & \\ S_{i1} & S_{i2} & & S_{ij} & & S_{in} \\ & & & & \ddots & \\ S_{n1} & S_{n2} & & S_{nj} & & S_{nn} \end{pmatrix} = \begin{Bmatrix} b_1 \\ b_2 \\ \vdots \\ b_j \\ \vdots \\ b_n \end{Bmatrix} \tag{2.59}$$

S-Parameters of a network are calculated considering single port excitation and matching conditions on the non involved ports. Lossless Networks satisfy the conservation of total power:

$$| S_{11} |^2 + | S_{21} |^2 + | S_{31} |^2 + | S_{41} |^2 = 1; \tag{2.60}$$

If a network is passive and made up of reciprocal materials only, it will show a symmetric Scattering matrix and will be named reciprocal.
The definition of the scattering parameters comes, as we have seen, from an analogy between waveguides and transmission lines, but can be generally used to describe a general n-port network of desired complexity.
Nowadays computational methods are largely used in microwave engineering to design complex devices whose performances might be difficult to find through the transmission line analogy without being too approximative, and their reliability, together with efficiency, is always increasing.

Computational ElectroMagnetics

Computational electromagnetism (CEM) comprise a wide variety of numerical algorithms, finding approximate solutions to the exact Maxwell's equations over cells of finite dimensions in which the whole domain is divided, rather than solving exactely the approximate equations given by the transmission line approximation.
These methods can be classified with respect to the form of hyperbolic Maxwell's equation they base on, differential or integral.

The most popular integral equation solver is the MoM (Method of Moments): it requires calculating only boundary values, rather than values throughout the space, and is therefore more efficient in terms of computational resources for problems with a small surface/volume ratio. Conceptually, it works by constructing a mesh of elements over the modeled surface, but, for many problems, is significantly less efficient

than volume-discretization methods, since boundary element formulations typically give rise to fully populated matrices; this means that the storage requirements and computational time will tend to grow according to the square of the problem size. FEKO is a popular software to solve RF problems using MoM solvers.
Other Integral methods for CEM are DDA (DIscrete Dipole Approximation), FMM (Fast Multipole Method), and PEEC (Partial Element Equivalent Circuit).

Differential equation solvers are the most used to solve CEM problems.
Many commercial and university-developed tools use FDTD algorithms, which has been since the early 1990s the principal implemented method. FDTD belongs to the general class of grid-based differential time-domain numerical modelling methods. Maxwell's equations are modified to central-difference equations, discretized, and implemented in software. The equations are organized in matrix form ($\mathbf{A}\vec{x} = \vec{b}$) solved in a cyclic manner: the electric field is solved at a given instant in time, then the magnetic field is solved at the next instant in time, and so on.
Since it is a time-domain method, solutions can cover a wide frequency range with a single simulation run, provided the time step is small enough to satisfy the Nyquist Shannon sampling theorem for the desired highest frequency.
The finite integration technique (FIT) is a spatial discretization scheme to numerically solve electromagnetic field problems in time and frequency domain. It preserves basic topological properties of the continuous equations such as conservation energy. This method covers the full range of electromagnetic (from static up to high frequency) and optic applications and is the basis for commercial simulation tools, such as CST.
The basic idea of this approach is to apply the Maxwell equations in integral form to a set of predefined grids. This method stands out due to high flexibility in geometric modelling and boundary handling as well as incorporation of arbitrary material distributions and material properties such as anisotropy, non-linearity and dispersion. Furthermore, the use of a consistent dual orthogonal grid in conjunction with an explicit time integration scheme leads to compute and memory-efficient algorithms, which are especially adapted for transient field analysis in radio frequency (RF) applications.[31]

Finite element method (FEM) is widely used to find approximate

solution of partial differential equations and integral equations. It consists on rendering the exact equations in an integral weak form, using weighted shape functions as a solution base: the mathematical smoothness of such functions must fit the order of the derivatives present in the equations to solve.
The domain volume is divided in geometrically simple elements whose definition must be made with care, since accuracy and stability of results depend on it.
The FEM was first proposed to solve elastic problems, but apply well to solve different phenomena, including electromagnetic ones.
COMSOL is a software which exploits the versatility of the FEM to solve problems involving different physics contemporary. Yet FEM is more expensive in terms of CPU load: computational cost grows with the square of the number of total elements; therefore FEM solver algorithms optimization is one of the principal aims of software developers.
In my work I used COMSOL release 4.1 RF module to define the electromagnetic design which will be presented in next chapter.
This choice is based on two considerations: the disponibility of a licensing contract for this module and the possibility of a future refining of the design taking into account other physics, such as heat transfer and mechanical stresses.
Preliminary study of the software was required to get familiar with its RF module.
The model and simulation parameter definition will be related in next section.
Here I propose the first simulations carried out to obtain the known results of field modes propagation through a circular and rectangular waveguide, as Figure2.11 illustrates.

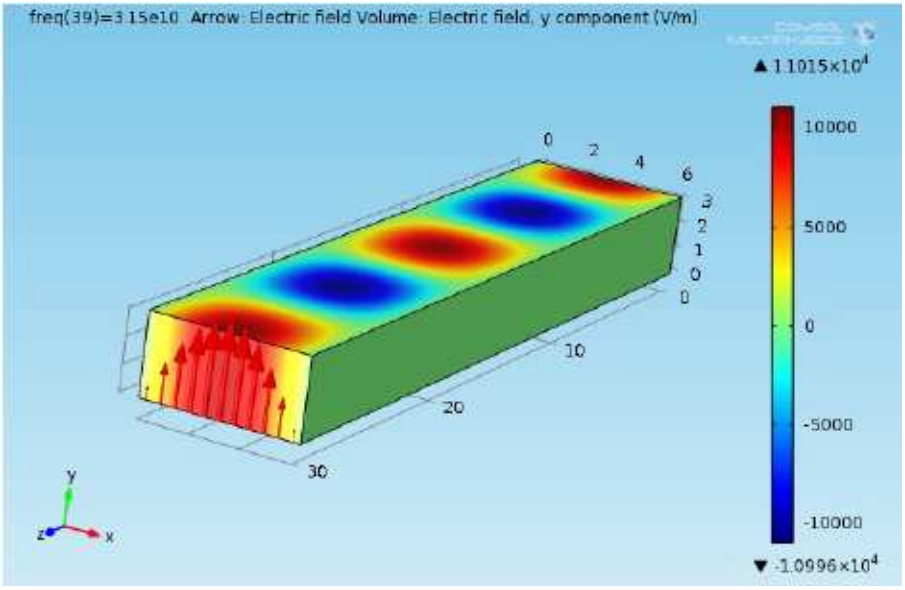

(a) TE10 in rectangular guide: arrows represent the Electric field direction; colors plot the magnitude of its y component. Dimensions are 6.25 x 3.12 x 30 mm; the plot refers to a frequency of 31.5 GHz, that is in the single mode band above the first cutoff frequency, about 25 GHz.

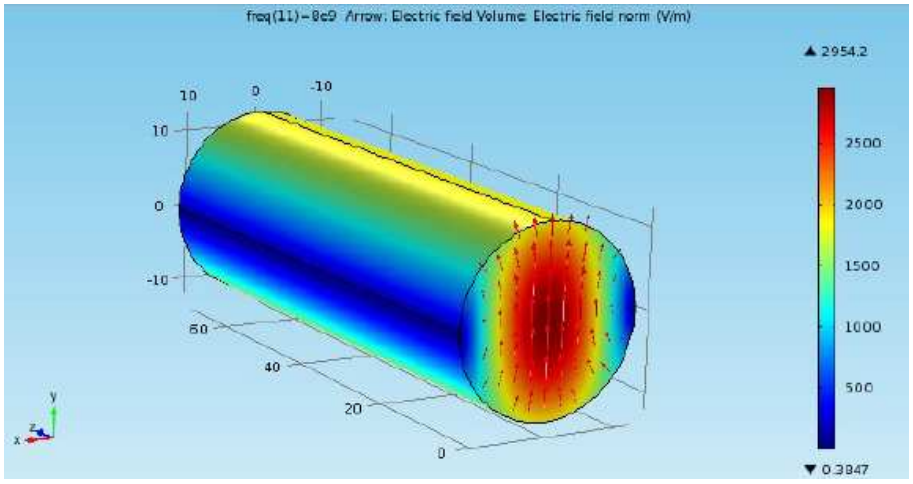

(b) TE11 in circular guide: arrows represent the electric field direction; colors plot its magnitude norm. Radius is 10.9 mm, with a cutoff frequency for the dominant mode at about 8 GHz. Plot refers to 9.8 GHz, that is in the single mode band above the first cutoff frequency.

Figure 2.11: Simulation of two simple waveguide field main modes.
A comparison with analytical results shows good accordance both in modal form, cutoff frequency and scattering parameters.

Chapter 3

OMT state of art

3.1 OMT work principles

Orthomode transducers are passive devices which allow, through geometrical design properties, the transduction of a generic EM wave in two orthogonally polarized signals, or viceversa.
As we have shown in Chapter 1, OMTs collocates in the radiometric chain between the feed horns and the receiving system, and must be designed to adapt both to the circular section of the antenna and to the electric properties of the cabling.
OMTs are commonly used in TMTC systems where a single antenna is used both in receiving and transmission modes: if the incoming and outgoing signals are generated with orthogonal polarizations, they will follow different paths in the two directions on the OMT without interfering in the common guide, as schematically shown in Figure 3.1.

In scientific instruments for the investigation of microwave sources and their polarization properties, OMTs are used to distinguish the or-

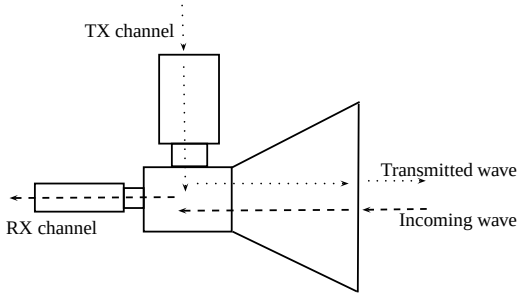

Figure 3.1: Typical use of an OMT in telecom systems

thogonal polarization modes perceived by the antenna.
Under the electromagnetic point of view, OMTs are four-ports devices, with two port sharing the same physical position(Port1 e Port2 in Figure 3.2) and the remaining two respectively corresponding to the two principal modes of the input signal.
As introduced in Chapter 2, inside an OMT the electric quantities can't

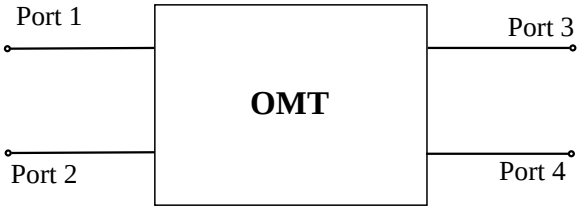

Figure 3.2: Schematic of an OMT as a 4-port device.

be defined uniquely defined, since they vary significantly through its length. Thus, the most common performance check method is to consider it as a black box and build the transfer functions matrix between all possible combination of input-output pairs.
If we call a_i the generic amplitude of an incoming signal at the i-th port, and b_j that of a outgoing signal at the j-th port, we can build the matrix of correlation between inputs and outputs, called scattering matrix **S**, which in the case of an OMT is 4×4.

$$\begin{Bmatrix} a_1 \\ a_2 \\ a_3 \\ a_4 \end{Bmatrix} = \begin{pmatrix} S_{11} & S_{12} & S_{13} & S_{14} \\ S_{21} & S_{22} & S_{23} & S_{24} \\ S_{31} & S_{32} & S_{33} & S_{34} \\ S_{41} & S_{42} & S_{43} & S_{44} \end{pmatrix} = \begin{Bmatrix} b_1 \\ b_2 \\ b_3 \\ b_4 \end{Bmatrix}$$

The diagonal parameters S_{ii} represent the reflection coefficients on the four ports; the square of their module $|S_{ii}|^2$ define the Power Loss ($\mathbf{PL}_i$) due to the electrical mismatch of port i, while its reciprocal are called Return Loss ($\mathbf{RL}_i$); an ideal OMT should exhibit a power loss parameter as close as possible to zero.
The values $|S_{31}|^2$ and $|S_{42}|^2$ are the transmission coefficients along the paths from port 1 to port 3 and from port 2 to port 4 respectively, and should be maximized for high quality reception; their reciprocals are named insertion losses $\mathbf{IL}_{ij}$.
The quantities $|S_{41}|^{-2}$ and $|S_{32}|^{-2}$ represent the power amount of one polarization mode reaching the wrong port, i.e. the one designed to transmit the other mode; these are then called cross polarizations, $\mathbf{XP}_{ij}$.
Eventually, S_{34} and S_{12} indicate respectively the reciprocal insulation

of the output ports ($|S_{34}|^{-2}$, Output Insulation) and of the input ones ($|S_{12}|^{-2}$, Input insulation). For these considerations, an ideal OMT must have this scattering matrix:

$$\mathbf{S_{id}} = \begin{pmatrix} 0 & 0 & e^{j\phi_1} & 0 \\ 0 & 0 & 0 & e^{j\phi_2} \\ e^{j\phi_1} & 0 & 0 & 0 \\ 0 & e^{j\phi_2} & 0 & 0 \end{pmatrix} \tag{3.1}$$

where ϕ_1 and ϕ_2 are the phase delays due to the waveguide length between port 1 and 3 and between port 2 and 4, respectively.
Regarding real OMTs, the main design criteria are then indicated by the minimum required performances, i.e. some specific requirements on the S parameters, reaching whom is often not simple, as some design choices improving one parameter might worsen some others.
On the other hand, it is often not required to all of the parameters to approach the ideal case values, especially in commercial devices, and in many cases some trade-offs between performances and production costs are necessary.
A variety of design solutions are widely diffused to satisfy different requirements at different frequency bands, as the following will summarize.

3.2 OMT typologies

There exist diverse types of OMTs with different characteristics in terms of performances, work frequency bands, geometry, production technology and therefore costs. A useful classification is based on the geometrical structure of the device, as presented in the following. [8]

- Planar [18];
- Waveguide based [19];
- Finline [20].

Planar OMTs

Planar OMTs use dielectric probes in rectangular or circular waveguides: the typical and most researched configuration since the early 2000s ([18]) uses four probes at right angles in a cylindrical waveguide; two orthogonal polarisations are extracted by combining the signals from each pair of opposite probes.
It is compact, simple to construct, and easy to scale to any frequency band.
Because of the advantages in integration, scalability and mass of planar OMTs compared to external waveguide OMTs, a planar OMT coupled to a corrugated horn is a good option for future CMB polarisation missions such as B-Pol, in particular at submillimeter wavelengths using micromachining.
The realization of a high performance Planar OMT to achieve the stringent requirements of new polarisation cosmology instruments requires nonetheless extreme precision and some corrective expedients, either to increment the bandwidth or to tear the cross-polarisation down, which in turn require higher costs [21][18] [9] [10].
In Figure 3.3 is shown an example of Planar OMT, with a schematic representation of the electric circuit.
Typical materials for these devices are metals (gold, copper, aluminium alloys) at low frequencies, while superconducting materials (Silicon nitrides, Niobium) are commonly used at higher frequencies, i.e. at extremely small dimensions.

Waveguide based OMTs

Waveguide based OMTs exhibit the best demonstrated performances at millimeter wavelengths [8], and can be produced with a wide variety of techniques.
As for any waveguide devices, the broadband operation is tied to its symmetry properties; symmetrical or non-symmetrical transitions in waveguides produce high order modes which, though evanescent, subtract power to the desired principal modes.
These OMTs can be classified with Bøifot after their increasing symmetry.
Class I contains the simplest solutions, with one arm for each orthogonal mode: the main mode arm is coaxial to the feed horn, and is therefore symmetric, while the side arm mode is orthogonal and thus

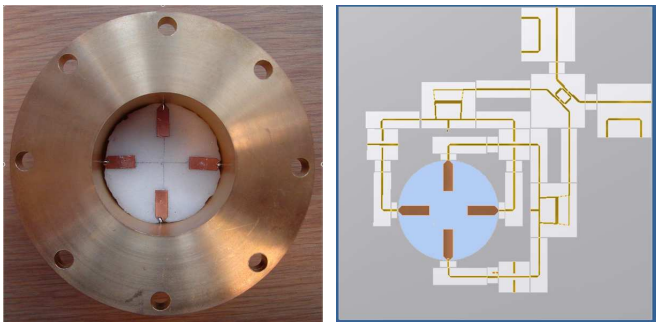

(a) *OMT and probes*

(b) *OMT and striplines simulation model*

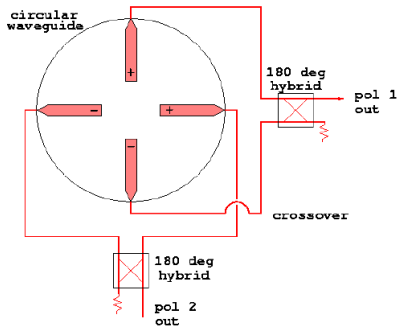

(c) *electrical scheme*

Figure 3.3: Planar OmT, waveguide and probes [21] and complete electric circuit

non-symmetric, as shown in Figure 3.4a. For what said, this asymmetry causes limitation on the bandwidth.
This solution is compact and geometrically very simple, and therefore proves to be very versatile and realizable with many techniques, from electro-forming to direct machining.
Class II configuration is a bit more complex, presenting a symmetric solution for the side arm: two symmetric side arms depart from the main one, and are then joint together in a second time, so both arms modes see a symmetric device. A scheme o a Class II OMT junction is represented in Figure 3.4b.
This expedient makes it easier to reach a good bandwidth even in the side arm, though increases the complexity of the device and complicates its fabrication.
A further increase of complexity is present in class III OMTs, where the main arm is also split in two and then rejoint, just like the side one. The splitting junction essentially forms a classic turnstile junction which has

been widely investigated [11][8],[12]. In Figure 3.5b is shown an example of such an OMT in submillimeter band.
The complexity of such an OMT naturally provides good compensation of higher order symmetric modes on both arms, but lets production costs increase.
Among these types of OMT, some other expedients can be taken and are often necessary to adjust the EM fields to match the requirements: posts, septums and transitions are some examples.[8] [11].
A particular class II OMT is shown in Figure 3.5a. It was designed by Bøifot himself, using a thin metallic septum in the main arm, long enough to select the only desired mode; this solution acts in the same principle of the double split in class III OMTs, and is therefore referred to as a Class IIb device.
Typically, the common port has square or circular section, since it must host both the vertical and horizontal principal modes coming from the horn, while the output single mode standard ports are rectangular with a typical ratio between the two edges of 1:2.
A circular port can be directly joint to the feed horn, while a square one requires a circular-to-square transition which must not introduce mismatch power losses between the feed horn and the OMT.
Section transformers from circular or square to rectangular standard ports, just like junctions, are very critical to design with good matching properties, since any section variation has consequences on the impedance seen by the travelling fields, as explained in the previous chapters (**ref: chap2**) Splitting junctions are actually the most important part of a waveguide based OMT to get good separation between the two orthogonal modes.

Finline OMTs

A Finline OMT consists of a square or circular waveguide fitted with diametrically opposite thin tapered metallic fins. The dominant mode electric field parallel to the fins is gradually transformed to a finline mode whose energy is essentially confined to the narrow gap between the fins in the center of the waveguide. This energy then can be removed from the waveguide by curving the finline and bringing it out through the side wall of the guide. The mode polarized orthogonal to the fins passes through the guide virtually unperturbed when the fins are sufficiently thin. This design is thought to be easier to fabricate at millimetric frequencies than class II and class III OMTs, and is therefore

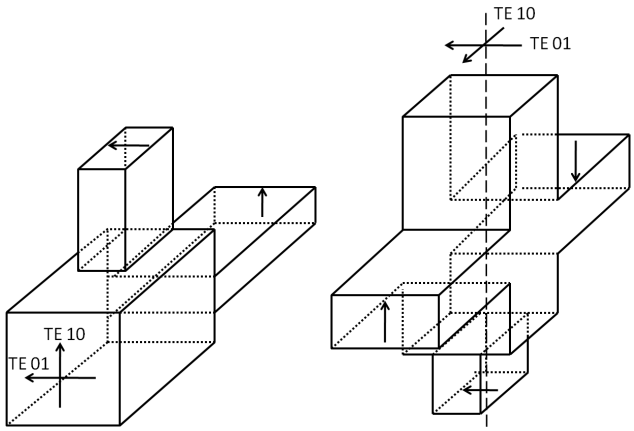

(a) *ClassI junction* (b) *ClassII Junction*

Figure 3.4: Rappresentations of waveguide junctions of ClassI and ClassII OMTs.

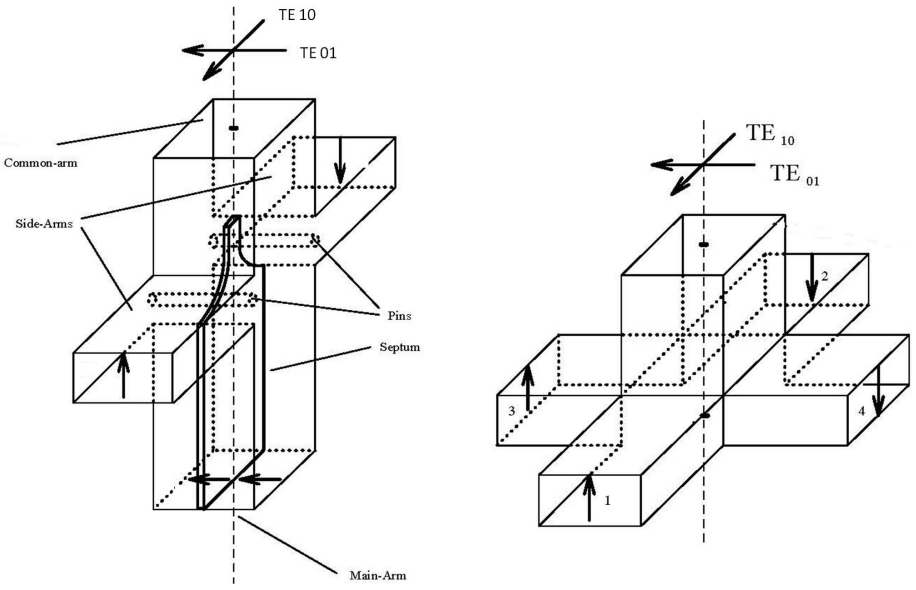

(a) *Boifot Junction* (b) *Turnstile Junction*

Figure 3.5: Rappresentations of waveguide junctions of ClassIIb (Boifot) and ClassIII (Turnstile) OMTs.

looked into as a viable design in these bands.
Figure 3.6 illustrates a section of a finline OMT.

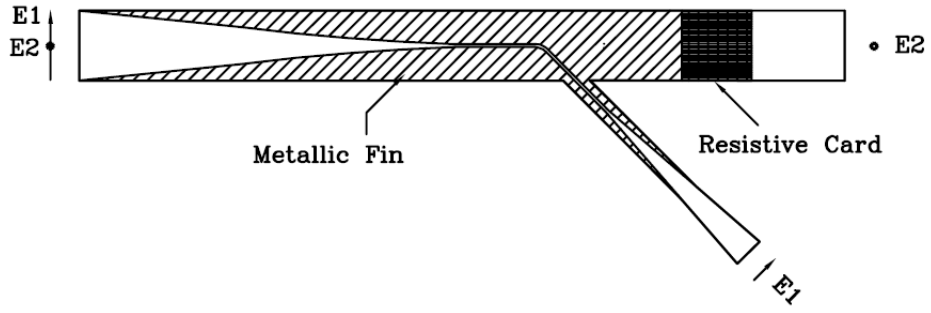

Figure 3.6: Finline OMT solution

3.3 Fabrication technologies

Let us now introduce some of techniques of fabrication of waveguide based OMTs and waveguide components.
As for all technological processes, the choice of materials to use is critical for both the operative life performances (mechanical, thermic, electric) and the machining techniques they allow or can't undergo.
A component as an OMT we will propose must be rigid and keep shape without significant deformations from ambient to cryogenic temperatures, where it is designed to operate; for this reason low thermal expansion coefficient at low temperatures is required.
Under an electric point of view, materials with low bulk resistivity are required to grant low transmission losses. Since transmission of the EM power in high conductivity materials involves only a thin depth (skin depth), it is possible to use metals with poor conductivity characteristics, if the interior walls are properly plated.
The skin depth is defined as the depth below the surface of the conductor at which the current density has fallen to about 37%, and depends principally on frequency f, resistivity ρ and magnetic permeability μ, as indicates its most common expression:

$$\delta_s = \sqrt{\frac{\rho}{\pi f \mu}}. \tag{3.2}$$

It is accepted that a depth five time δ_s is sufficient to carry almost the whole electrical power.

Table 3.1: Main properties of some metals and materials.

Material	Ni	Cu	Fe	Au	cr	Al	Ag	Ti
Bulk resistivity [$\mu\Omega/cm$]	8.707	1.673	9.66	2.44	18	2.65	1.59	55
Density [g/cm^3]	8.9	8.92	7.81	19.3	7.1	2.702	10.5	4.5
Heat capacity [$J/kg/K$]	442.6	385.2	386	238.7	449	902	236.3	523
Thermal expansion [ppm/K]	12.8	16.6	12	14.2	8.2	23.03	18.9	8.5

Figure 3.7 presents a plot of δ_s versus frequency for some good conductors.
Typical materials are metals such as brass, copper, silver and aluminum

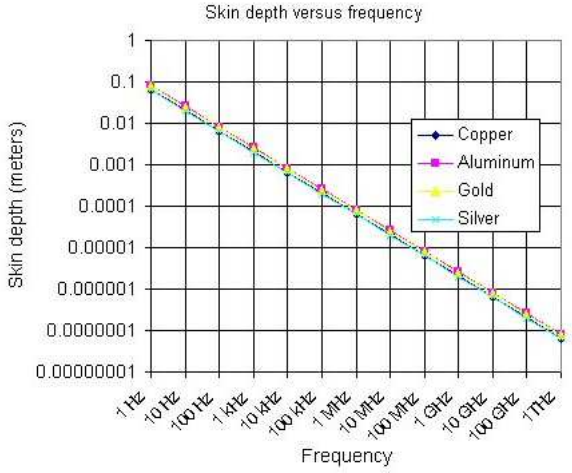

Figure 3.7: Skin depth versus frequency for different conductors. Notice that the magnitudes are of the same order and decrease with increasing frequency, shown in logarithmic scale.

alloy. A table of some materials and their bulk resistivity is shown in Table3.1
Different methods can be used to product a metallic OMT, either conventional, where material removal mechanism is essentially based on mechanical forces, or non conventional, based on other principles such as electric and chemical processes.

Non conventional machining

Electroforming is a good technique to product waveguides and cave parts. It requires more lavoration steps, and is up to now limited to single object production: this means it is hardly extendible to the parallel production of OMT or feed horn arrays.
A metallic material is forced via galvanic deposition to cover a mandrel (a sort of negative of the final product) of the desired form of the OMT cavities, which will then be removed.
Thereafter, the product must be treated and refined to avoid imperfections and to gain the desired mechanical properties.
The choice of the materials is critical: to allow galvanic deposition, the mandrel must be made of a conductor material which can act as anode, like aluminium, copper or silver; the final OMT material must on the contrary be the cathode of the process.
Copper is generally used for applications requiring high thermal or electrical conductivity. Nickel, gold, silver and rhodium are used where unusually high resistance to corrosion or oxidation are required. Iron can be electroformed but has an important drawback on corrosion affection [24].
Residual stresses may occasionally cause problems for highly loaded parts, but this is not the case of typical waveguide components.
The removal of the mandrel must be studied accurately, too: a complex object may let mechanical separation become impossible, and would require chemical corrosion of the mandrel in an acid bath. This in turn has important consequences on the choice of materials, since the mandrel must erode while the OMT must not.
Thanks to its intrinsic ability to reproduce any given shape with extremely high accuracy, it is a very interesting technique for the fabrication of metallic passive microwave components used at frequencies ranging from tens to a few hundred gigahertz (upper microwaves and far infra-red). At such high frequencies, it is much simpler to get accurately machined mandrels than cavities, and electroforming proves to have many advantages.
In conclusion, electroforming is an accurate but long and expensive method, not extendible to parallel production of many OMTs in array structures. Advantages in time and money could be obtained with reusable mandrels, but this is often not practicable with complex cavity shapes.
Figure 3.8 shows an electroformed copper OMT working around 43 GHz and aluminium mandrels.

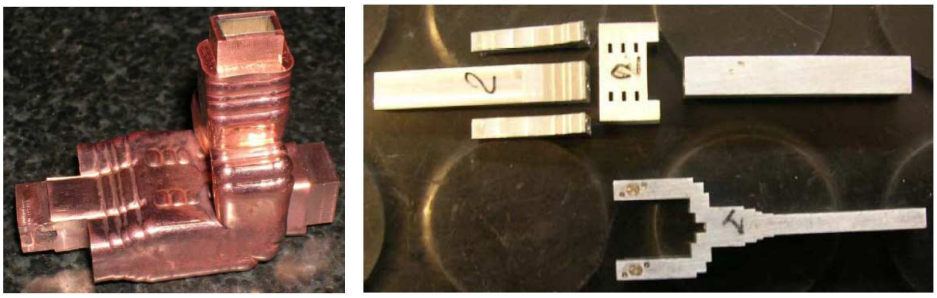

(a) *Copper electroformed OMT* (b) *Aluminium mandrels*

Figure 3.8: Class II electroformed OMT [22].

Another interesting method is the electronic discharge machining, or electroerosion, of which two types exist: wire EDM and plunge EDM. Both methods use high-voltage to melt away metal, rather than mechanically removing metal with cutting tools.
Wire EDM uses a very thin wire that travels from one spool to another, is energized with high voltage, and is placed in contact with the part being machined to make a linear cut by blasting away material. The part being machined is typically held stationary, while the two spool feeds are moved to steer the saw. In the best wire EDM machines, the top and bottom spools can be moved independently, but that does not work with complex OMTs. The part being machined is suspended in an oil solution, which is used to carry away and suspend the machining gases. Wire diameter for wire EDM is typically a few millimeters, so accuracy hardly exceeds one millimeter; brass is the typical material of choice.
Plunge EDM uses carbon elements that are energized to high voltage, and are pushed into the part being machined to blast away unwanted material. The part being machined is suspended in an oil solution. The plunger can be moved in X, Y, and Z axis, as well as rotated, enabling more complex shapes than wire EDM. Accuracy is better, but also expenses are superior, because the plunger must be machined, and it has a short life.
EDM methods can be used to get cavities and ribs relatively quickly, but have limitations on the geometry complexity obtainable, and remain less accurate than electroforming, with precision limits which prevent the use of this technique for objects working at frequencies over some tens of GHz.
In the Planck satellite, for instance, only the feed horns at the two

lower frequencies (30GHz and 44Ghz) where fabricated by electroerosion, while electroforming was adopted both for the 70 GHz LFI horn and all the HFI feed horns ranging from 100 to 857 GHz[13].
Electroerosion is therefore an accurate and cheap technique only for simple object without submillimetric lavorations, which could be in principle used to product small clusters of feed horn arrays.

Another option is dip-brazing, a specialized process for joining aluminium pieces, cheaper than electroforming. Pieces of the waveguide must first be machined from a solid block of material, commonly an aluminium alloy; a thin doping layer is applied to the aluminium pieces on surfaces to be joined; this drops the melting temperature of the metal only where it contacts. The finished waveguide is then placed into a bath of molten salt and then brought up to the metal's near-melting point. Of great importance is the exact temperature profile that will braze the joints but not melt the waveguide pieces. After the waveguide is removed from the bath it must be hardened. During the brazing and hardening process the walls of the waveguide can become deformed from their ideal geometry. In Ku-band and lower frequencies this is not much a problem; errors up to few millimetres represent less than 1% error w.r.t. the characteristic dimensions and do not have appreciable effects on the insertion and phase of the signal at these frequencies. However, when reaching higher frequencies such as Ka, V, and definitely W, this becomes a problem worth thinking about when considering dip-brazing.
All of these fabrication techniques are non conventional, since they don't use mechanical forces to model objects.

Conventional machining

Let us now introduce conventional machining, since this is the method the current project will be based on, though realization of the designed object will not be part of the work.
Conventional machining is a form of subtractive manufacturing, in which power-driven machine tools, such as saws, lathes, milling machines, and drill presses, are used with a sharp cutting tool to physically remove material to achieve a desired geometry. Machining is a part of the manufacture of many metal products, but it can also be used on wood, plastic, ceramic, and composites.
When using conventional methods, many factors must be considered

to grant the quality of the final product, such as elements of fixture, which must be designed ad hoc and often requires deep study and optimization steps, choice of the cutting tools, speed and trajectory of the processings, lubrification and cleaning of tools and object.
Industrial conventional machining are highly automatic, with numerical controlled motion of tools on one or more axes. Indeed, automation has notably increased the performances, allowing nowadays to obtain processings on the order of few micrometers, which can be useful for high frequency components.
In conventional machining, the shapes are modelled using rotating cutting tools, which motion is governable on one or more axes depending on the type of machinery they are mounted on.
A hollow structure like an OMT is still too complicated to manage with a milling machine from a unique metal piece.
There exist a variety of OMT prototypes obtained via direct machination of junctable blocks, designed at different frequency bands, from few to several hundreds GHz.
Some examples of directly machined microwave devices are presented in the following.

Ultra-Thin conventionally machined OMT with Turnstile Junction, for the X-Band EVLA receiver

The first is a project of a turnstile junction OMT, designed to be as flat as possible, with a central frequency of 10GHz, illustrated in Figure 3.9 [11].

As can be seen, an assembly of this type requires a great amount of junctions to grant a good bearing between the parts, which increase the total weight.
Such a structure will also be very inefficient at high frequency, since the bulk of the junctions can't be reduced much, and cannot follow the trend of electromagnetic lengths.
The great advantage due to simplicity of realization of the single blocks meets the drawback of the assembly requirements, which also doesn't fit the necessity of a modular approach for CMB polarization instruments.

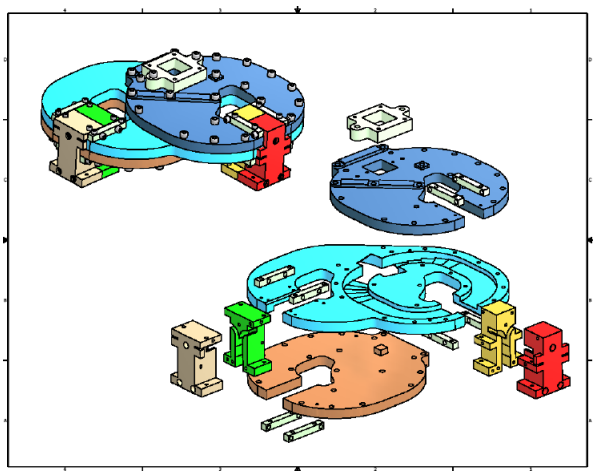

Figure 3.9: Representation of the juncted blocks of the project EVLA in X-Band.

Turnstile Junction OMT for CARMA project.

A different approach is presented in Figure3.10; here, the waveguide paths are obtained from two (or more) geometrically simple blocks, using essentially superficial cave milling and avoiding deep boring. The blocks are then puzzled up and joint[8].
This method is particularly used in high frequency designs, where micromachining is required to obtain high accuracy, and deep lavorations should be avoided or in some cases are not practicable by conventional machining, for stability or limited stiffness of the cutting tools.
This technique is also well promising in view of OMT array production thanks to it's high modularity.
Alignment is here very important: any even small misalignment would hit performances down, since influencing directly the line impedance of each waveguide section.

Platelet Feed Horn Array

An already tested technique to obtain complicated waveguide structures is the superposition of simple bored metal plates of small thickness, to which we refer as *platelet method*.
This method is intrinsically modular and can easily be extended to product small clusters of more than one object at the same time.
The most efficient way to build up arrays is to use hexagonal elementary cells, learning from the honeycomb structures,each hosting the cross sec-

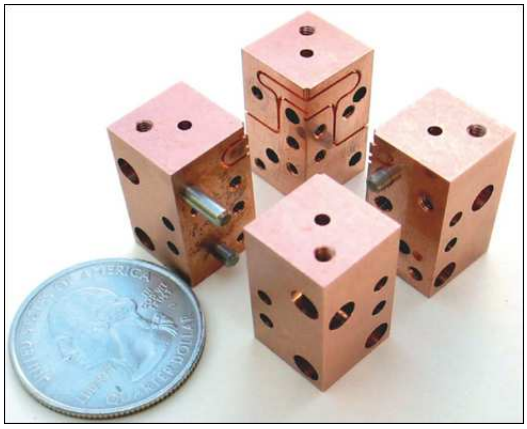

Figure 3.10: A turnstile junction OMT obtained from milling of four complementary blocks.

tions of one or more feed horn.
This approach fits well with the production of corrugated feedhorns, which are obtained by superposition of plates with just circular bores, simply varying the diameter of the processing.
Modularity, simplicity both of geometries and lavoration technique (and therefore speed), also have the important advantage of cost effectiveness per unit.
The possibility of producing OMTs with this last method seems very

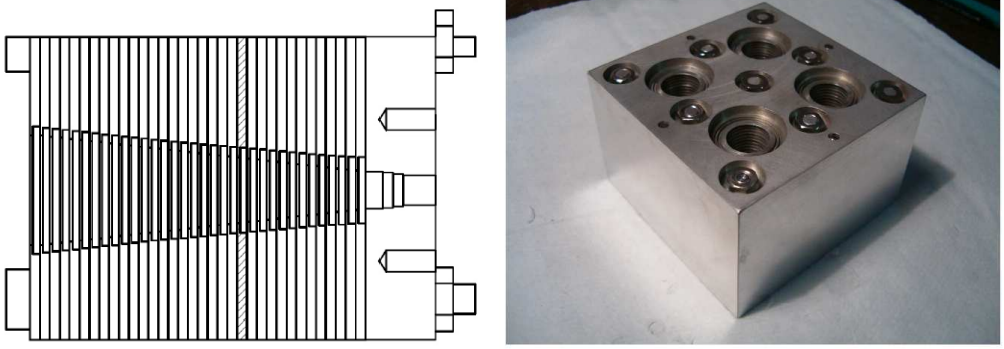

(a) *Section view* (b) *realized prototype*

Figure 3.11: Platelet feedhorn sectional view (a) and realization of a four element cluster (b).[25]

interesting, both for the just mentioned advantages and for the natural coupling with a platelet feedhorn array.

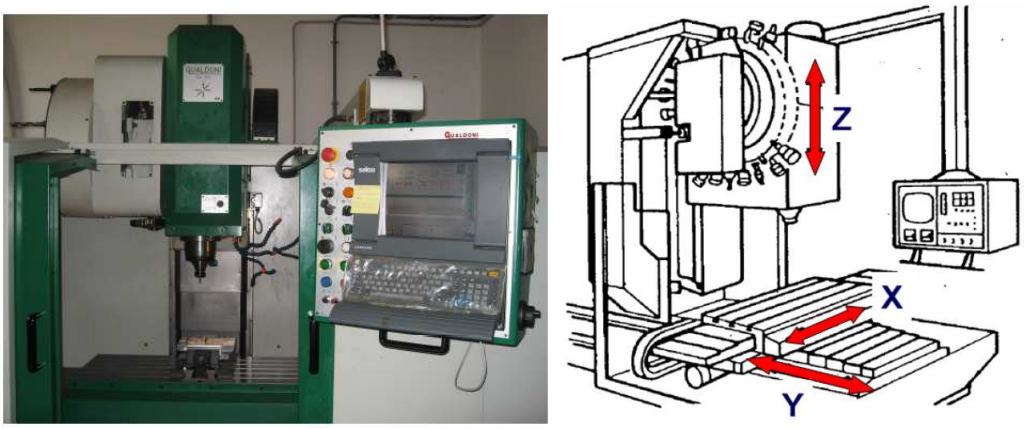

(a) (b)

Figure 3.12: The Gualdoni GV-94 three axes CNC miller (a)and its motion representation (b).

As already mentioned, this work will propose a prototype of OMT to be realized with this technique.

Cutting tools

Milling is thus the mechanical process the different plate will undergo, using the CNC milling machine of the university laboratory (see figure 3.12a)as reference, whose three degrees of freedom are illustrated in Figure 3.12b. The horizontal plate is able to interpolate almost any trajectory on its plane (say XY), thanks to a computer based motion control.
Above the base the mandrel can be seen, where to mount the cutting tools. The mandrel can rotate with a speed of 50 to 10000 rpm and move along the vertical axis (Z).
A CNC machine has advantages in the programmability and therefore repeatability of the process.
The precision of the illustrated machine reaches 0.01mm, a typical value for its class.
To program a machining, the mechanical drafts must be translated in the programming language; before starting the process, it is good practice to simulate it via software to verify the translation and prevent it from programming errors which can deface the final object in the best case,and damage the machinery in the worst.

It is therefore necessary to carefully choose both the mechanical parameters and the cutting tools (mills) to use.
The choice of the cutter depends on the material it must remove and the dimensions of the processing. A general rule is that a cutter with diameter D cannot be used for processing depths greater than $s = 2D$ (See Figure3.13).
As will be explained in the next section, in the current design process we tried to obtain the maximal radiuses of edge machining (which is directly related to the diameters of the mills to use), granting the goal performances, and accomplished a prototype requiring a minimal diameter of 1.5 mm on a thickness of 2 mm.
The rotational speed ω[rpm] of the cutters is than associated to this

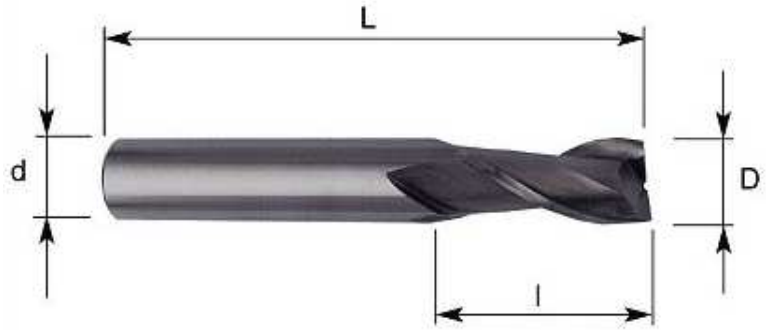

Figure 3.13: Schematic of the main dimensions of a mill.

diameter D_E[m] through the linear cutting velocity v_c[m/min]:

$$\omega = \frac{v_c}{\pi D_E}; \tag{3.3}$$

while the effective advance speed v_a is related to the number of cutting teeth (n) and the advance rate per tooth a_n:

$$v_a = n a_n \omega; \tag{3.4}$$

These two speed parameters are requested to program the process; the diameter parameters involved in this project, associated with aluminium sheets and mills with two teeth, result in rotating speeds affordable by the reference work station.
Several other aspects have to be taken in consideration when directly machining an object, such as the fixture, to locate, hold and support the

workpiece during the manufacturing operations.
Fixtures must correctly locate a workpiece in a given orientation with respect to a cutting tool or measuring device, or with respect to another component, as for instance in assembly or welding. Such location must be invariant in the sense that the devices must clamp and secure the workpiece in that location for the particular processing operation.
Fixtures are normally designed for a definite operation to process a specific workpiece and are designed and manufactured individually.[28]
The fixture design for our OMT is not part of this work, but will be a necessary step to the future realization of a prototype.
Since one of the aims of modern manufacturing in general, and of the proposed design in particular, is unit cost reduction, it is suggestible to design the fixtures to let load and unload cycles be as simple and efficient as possible, to reduce the manifacturing cycle time.
The clamping procedure must provide an invariant location to the object w.r.t. the external load due to the machining process, and must not infer a state of stress to the unloaded piece. This second requirement can be not trivial satisfy, and may require different clamping steps [25].
An initial non zero stress field on our plates may result in undesired deformations and thus misalignments when unloading the workpieces, which in turn could prevent the correct superposition of the laminas or modify the impedance characteristics of sections, thus worsening the electromagnetic performances.
Surface roughness has a big effect on electromagnetic losses, too: when roughness becomes on the order of skin depth, attenuation of transmission lines increase. Although an Root Mean Square value is typically used to define global roughness, imperfections are very unlikely regular, and could give way to anisotropic attenuation.

Chapter 4

Design of a platelet OMT at 40 GHz

The objective of this work is the design of an OMT in millimetric band intended to be produced with the platelet technique, in which each layer is directly milled.
Let us now introduce the chosen geometry and the final design following the driving ideas which guided the design process.

4.1 Constraints and objectives

Desired performances and mechanical constraint are the first aspects to be taken into account to start the project. Nonetheless, in our case the design had no fixed constraint since the work is thought as pilot project and was not commissioned by any agency.
Some initial considerations were necessary, and some literary research about the typical performances in cosmological instruments, different design solutions (already introduced in Chapter 3) bulk of feed horns at 40 GHz, interface flanges dimensions for Q-Band single mode waveguides was made to let us take reasonable design parameters.

Q-band feed horn bulks

this informations were researched to have some reference of the overall acceptable dimensions of a Q-band OMT and choose an interesting level of compactness.

This in turn plays a role in view of a future compact n-receiver module design: feed horn arrays have already been proposed, using hexagonal cells, easy to place side by side just like honeycomb structures; the smaller the projected surface of the OMT are with respect to the large section of the feed horn, the more it will be possible to design coupled OMT and horn arrays without losing compactness.
The dimensions of the low frequency feedhorns mounted on the Planck focal plane are shown in Figure 4.1: R on the y-axes is the radius in millimetres, since each horn is obtained revolving these sections around the x-axis.
The 44GHz operates at frequencies close to our work goal, so we can

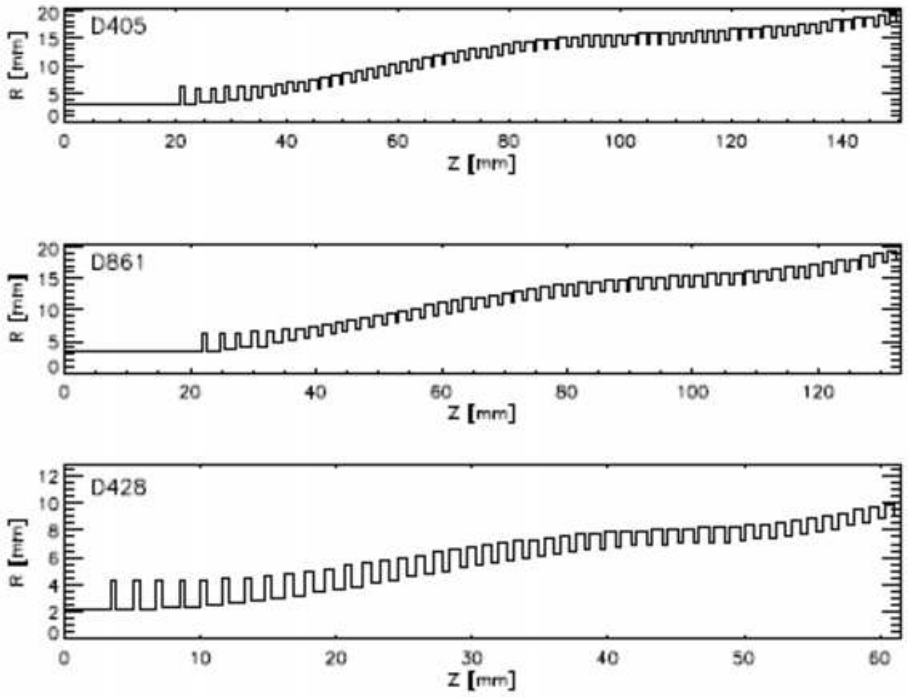

Figure 4.1: Low frequency feedhorns dimensions on the Planck focal plane, working at 30GHz, 44GHz and 70GHz, in the order from the top.

foresee similar dimensions.
We will then consider the maximum and minimum section diameters to be respectively 40mm and 7.35mm.

Ports configuration

A significant consideration following the layer superposition technique is that the waveguide path must have input and output ports sections perpendicular to the boring direction of the foils (that is parallel to foils' surfaces), and that the last foil have to host the two output ports.
Actually, this is not as much a direct requirement of the platelet technique, but rather of its extension from single OMTs to compact arrays, which is its most encouraging employment.
This results in the necessity to design bended arms to redirect the side ports of the OMT junctions: a single bend is sufficient if a simple ClassI OMT is chosen as in Figure 4.2, while a class III one would require at least one bend on each of the four arms.

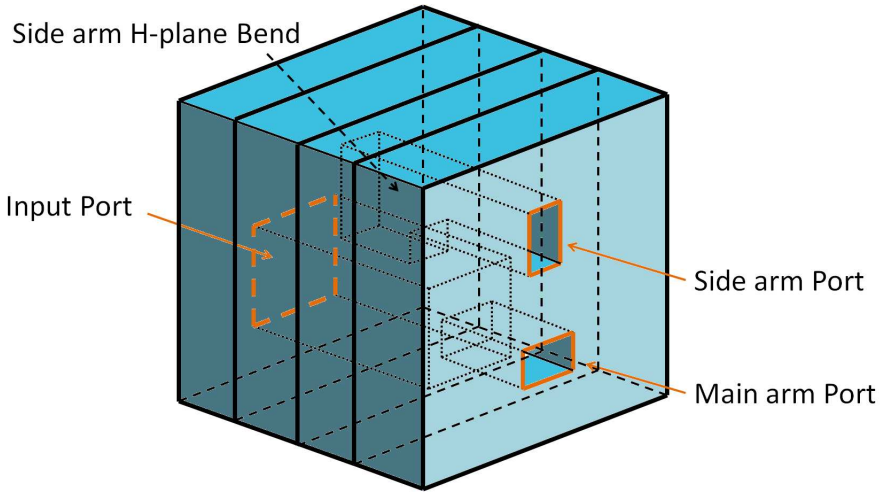

Figure 4.2: representation of the input and output ports positions in a platelet design concept.

Q-band flanges dimensions

: The link between the OMT and the subsequent items (either with guided or cabled input) is usually managed through flanges with standard dimension. Figure 4.3 shows some commercial waveguide to coaxial cable matching flanges, corresponding to rectangular single-mode ports.
Their dimensions must be taken into account in particular to design the test prototype, and infers a minimal distance between the two output

ports.
Since this project refers to Q-band, the standard flange dimensions are those indicated in Figure4.4, where WR22 is the standard rectangular waveguide on this band.
Instrumental spcifications could require non-standard flanges, but in this project we will consider the WR22 in order to preserve the general and low cost character of the design solution.

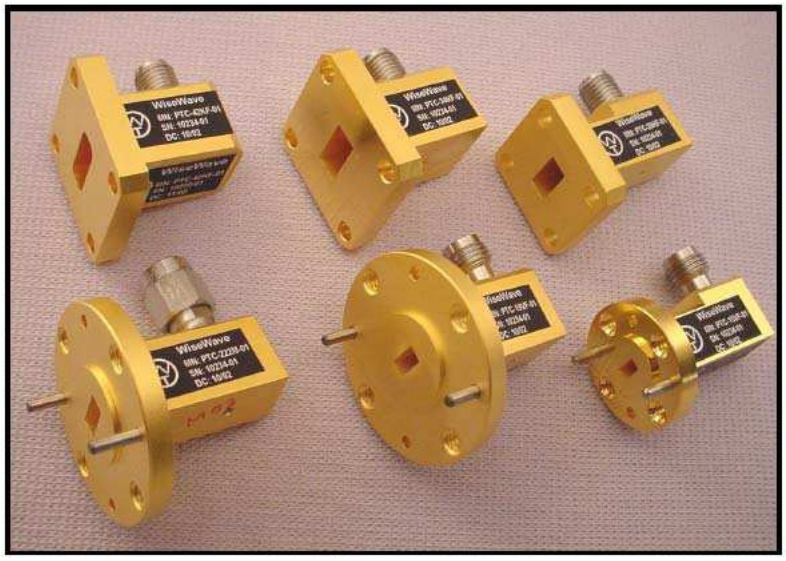

Figure 4.3: Commercial flanges with rectangular waveguide input and coaxial output. Figure provenance: wisewave technology inc. catalogue

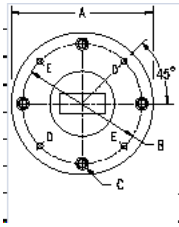

WR22	WG23	R400
UG383/U		
Dimension	mm	
A	28.850	
B	23.810	
C Holes	4 - 40 UNC-2B	
D Holes	1.613	
E Dowels	1.555	

Figure 4.4: Standard Flange for Q-band devices with rectangular ports. Figure provenance: Maury microwave corporation catalogue

Existing OMT designs and performances

: As already introduce in Chapter 3, an ideal OMT should have the Scattering matrix described in (3.1). These performance are not practica-

Figure 4.5: The three Class I OMTs on the LFI.

Table 4.1: Project requirements for the OMTs in Planck LFI.

	30GHz	44GHz	70GHz
$Bandwidth[GHz]$	$27-33$	$39.6-48.4$	$63-77$
$\mathbf{IL}_{dB}$ at 20K	<0.15	<0.15	<0.15
$\mathbf{IL}_{dB}$ at 300K	<0.3	<0.3	<0.3
$\mathbf{RL}_{dB}$	>20	>20	>20
$\mathbf{XP}_{dB}$	>25	>25	>25
$\mathbf{IS}_{dB}$	>40	>40	>40

ble, and is actually unnecessary to reach the same level of approximation of the ideal case.
Nonetheless, cosmological instruments for polarization measurements exhibit hard requirements in order to guarantee the operating performances.
Planck is the most recent and more accurate instrument to detect cosmic background radiation pattern, sensible to a wide range of frequencies through two instruments sharing the same focal plane: LFI (Low Frequency Instrument) and HFI (High Frequency Instrument), ; LFI is based on radiometric technology uses OMTs for the detection of the signal polarization; HFI, instead, mounts polarization sensible bolometers.
Three frequency bands are covered by LFI (30, 44, and 70 GHz), each using optimized classI OMTs, (see Figure4.5) whose performances are presented in Table 4.1 [13]. Some other studies and projects presents similar performance requirements.
In the Polatron experiment , the 96 GHz class I OMT were required $\sim$ 20dB or better **RL** over 20% bandwidth for both polarization channels, isolation better than 30 dB and low (not specified) **IL** for both polarizations.[23] Very high performances are given by NRAO for the

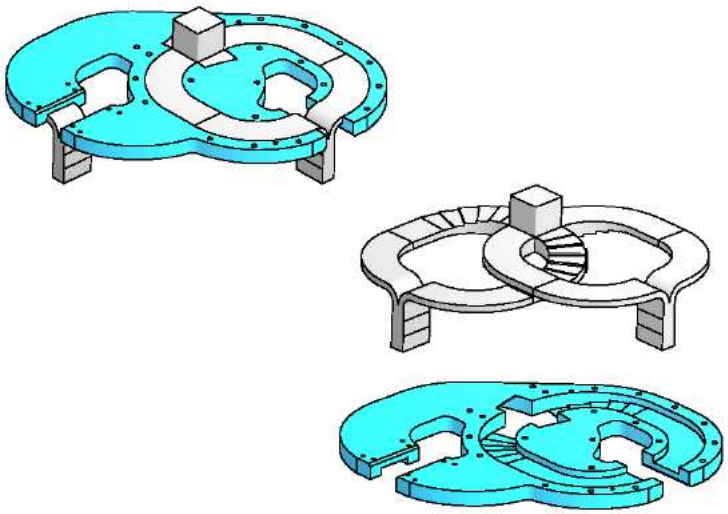

Figure 4.6: EVLA turnstile design solution.

EVLA X-band receiver, which required the design of a turnstile junction OMT, shown in Figure 4.6:

- Return Loss > 25dB;
- Insertion loss $= 0.2$dB;
- Crosspolarization $= 40$dB;
- Isolation $= 40$dB.

A last example is the Boifot type OMT in W-Band shown in Figure4.7, which exibits ~20dB of **RL** and an Insertion Loss of less than 0.2 dB in the 75-110 GHz band [19].

Commercial metal laminates

Prototypes of platelet feed-horn arrays, using anticorodal laminates with standard thickness, were realized at the Physics Department of the University of Milan. [25].

The choice of the laminates thickness represents a first guess in the design process: we found commercial sheets with thickness between 0,1 mm and 10 mm, as shown in Figure 4.8.

In this work, we tried to keep similar thickness for each foil, and not

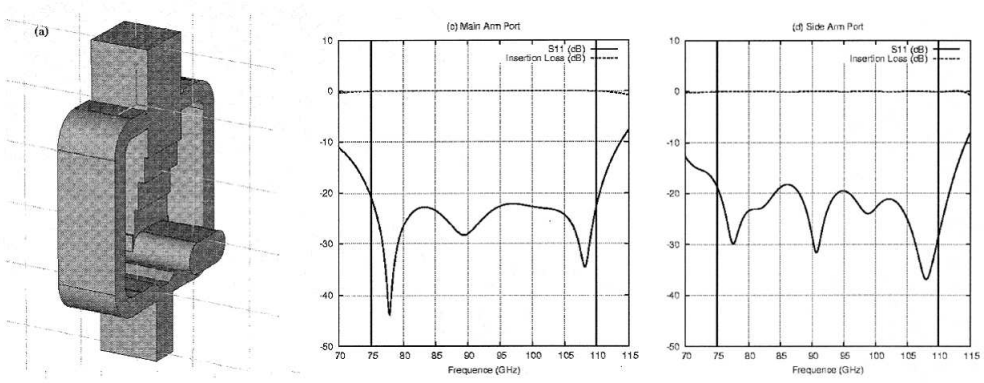

Figure 4.7: Boifot OMT in W-Band with the main scattering parameters on the two arms.

Table 4.2: Project requirements for the OMT object of this work.

Goal	Value	Notes
$\mathtt{Bandwidth}$[GHz]	36 - 44	20% around 40GHz
$\mathbf{IL}_{\mathrm{dB}}$	< 0.1	Efficient transmission
$\mathbf{RL}_{\mathrm{dB}}$	> 20	Low power reflection
$\mathbf{XP}_{\mathrm{dB}}$	> 30	Clean separation of modes
$\mathbf{IS}_{\mathrm{dB}}$	> 30	Clean separation of modes

to use submillimeter sheets, which require special tight and support during the machination.
Directly dependent on the workpiece thickness is the choice of the cutting tools (mills), which typically allow the realization of cavities not exceeding the double of their diameter in depth.

4.1.1 Definition of goal performances

Up to these preliminary considerations, goal performances of this work have been defined as follows in table 4.2.

Compactness requirement leads to a Class I OMT with a 90 degree bend on the side arm as first choice, though its intrinsic asymmetry affects bandwidth requirements, as explained in Chapter 3.

ALUMINIUM SHEETS AND PLATES (WEIGHT PER UNIT IN KG)							
mm.	1000X2000	1250X2500	1500X3000	1500X3500	1500X4000	2000X4000	2000X6000
0,1	0,54	0,85	1,22	------	------	------	-------
0,2	1,08	1,69	2,43	------	------	------	-------
0,3	1,62	2,54	3,65	------	------	------	-------
0,4	2,16	3,38	4,86	------	------	------	-------
0,5	2,7	4,23	6,08	------	------	------	-------
0,6	3,24	5,07	7,29	------	------	------	-------
0,8	4,32	6,76	9,72	11,34	12,96	------	-------
1	5,4	8,45	12,15	14,18	16,2	21,6	-------
1,2	6,48	10,14	14,58	17,01	19,44	25,92	-------
1,5	8,1	12,68	18,23	21,26	24,3	32,4	-------
2	10,8	16,9	24,3	28,35	32,4	43,2	-------
3	16,2	25,35	36,45	42,53	48,6	64,8	97,2
4	21,6	33,8	48,6	56,7	64,8	86,4	129,6
5	27	42,26	60,75	70,88	81	108	162
6	32,4	50,71	72,9	85,05	------	129,6	194,4
8	43,2	67,61	97,2	113,4	------	172,8	259,2
10	54	84,51	121,5	141,75	------	216	324

Figure 4.8: Commercial thicknesses of aluminium laminates. Figure provenance: Ambrogio Colombo S.R.L. online catalogue.

4.2 Preliminary software simulations

The design tool used in this work to get performance analysis is a multiphysic software simulator, COMSOL release 4.2, containing a RF simulation module.
Getting to know the software and its simulation philosophy and performances was the first step of the current work: starting with simple rectangular and circular waveguide transmissions, I took more confidence with it replying some simple and complex existing OMT designs obtained with other softwares (such as CST and HFSS).
COMSOL RF module showed good approximation of analytical solutions, as already mentioned in Chapter2.

We then tried to compare COMSOL with CST MW Studio, using known simulation results of other OMT designs found in literature [11].
Here I propose the already cited turnstile junction OMT of the EVLA research for the ALMA project.
The design parameters, dimensions and simulation results were attainable in the study report.
The input square waveguide section edges measure 22.86mm; a Turnstile junction (Figure4.10a) splits the signal into four orthogonal arms with a starting section of 22.86 x 10.16 mm (WR90 waveguide), which in couples carry the two polarisations through a stepped E-plane bend and Y-junctions (Figure4.10c) to the two output ports, matching again the WR90 waveguide dimensions.

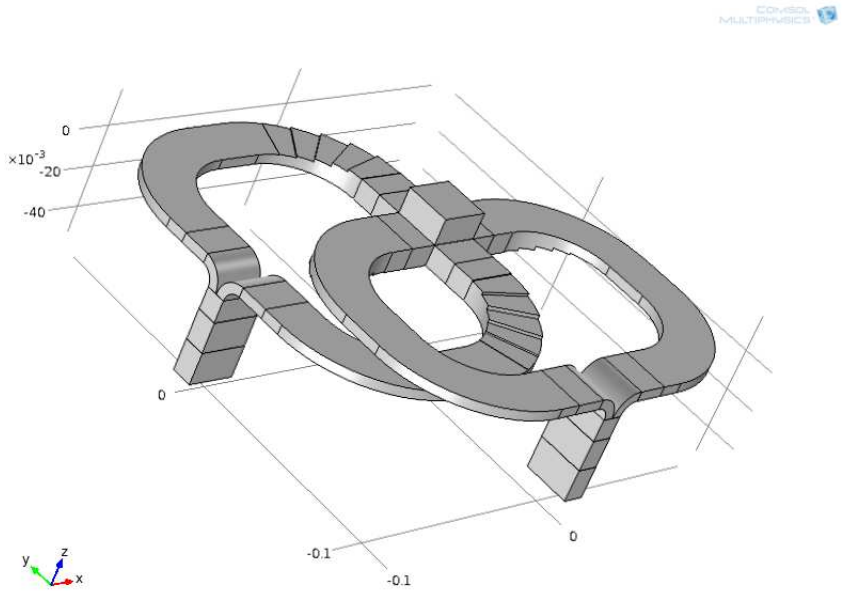

Figure 4.9: COMSOL snapshot of the complete turnstile OMT of the EVLA project.

The frequency range is a 20% band centred on 10GHz; the whole domain is considered empty space ($\epsilon = 1$ and $\mu = 1$), while boundary material is imposed to be perfect electric conductor (PEC), which is set by default. The boundary conditions are then automatically set to $E_t = 0$.
The last step before running the simulation is the choice of a good mesh: COMSOL has automatic meshing algorithms which can be directly se-

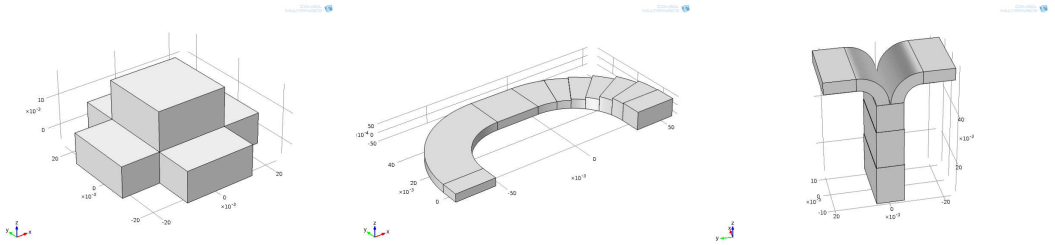

(a) EVLA Turnstile junction (b) E-plane 180° bend with Chebyshev stepped transition (c) Y Junction

lected by the user, as well as allowing a customization of the elements. Simulation of a single mode transmission solves the problem on an extra fine mesh (306513 elements) in about 10900 seconds on a dual core processor[1].
Figure4.10 presents the S-parameters obtained, compared with CST results.
Here we can see the similarity of the results, which are also comparable with the performances of the real OMT [11]. With this model the reliability of the software was proved,despite the high memory consumption due to the fine mesh and the consequently long simulation time.
This type of OMT is efficient but bulky in the focal plane, and rescaling it in Q-Band - as required in our project - may not be trivial, so that it was not chosen for our platelet OMT prototype. Its performances are nonetheless interesting and it can adapt well to the platelet design concept.

4.3 Design process

On the basis of the driving ideas explained in the previous sections, a ClassI OMT was designed to fit the defined requirements.
It was then chosen as reference design the OMTs mounted on the already cited Low Frequency Instrument on the Planck satellite, optimized to grant high performances over a bandwidth of about 20%, realized by electroforming. The first step was the initial design of an OMT at 40 GHz with a bandwidth of 20%, similar in structure to the reference ones; then, each part of the OMT was modified taking into account for the fabrication limits and the thickness of the aluminium plates.

[1]Intel I7-2600K with 16Gb RAM

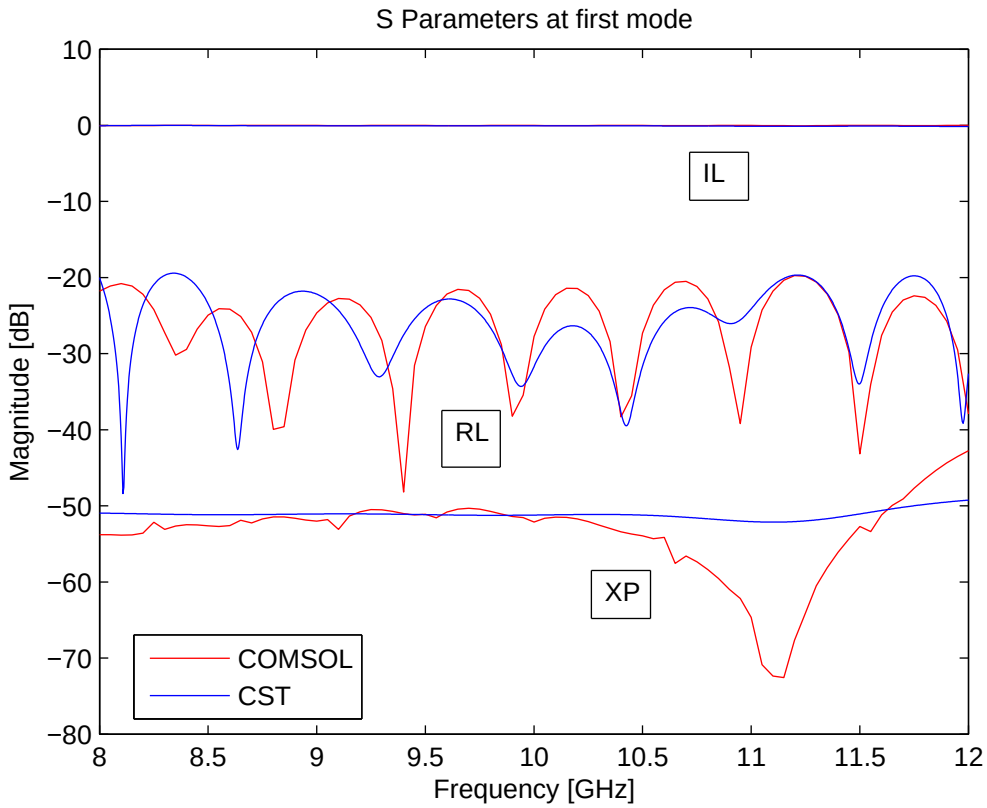

Figure 4.10: Software simulations results: return Loss (RL), Insertion Loss (IL) and Cross Polarization (XP) in the ClassIII OMT, generated by excitation of the first mode at the common port (Port 1). The figure compares our results using COMSOL with known results of CST Microwave Studio.

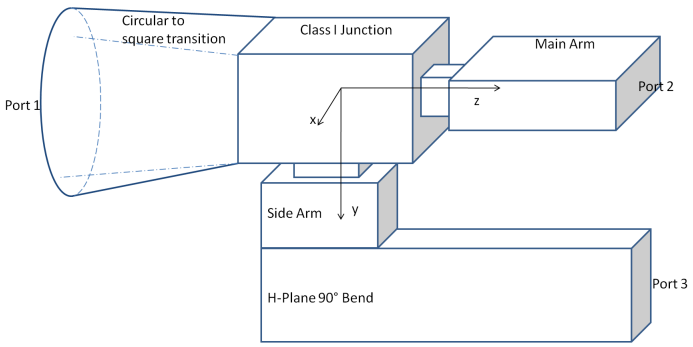

Figure 4.11: Schematic of the geometry and critical part of the proposed OMT.

4.3.1 Preliminary design

The first step was the design of an OMT at 40 GHz with a bandwidth of 20%, similar in structure to that mounted on Planck, without considering technological limits.
When handling with simple waveguide transmission, dimensions are directly dependent on the cutoff frequency of the first mode (see Chapter2), so a change in the desired central frequency can be obtained by scaling the waveguide dimensions.
In the design of more complex devices, direct scaling of the whole object is not always possible, because the irregularities and discontinuities have non linear effects on the electric impedance seen by the travelling waves.
The chosen geometry concept is outlined in Figure4.11: here the most critical parts are the ClassI junction and the section stepped transformers on the Side and Main arms. The bend and the circular to square transition are easier to scale and less problematic in this initial phase.
The coordinate system is also outlined in the figure. It is useful to remark that throughout this work the z-axis will be always taken in the longitudinal direction, laying on the geometric centres of the main arm, while the y-axis is directed as the side arm main direction; the x-axis completes the right tern.

ClassI junction

It is a three port device, usually consisting of a square or circular waveguide - the former in this work - hosting two identical orthogonal modes, and two rectangular isolated ports; location and dimensions of these two ports are the design parameters of such a device. A typical configuration is that presented in the assonometric view in Figure4.12, with one port (Main port) sharing the propagation direction with the common guide, to select the first mode, and the other (Side port)opening orthogonally on one of the lateral surface, where the second mode can be isolated.
It is common to design them in succession: starting with the side port, the waveguide is considered closed on a short circuit in the through direction, thus obtaining a phase difference on the short circuit of $= 180degree = \pi/2$; the center of the port is then located at $dz = (\lambda\pi/2)/(2\pi) = \lambda/4$, where λ is the center wavelength in the band. Its dimensions are then defined to get low **RL** on the corresponding mode.

Next, the through port is considered, closing up the side: its center

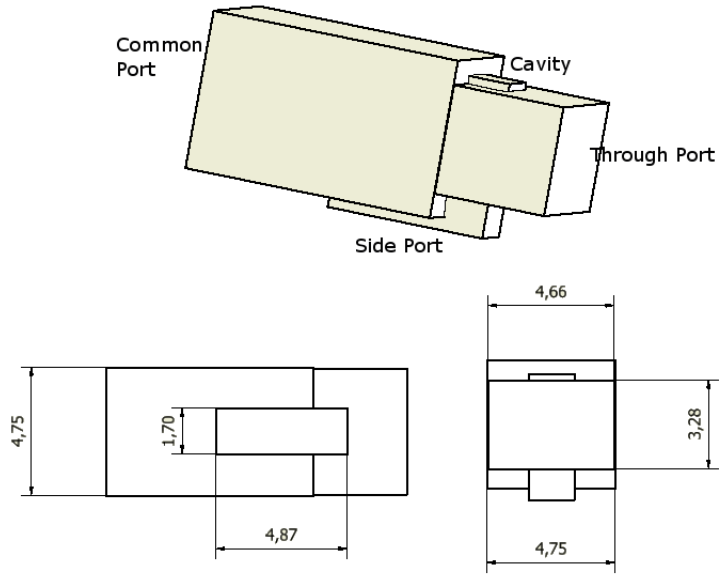

Figure 4.12: Class I Junction: assonometric view and preliminary dimensions. Note the position of the side port and the small cavity over the through port. Recall that these figures refer to waveguides and therefore represent empty domains.

is imposed on the symmetry axis of the guide, and dimensions should

return low reflection of the main port mode and a short circuit for the second port mode (**RL** = 1).
The presence of the longitudinal port acts as a phase shift of the side port mode, so the position of the side port has to be consequently varied by $\lambda\phi/(2\pi)$.
The side port partially overlaps with the main arm first step. An useful expedient to broaden the bandwidth on the side arm is a cavity on the surface of the through port opposite to the side arm (Figure4.12), employed in Planck's OMTs too.

Side arm matched section adapter

A section transformer is necessary to match with standard waveguides in the desired band. This can be made through a stepped transition. On the side arm, the port is sufficiently small to manage the matching objective with 2 simple steps of growing dimensions.
The length (read on the y-coordinate) of the side arm before the 90° bend is imposed by two considerations: it has to be long enough to let high order modes vanish in favour of a single mode transmission, and should be at least as long as the minimum span required to mount the two circular flanges without mechanical interference. As previously indicated (Figure4.4), the diameter of the standard flange for Q-Band is 28.85 mm: this is the minimum distance allowable between the centres of the two output ports, which defines the length of the side arm consequently.

Main arm matched section adapter

The same stepped approach can be used to match the through port with the same standard output (WR22), but here the port is too wide and a first section reduction is necessary. This introduces an initial mismatch, which will be then recovered by the subsequent two steps.
This procedure is not unusual in microwave design, though requiring some experience.
With the definition of these three critical parts and the up-scaling of the circular-to-square transition and the H-plan 90° bend on the side arm, the initial design of the OMT was completed.
It is a prototype of a Class I OMT with a central frequency of 40GHz, and can be seen as the single block mandrel of an electroformed OMT with high precision.
The main dimensions and performances obtained are shown in Figure4.13

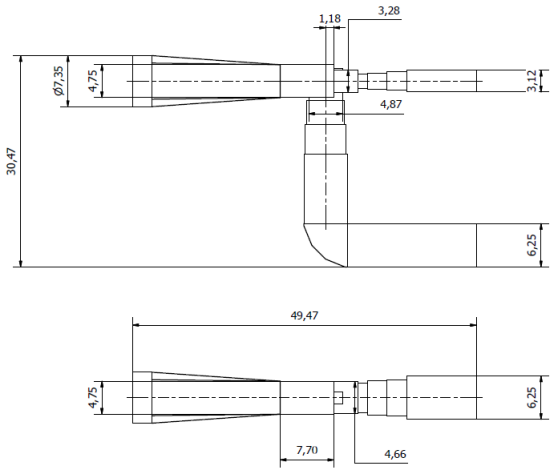

(a)

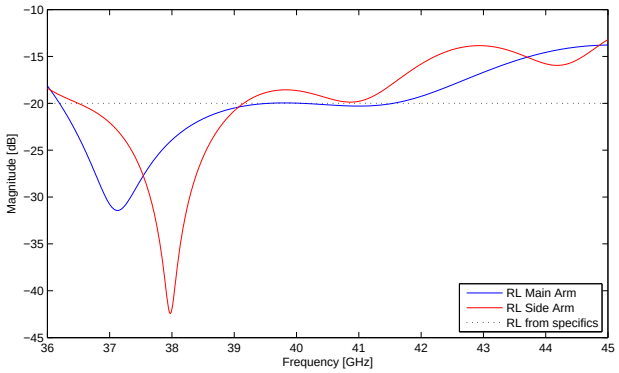

(b)

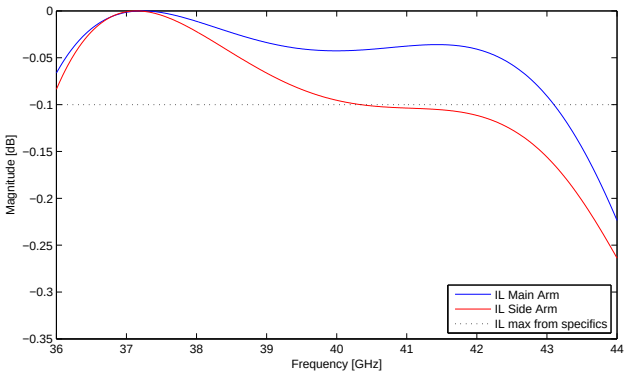

(c)

Figure 4.13: Initial design: (a) Return Loss and Insertion Loss; (b) main dimensions.

This geometry has to be modified in order to fit the machining limits and choices.
From the initial to the final design, a loop process has been followed, operating on the definition of the thickness of the laminas, the precision of the cutting tools (depending on their radius) and other geometrical parameters.

4.3.2 Cutting tools and edge radiuses

Adapting this design to the fabrication limits and to the thickness of the plates was next aspect to deal with.
Since milling was considered the first choice to machine the laminate, limits come mainly from the cutting tools dimensions: milling subtracts material from the workpiece through axial rotation of cutting teeth; the thinner the mill, the smaller the attainable edge radius, the better it is possible to approximate convex angles and polygonal hollow shapes.
The influence of a non zero fillet is critical especially on the main arm, where the directions of wave propagation and the machining axis coincide: it was therefore necessary to redesign the whole arm.
This was made with a parametric simulation, evaluating different fillet radiuses on each step of the guide; the other geometrical properties, i.e. length, width and height are instead fixed in simulation.
Figure4.14 shows how fillet radius changes the cut-off frequency and consequently the transmission properties of a simple rectangular section, through a parametric simulation.
Therefore, the whole main arm had to be redesigned to grant good

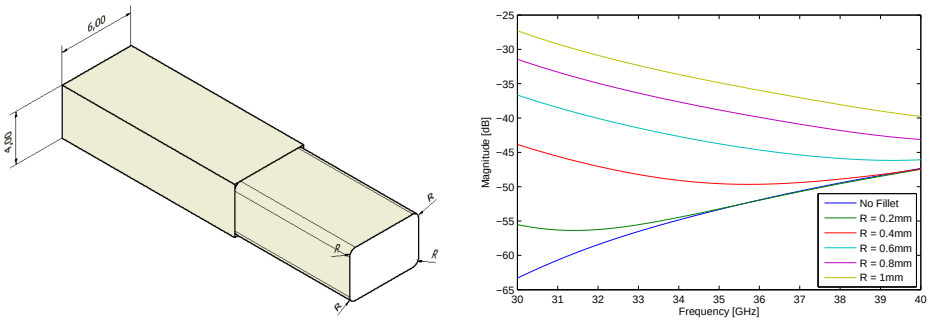

(a) (b)

Figure 4.14: Influence of fillet radius on transmission.

matching taking into account a minimal fillet radius of 0.5mm, corresponding to a diameter of 1mm and an allowable depth of machining of 2mm. As Figure4.15a shows, this operation was carried out considering the isolated arm: the number of possible combinations of different fillets is visibly high; some considerations were useful to get some constraints and reduce it:

- asymmetric solutions were neglected, because they would provide asymmetric effects on the propagating fields;
- only radiuses between 0.5 and 1.25 were considered, at intermediate values defined by the diameters of the commercial mills in that range (1mm, 1.5mm, 2mm, 2.5 mm).

At first, uniform fillet solutions were investigated, for convenience of realization; then, variations was driven avoiding large differences in the fillet between adjacent sections.
The design criteria was the minimization of the reflection coefficient (S_{11}) over the widest possible frequency band.
Results are outlined in Figure4.15, where the eventual choice is marked red. The sequence in the legend box refers to the different combinations of fillet radius.

4.3.3 Process of lamination

To divide the whole OMT in superposed sheets, the principal design parameters are their thickness and position along the longitudinal axis (z). This paragraph will introduce the driving ideas which lead to the final lamination.

Reference plane

The reference plane for the definition of the layers was not taken at the external ports positions, but on the bisection plane of the side arm, as shown in Figure 4.16. This choice has some advantages: with four 2mm layers, we cover the width of the side arm and get a simple machining on the central ones; moreover, the production of the stepped contours, which are symmetric, will be almost symmetric, granting the same order of accuracy (at least theoretically) on both sides. On the contrary, asymmetric machining might add asymmetric imperfections

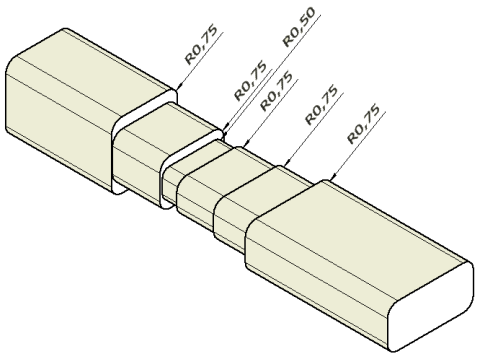

(a)

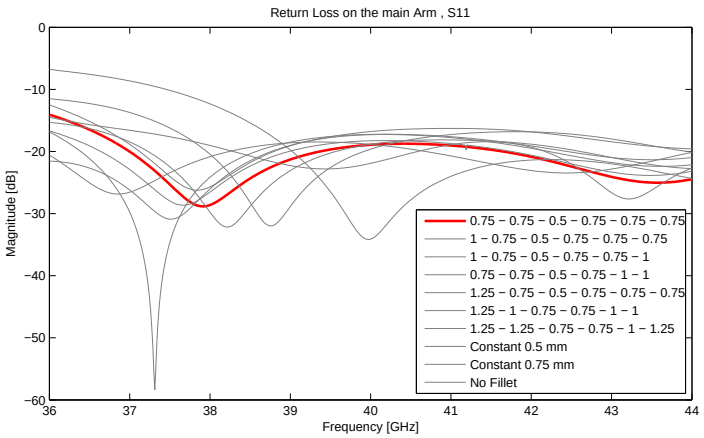

(b)

Figure 4.15: Resume of the parametric study on the main arm at different fillet conditions. The plotted parameter is Return Loss.

and have negative influences on the propagation of the modes. Nonetheless, Figure4.16 shows that a complete symmetry is not achievable within these four laminas. In particular, the bend in the starting model would require an asymmetric diagonal profile, which is possible with CNC machines, but would be very sensitive to misalignments at the interfaces between two laminas. The design of the bend introduces a further problem: referring again to Figure 4.16, it can be seen that the last plate on the right hosts the stepped profile of the side arm and an oblique profile of the bend, which can't be realized with a single process, but would require the plate to be milled from two opposite directions. This is not possible without overturn the plate on the working machine, by almost doubling the time of production, introducing misalignment

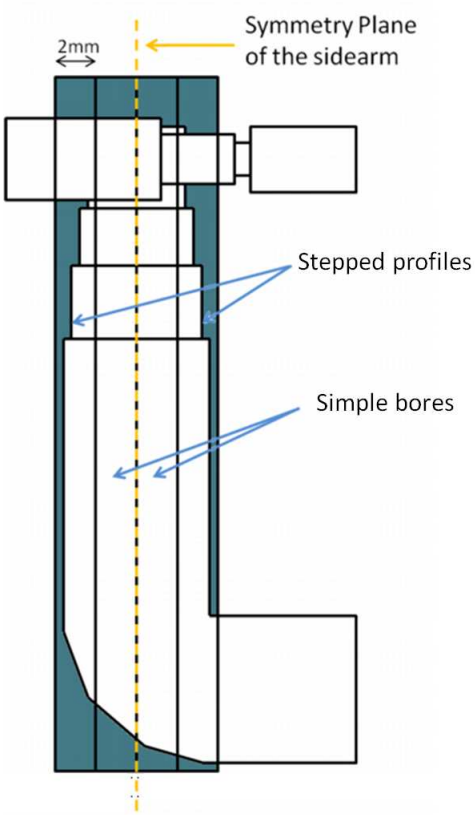

Figure 4.16: Sidearm laminate division. Four 2mm thick plates centred on the symmetry plane of the arm; only the external plates require partial machination to obtain the steps of the transition, while the two interior can be easily bored through thier whole depth.

errors.
A redesign of the bend was necessary to prevent this problem.

H-Plane Bend design

The best solution was to define a stepped H-plane bend; number, position and dimensions of the steps were the design unknowns.
The only constraint came from the will of avoiding multiple working

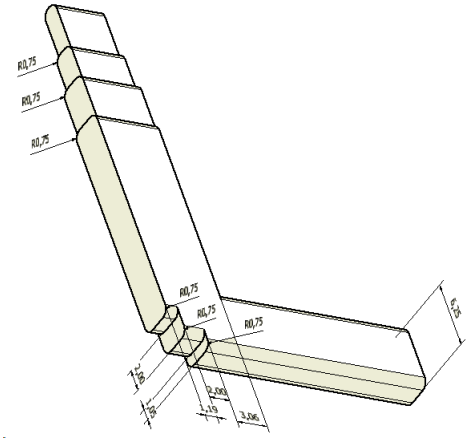

(a)

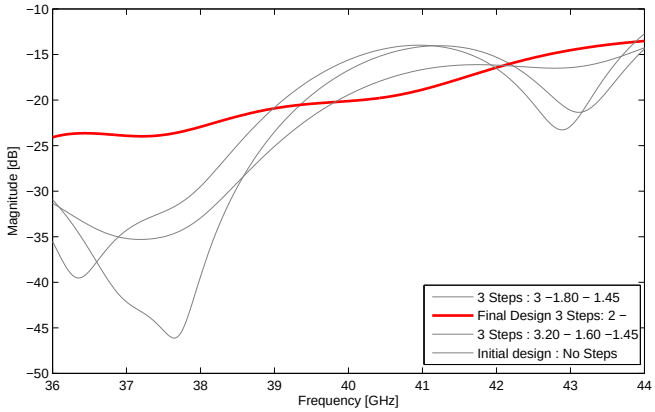

(b)

Figure 4.17: Comparison of results given by different choices for the geometry of the stepped Bend: the different values in legend refer to the height of the steps, in sequence from the lowest. In Figure (a) is shown the definitive geometry

directions, and led to impose that the last step must not be set on the last lamina.
A number of steps annealing the original bend geometry should provide good results but requires more complex and long machining.
It was then decided to search for designs with few steps, varying their dimensions to obtain satisfying performances.
A comparison of results given by different configurations is given with Figure4.17a, while the geometry of chosen bend is presented in Figure4.17b.

Effects of lamination on the complete OMT

The proposed position of the reference plane had consequences on the whole OMT design: using 2mm laminas on the whole OMT seemed advantageous, but it would require some extremely fine machination on some steps on the main arm, avoidable with a further refinement of geometry.
At first, a parametric change of the step lengths on the main arm was simulated, but it appeared clear that even small variations in this sense influenced performances negatively.
The alternative was to move the whole longitudinal arm with respect to the reference plane, kept solidal with the center of the side arm, searching for a placement granting both satisfactory performances and reasonable machining measures.
The sensibility of S-parameters to small displacements of the side port on the common guide was found to be less critical, and this second solution was investigated, obtaining good results with the configuration shown in Figure4.18

4.3.4 Circular to square transition

A last part to adapt with the platelet technique is the transition guiding the incoming signals from the circular feed horn to the square port.

A typical solution in electroformed OMTs is the one proposed with the preliminar design, with a continuous section variation from circular to square: this is expected to be exhibit the best performances, too.
Although CNC working machines can theoretically interpolate and realize lofted section variation, it was preferred to search for alternative

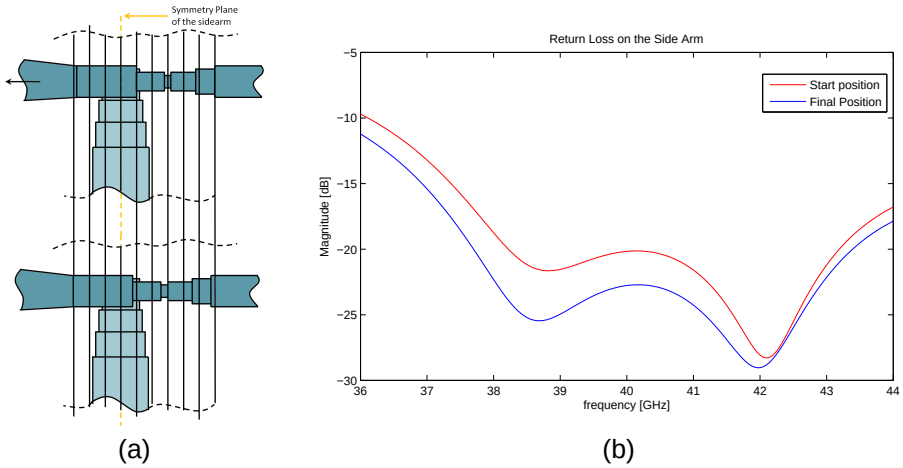

(a) (b)

Figure 4.18: initial and final insertion position of the side arm and relative Return Loss.

and more simple designs.
Two possibilities were investigated:

- A conical trunk with its final radius satisfying impedence matching with the square waveguide, and an abrupt section variation, after Figure4.19b;

- A stepped transition approximating the continuous variation, as shown in Figure4.19c to 4.19f.

Driving criteria to define the best transition were the global length of transition, which is desired to be minimal for weight reasons, good transmission and low reflection ($\mathbf{RL} < -30\text{dB}$).
Figure4.19 shows the different geometries investigated and Figure4.20 simulation results of different transitions: the chosen one is a stepped solution consisting in six 2 mm thick plates, suitably worked to obtain the intermediate sections.

4.3.5 Final design

In conclusion of this section, let us present a resume of the final design and global performances of the OMT.
The complete OMT will be composed of 19 plates of different thickness, as follows:

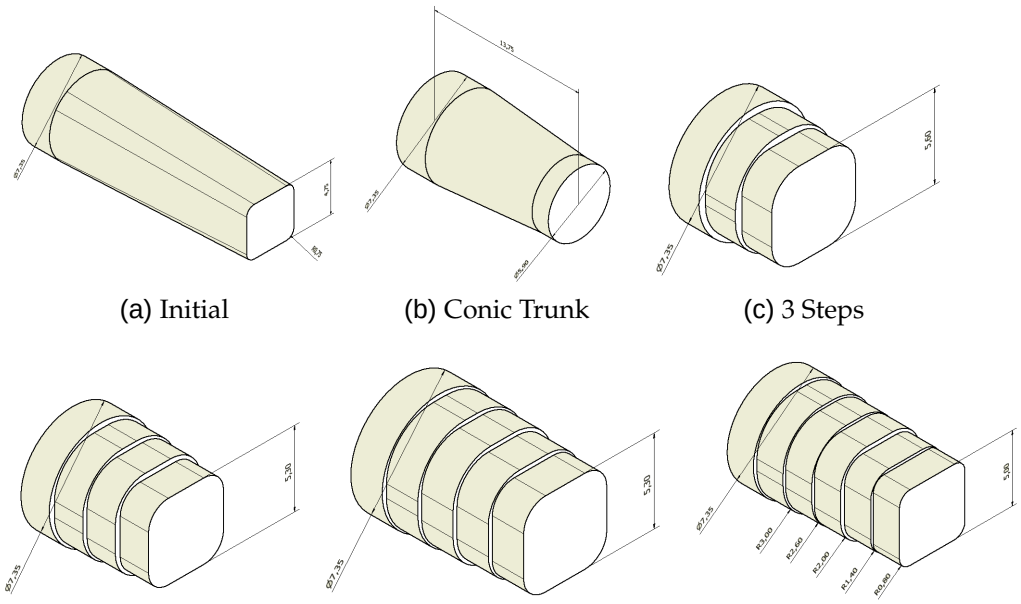

(a) Initial (b) Conic Trunk (c) 3 Steps

(d) 4 Steps (e) 5 Steps (f) 6 Steps

Figure 4.19: Different investigated geometries for the transition

- one 4 mm thick lamina, where the two output ports must be connected with the standard flanges; the ports will be machined with a 2.5 mm wide mill, flange holes will be drilled.

- Eleven 2 mm thick plates, hosting the two arms, the bend, the Class I junction, and a part of the common guide before the split. The most critical laminas to machine are those including the junction and the first steps of the main arm, since they include smaller details and more complex shapes.

- One 2.5 mm plate, interfacing the common port end and the sqaure-to-circular transition. This thickness was the best solution commercially availabel and fitting with the electromagnetic design.

- Six 2 mm thick laminas of the transition.

The main dimensions of the complete object are summarized in Figure4.21. Complete drafts are attainable in the appendices.
Simulations with COMSOL using a custom mesh and exciting the main two modes on the circular port, returned the global performances in

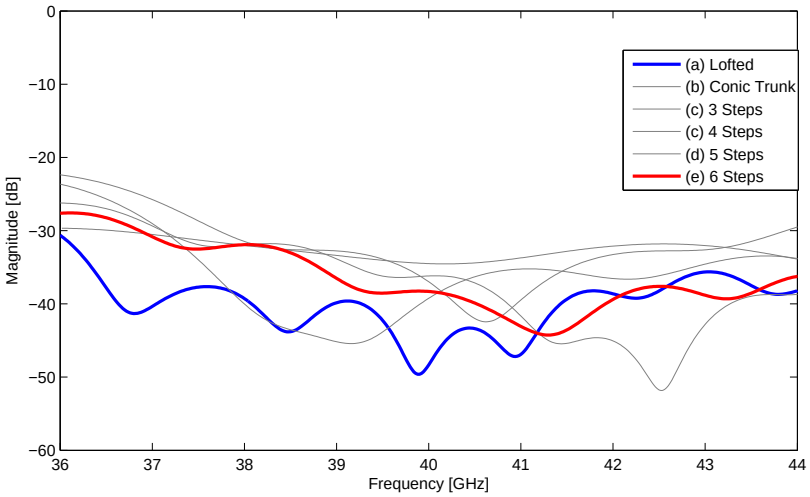

Figure 4.20: Simulation results of the transition. The labels refer to figure4.19

terms of Scattering parameters next explained.

4.3.6 Results

Performances are compared with requirements in the frequency band between 36 and 44 GHz: the main parameters analysed are return loss, insertion loss, cross polarization and isolation.
The final design was tested using the model configurations presented at the beginning of this chapter combined with an custom mesh. The domain of the simulation is the empty waveguide, while the conductive material of the laminas is introduced only through the effects at the boundaries. A resume of the model and simulation parameters is listed in Table4.3 and Figure4.22.

Return Loss

Figure4.23 shows the return loss performance of the OMT, exciting at the common port (Port 1) with both the dominant modes of the circular waveguide.
These correspond to the first two diagonal terms of matrix **S** and represent the amount of power associated respectively to these two propagation modes which, after reflections, returns at the input port.
The required performances of about -20dB are approached over the full band, though with differences between the two modes: RL on the main arm exhibits more than 25dB attenuation in the central range, but is less

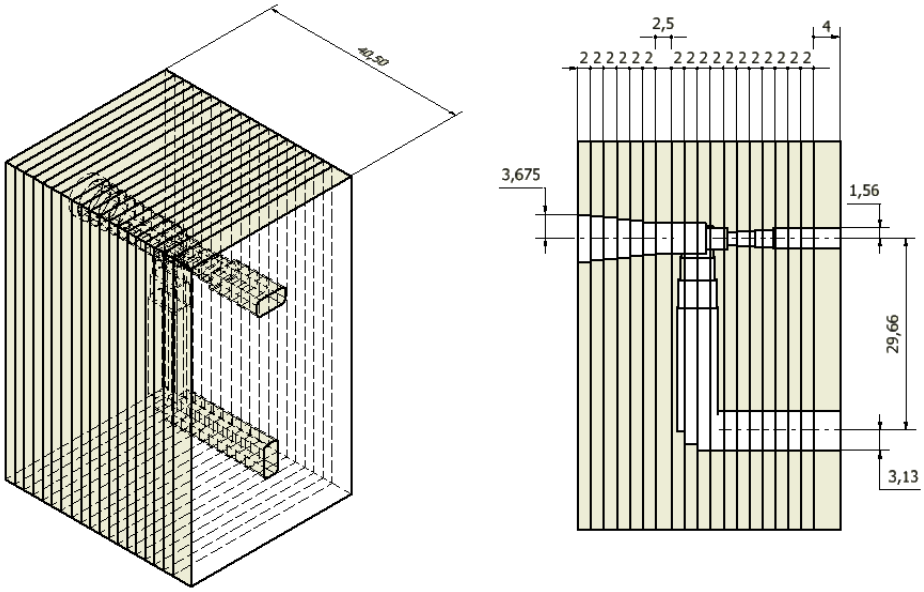

Figure 4.21: Quoted representation of the final lamination sequence and main dimensions of the OMT. Measures in mm.

Table 4.3: Summary of the final simulation settings

Object	**Setting**	**Notes**
Frequency [GHz]	36 - 44 (each 0.1 GHz)	desired bandwidth
Domain Material	Vacuum	empty waveguide
Boundary Conditions	$\vec{E}_t = 0$	Electric Wall Boundary
Boundary Material	PEC	Perfect Electric Conductor
Excitation	Port 1 - 2 - 3	One port at time
Mesh	custom	138840 elements
Processor	Intel I7-2600K	Dual Core
RA Memory	16Gb DDR3	
Simulation time	$\sim$ 11000 s	

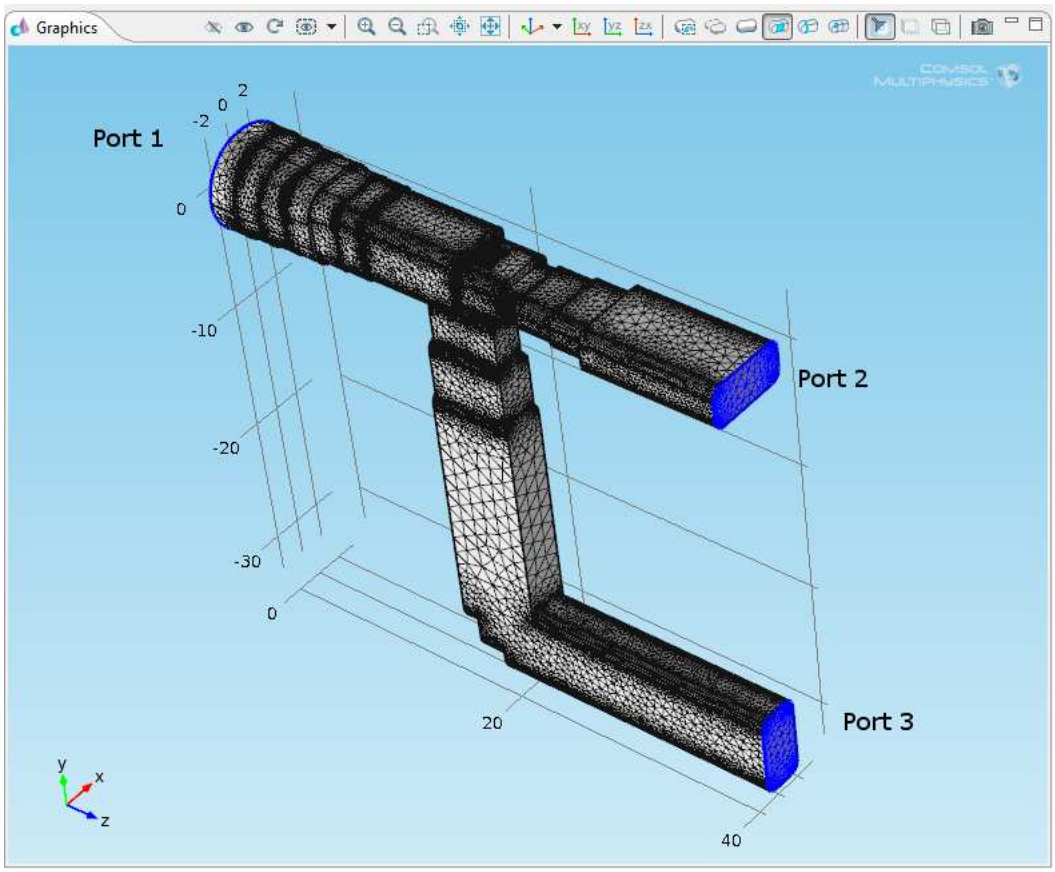

Figure 4.22: Snapshot of the final OMT mesh

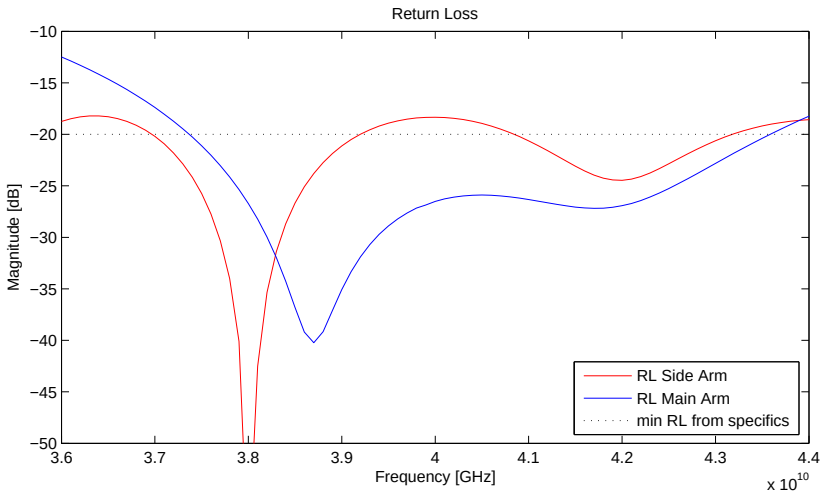

Figure 4.23: Return Loss on the main and side arm

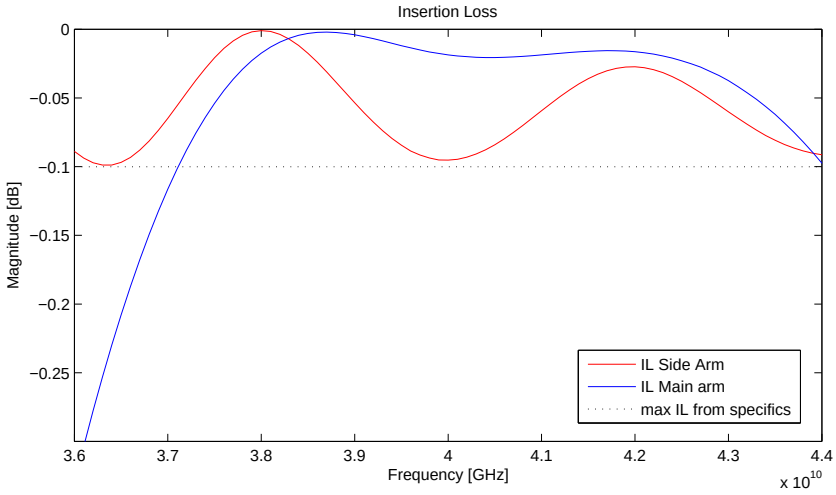

Figure 4.24: Insertion Loss on the main and side arm

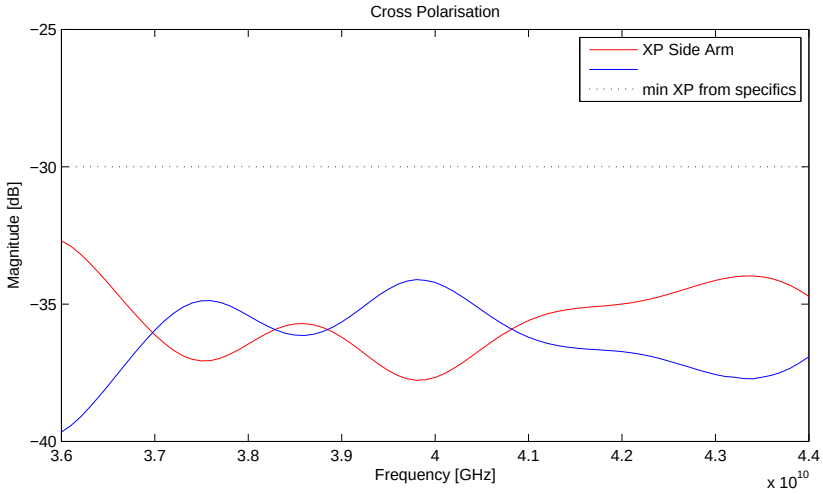

Figure 4.25: Cross Polarization on the main and side arm.

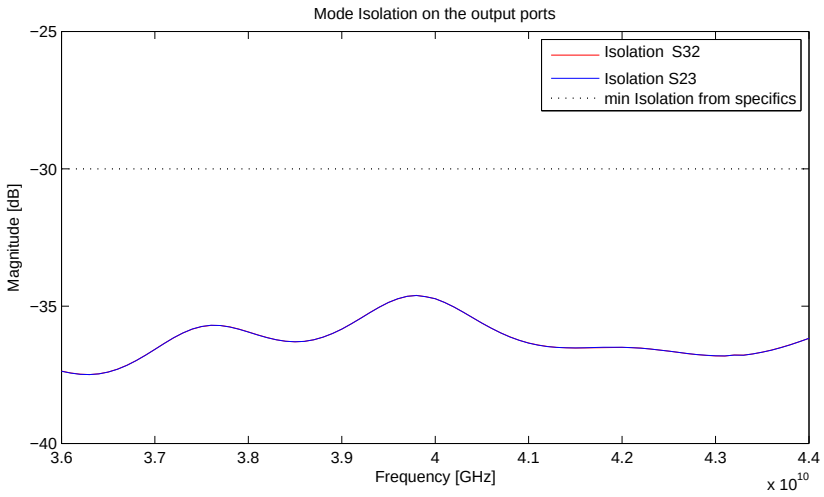

Figure 4.26: Mode Isolation of port 2 and 3.

performing in the low part of the desired Band, exceeding the specifications below 37GHz; the Side Arm is on the contrary less performing around the central frequency, but shows RL values not below 17dB on the full Band.

Insertion Loss

Insertion Loss from port 1 is calculated for mode 1 on the main arm output port, while for mode 2 on the side arm.
Prescribed performance on **IL** corresponds to a transmission parameter of about -0.1 dB.
As for RL, the Side arm shows good Insertion Loss on the full band, while the main arm exhibits the best performance at the centre of the band, but doesn't match the requirements below 37GHz.

Cross-polarization

XP for mode1 is measured on the side arm port, and viceversa for mode2 we get **XP** on the main arm port.
Figure4.25 shows that the desired values over the band are satisfied on both the arms.

Isolation

Isolation measure how much power transmitted from port2 to port3 and viceversa.
The proposed OMT fits the isolation goals, prescribed to be less than -30dB, as shown in Figure4.26.

Chapter 5

Conclusions and further steps

5.1 Critical results analysis and final considerations

In this work a new OMT for CMB polarization detection in Q-Band has been designed, taking into account the technological limits imposed by the milled platelet fabrication method.
The procedure and simulation software tools leading to the final design have been explained and justified. Results are satisfactory in terms of performances, though with enhancement margins in the low part of the band. The main goal has therefore been achieved, showing that it is possible to design platelet OMTs with good performances, to be coupled with platelet feedhorns.
Some critical considerations are all the same necessary.
This work proposes a prototype of an OMT working in Q-Band, that is a relatively low frequency band as regards CMB measures. As explained in Chapter 1 and 3, modern scientific satellites cover a wide frequency range from few tens to several hundreds GHz.
At higher frequencies characteristic dimensions decrease, and micromachining or other more precise techniques could become necessary on very small laminas. Costs rise consequently.
On scientific instruments, a wide range of frequencies is usually covered, with different OMT dimensions. The idea of fabricating an array with many different OMT using the same lamination can become very difficult or even impracticable. For this reason modularity seem to be a reasonable design way, where different modules could be realized with different lamination to fit the dimensions of devices working at different

frequencies.
Platelet is a relatively mature technology to realize feedhorn arrays, rated at a TRL (Technological Readiness Level) of 5 or higher [26], but has not been much employed to fabricate OMTs. The main reason for that is to be found in the critical performances required to OMTs in CMB mesuring instruments, to reach whom electroforming is the most reliable solution up to now.
Although the progresses in this technology are encouraging, in existing platelet feedhorn arrays can be observed some noticeable deviations between the measured platelet response and the theoretical prediction or the electroformed equivalent; the pathologies associated with the platelet arrays that would give rise to these deviations have not been fully investigated the most important effects depend on plate misalignments and bad clamping [26].

5.2 Further work

To complete the study of platelet OMTs, some further work is necessary, which is next briefly related.

Fabrication The natural consequence of this work is the realization of the OMT with CNC milling machines. To this aim, fixtures and clamping for each lamina have to be designed and made ad hoc, to prevent misalignments or deformations during the machining.

Electromagnetic analysis with VNA Then, tests are necessary to verify performances: EM measures in microwave bands are made with devices called Network Analysers, of whom two types exist: scalar and vectorial.
Scalar Network Analysers are only sensible to the magnitude of EM fields, while vectorial ones (VNA) allow to measure phase shifts.
An example of a test system to measure S-Parameters of an OMT is illustrated in Figure5.1.[27]

textbfStress and thermal analysis One of the advantages brought on by the use of COMSOL as simulating software is its possibility of get multiphysic simulations: stress and thermal analysis could be introduced to get a more compete knowledge of the behaviour of the OMT, both at ambient and cryogenic temperatures, where it is supposed to operate.

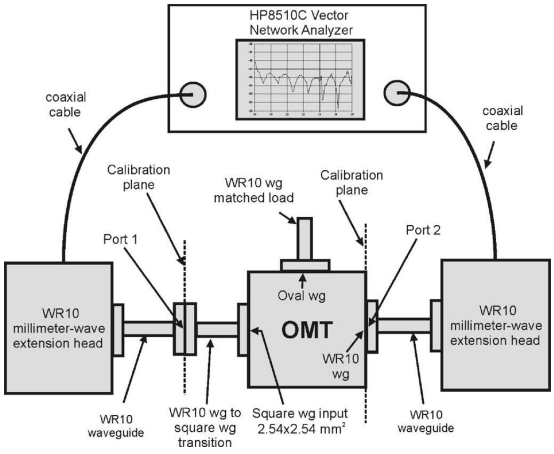

Figure 5.1: S-parameter measurement of the OMT with a vector network analyser

Platelet arrays Platelet is an interesting technique in that it fits with the concept of disposing several receivers in the same focal plane, organized in planar arrays. As previously observed, these can be made up of small modules (hexagonal or different) in which lay a limited number of receivers. Up to now, platelet has not been used to produce a complete waveguide path including feedhorn and OMT, but this possibility seems very advantageous in the economy of the a radiometeric chain. A potential disadvantage of the platelet is the presence of much non necessary material between the pixels which may excessively increase the global weight. Realization of optimal arrays for satellites should be lightweight: boring the laminas with additional holes may be a useful expedient to lower masses, if it is structurally critical.

Appendix A

Mechanical drafts

In this appendix I propose the final mechanical drafts of each lamina introduced in Chapter 4, with a first hypothesis of the holes for screws and, in the external 4 mm thick plate, the ones to correctly attach the flanges.
These might be used to fabricate a prototype of the proposed OMT.

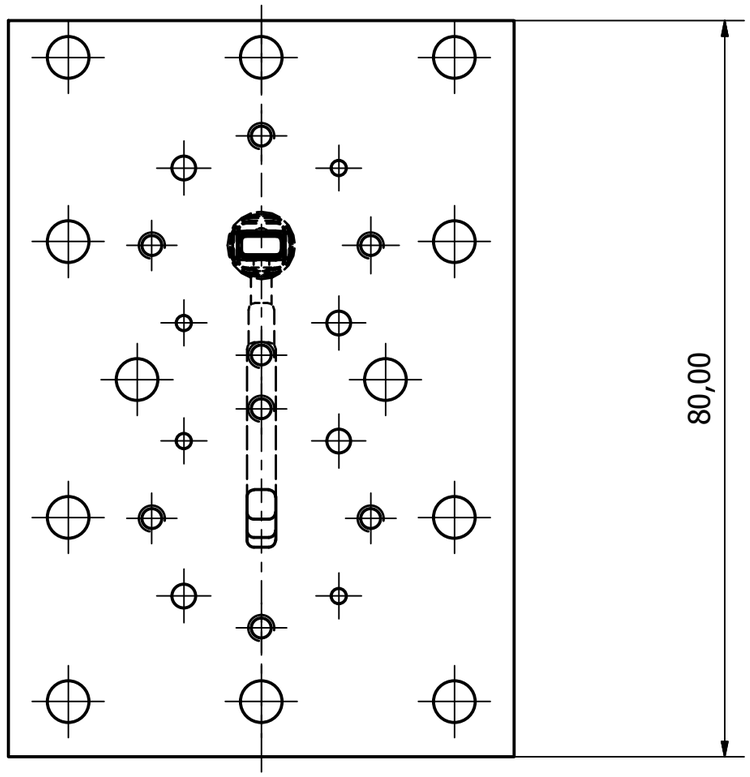

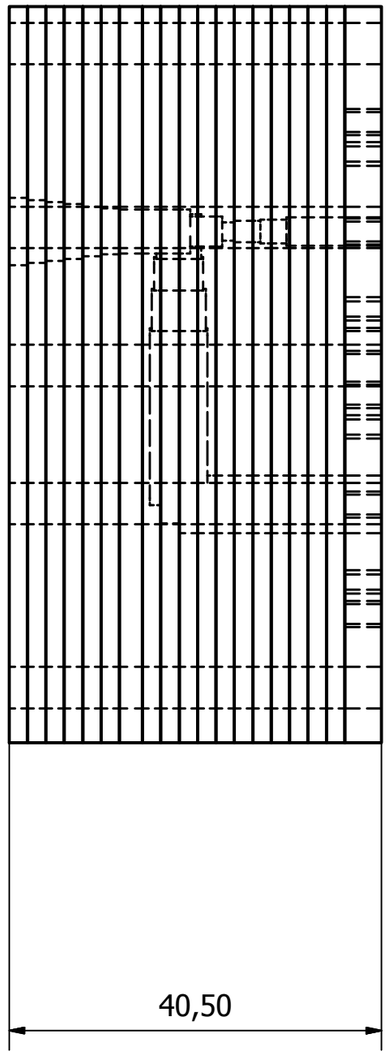

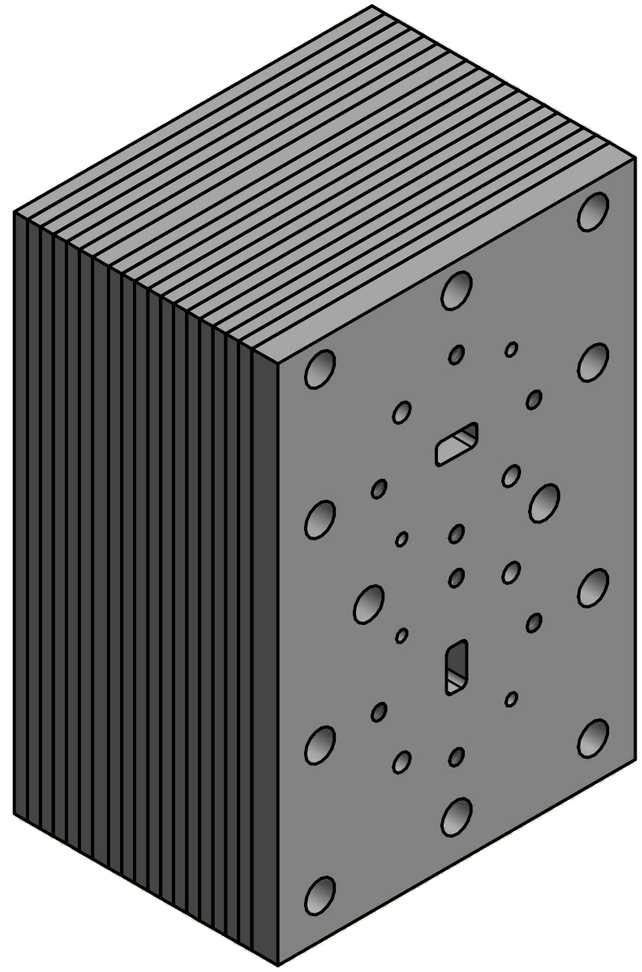

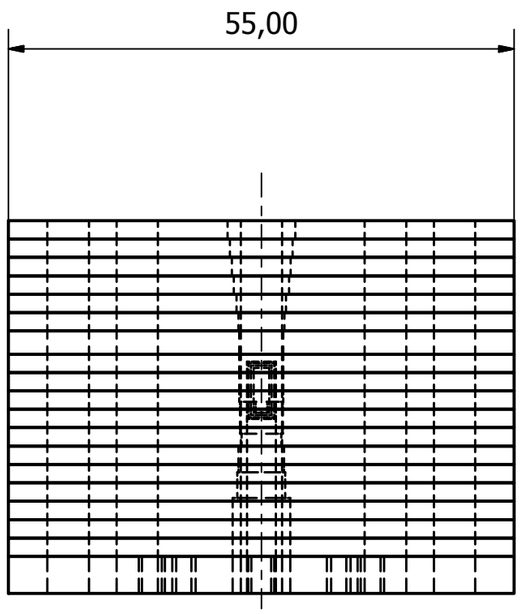

Progettato da	Controllato da	Approvato da	Data		Data	
Giacomo Trevisan					23/02/2012	

Finale - Laminato		Edizione	Foglio 1 / 1

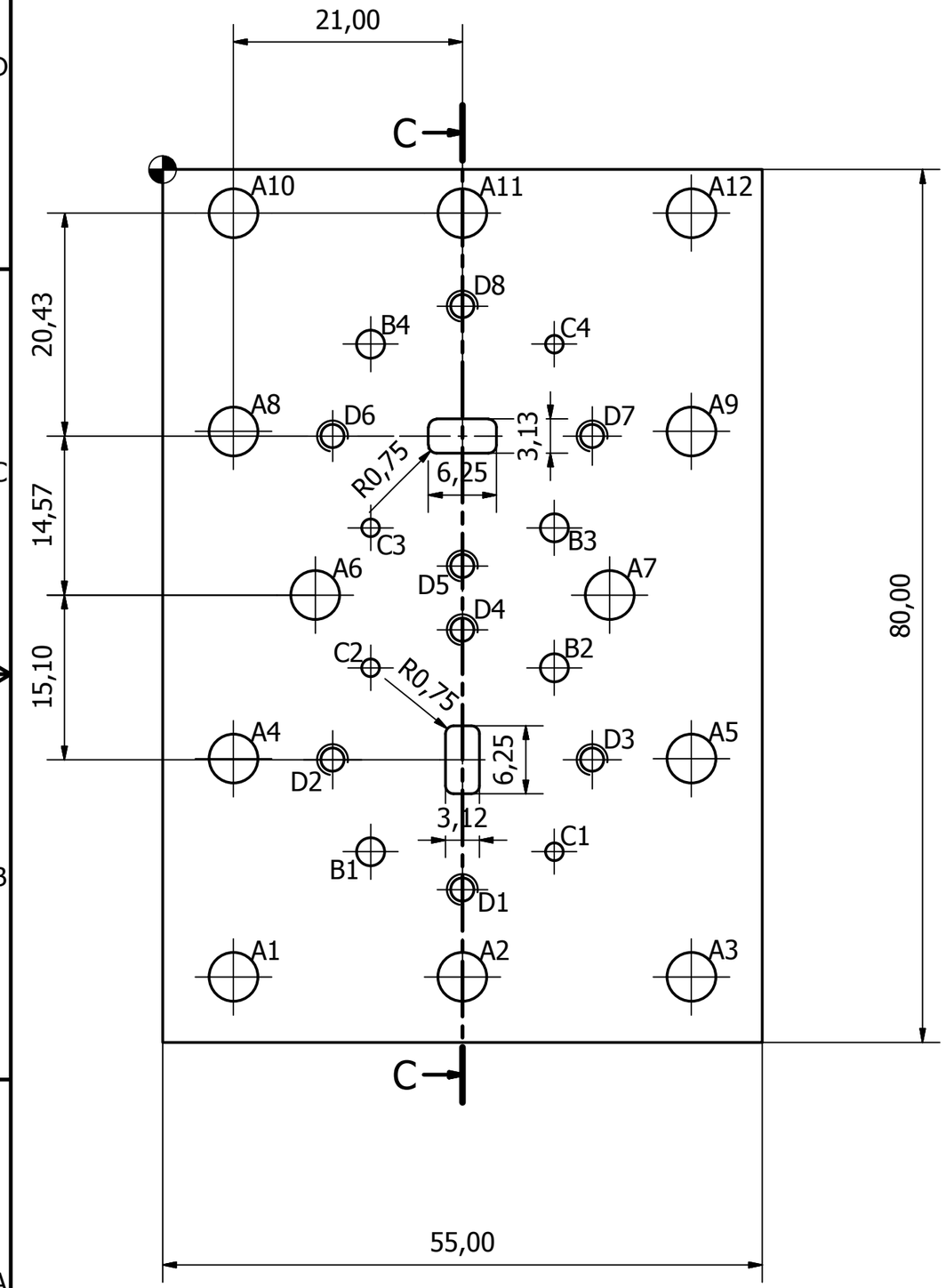

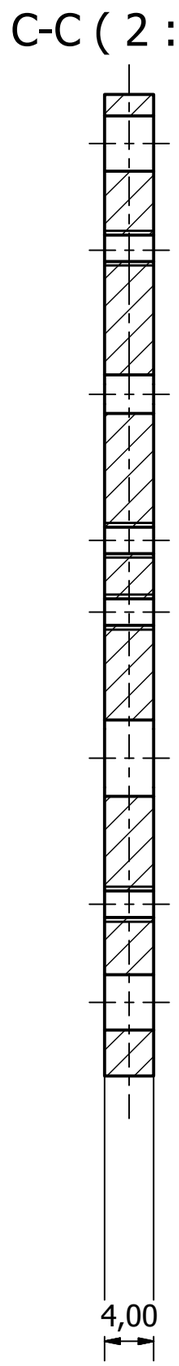

TABELLA FORO			
FORO	Quota X	Quota Y	DESCRIZIONE
A1	6,50	-74,00	Ø4,50 PASS.
A2	27,50	-74,00	
A3	48,50	-74,00	
A4	6,50	-54,00	
A5	48,50	-54,00	
A6	14,00	-39,00	
A7	41,00	-39,00	
A8	6,50	-24,00	
A9	48,50	-24,00	
A10	6,50	-4,00	
A11	27,50	-4,00	
A12	48,50	-4,00	
B1	19,08	-62,51	Ø2,55 PASS.
B2	35,92	-45,68	
B3	35,92	-32,85	
B4	19,08	-16,01	
C1	35,92	-62,51	Ø1,65 PASS.
C2	19,08	-45,68	
C3	19,08	-32,85	
C4	35,92	-16,01	
D1	27,50	-66,00	4-40 UNC - 2B
D2	15,60	-54,10	
D3	39,41	-54,10	
D4	27,50	-42,19	
D5	27,50	-36,34	
D6	15,60	-24,43	
D7	39,41	-24,43	
D8	27,50	-12,53	

Progettato da	Controllato da	Approvato da	Data		Data	
Giacomo Trevisan					23/02/2012	

Lamina1 flange	Edizione	Foglio 1 / 1

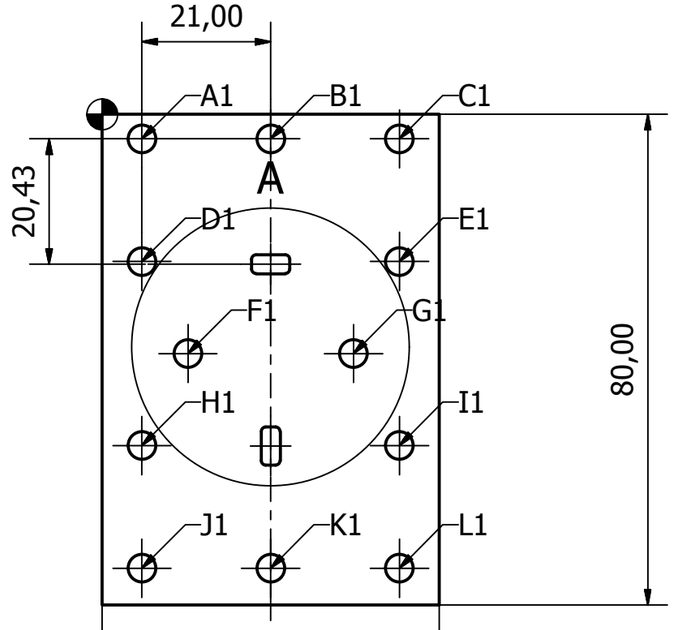

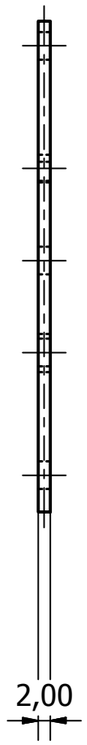

TABELLA FORO			
FORO	Quota X	Quota Y	DESCRIZIONE
A1	6,50	-4,00	-
B1	27,50	-4,00	-
C1	48,50	-4,00	-
D1	6,50	-24,00	-
E1	48,50	-24,00	-
F1	14,00	-39,00	-
G1	41,00	-39,00	-
H1	6,50	-54,00	-
I1	48,50	-54,00	-
J1	6,50	-74,00	-
K1	27,50	-74,00	-
L1	48,50	-74,00	-

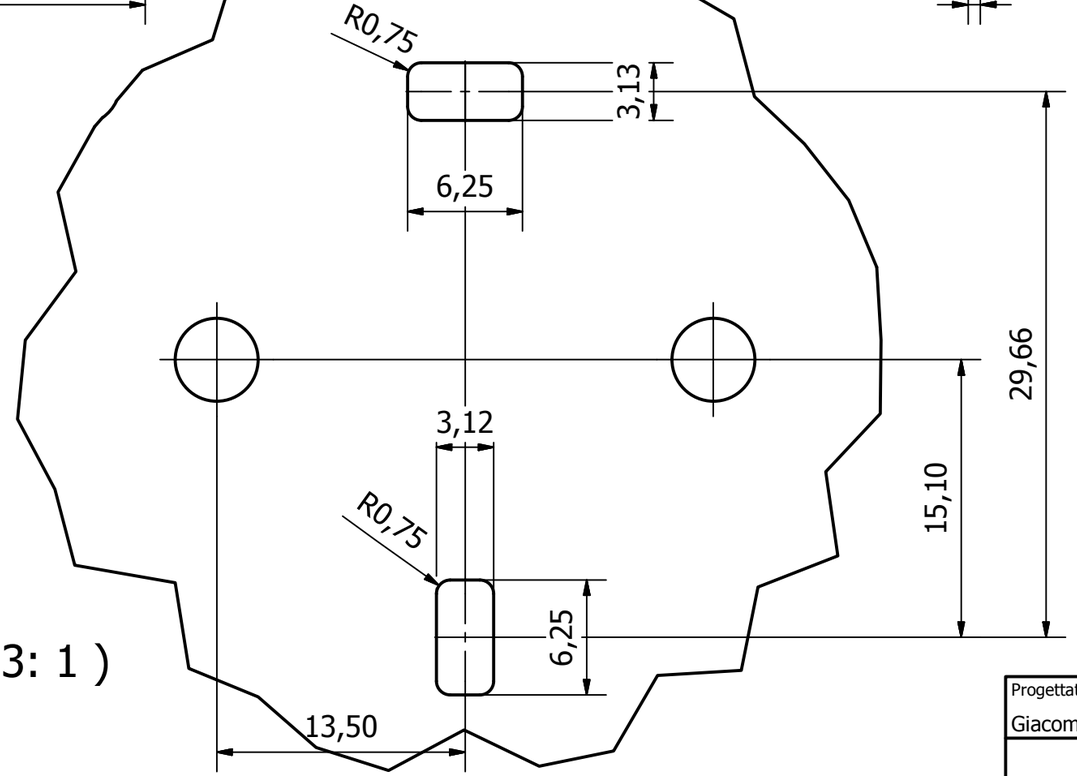

A (3: 1)

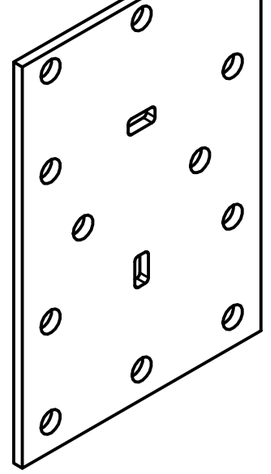

Progettato da	Controllato da	Approvato da	Data		Data	
Giacomo Trevisan					23/02/2012	

Lamina2		Edizione	Foglio 1 / 1

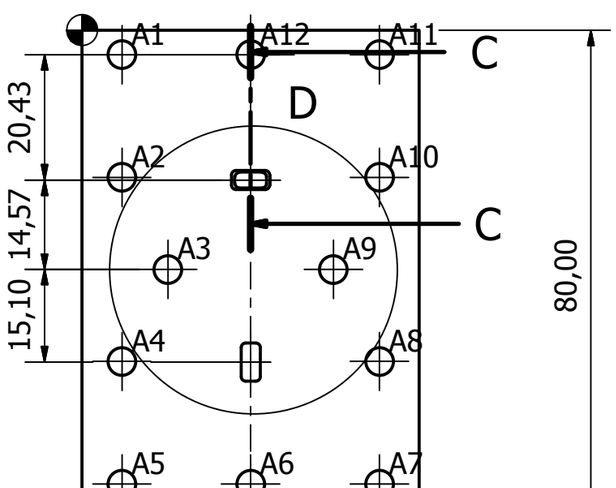

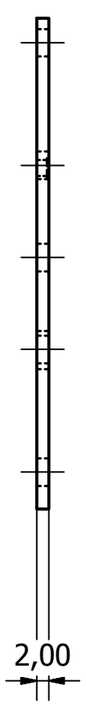

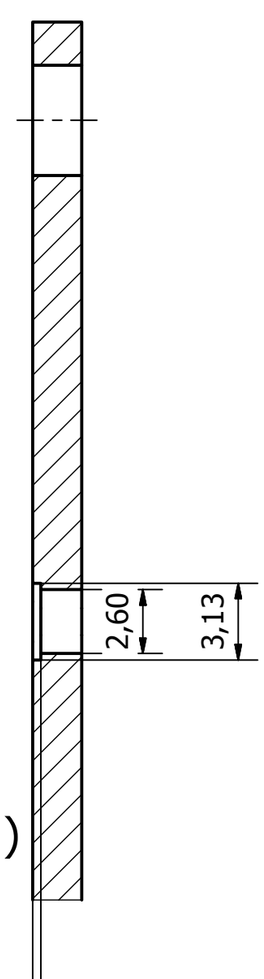

TABELLA FORO			
FORO	Quota X	Quota Y	DESCRIZIONE
A1	6,50	-4,00	Ø4,50 PASS.
A2	6,50	-24,00	
A3	14,00	-39,00	
A4	6,50	-54,00	
A5	6,50	-74,00	
A6	27,50	-74,00	
A7	48,50	-74,00	
A8	48,50	-54,00	
A9	41,00	-39,00	
A10	48,50	-24,00	
A11	48,50	-4,00	
A12	27,50	-4,00	

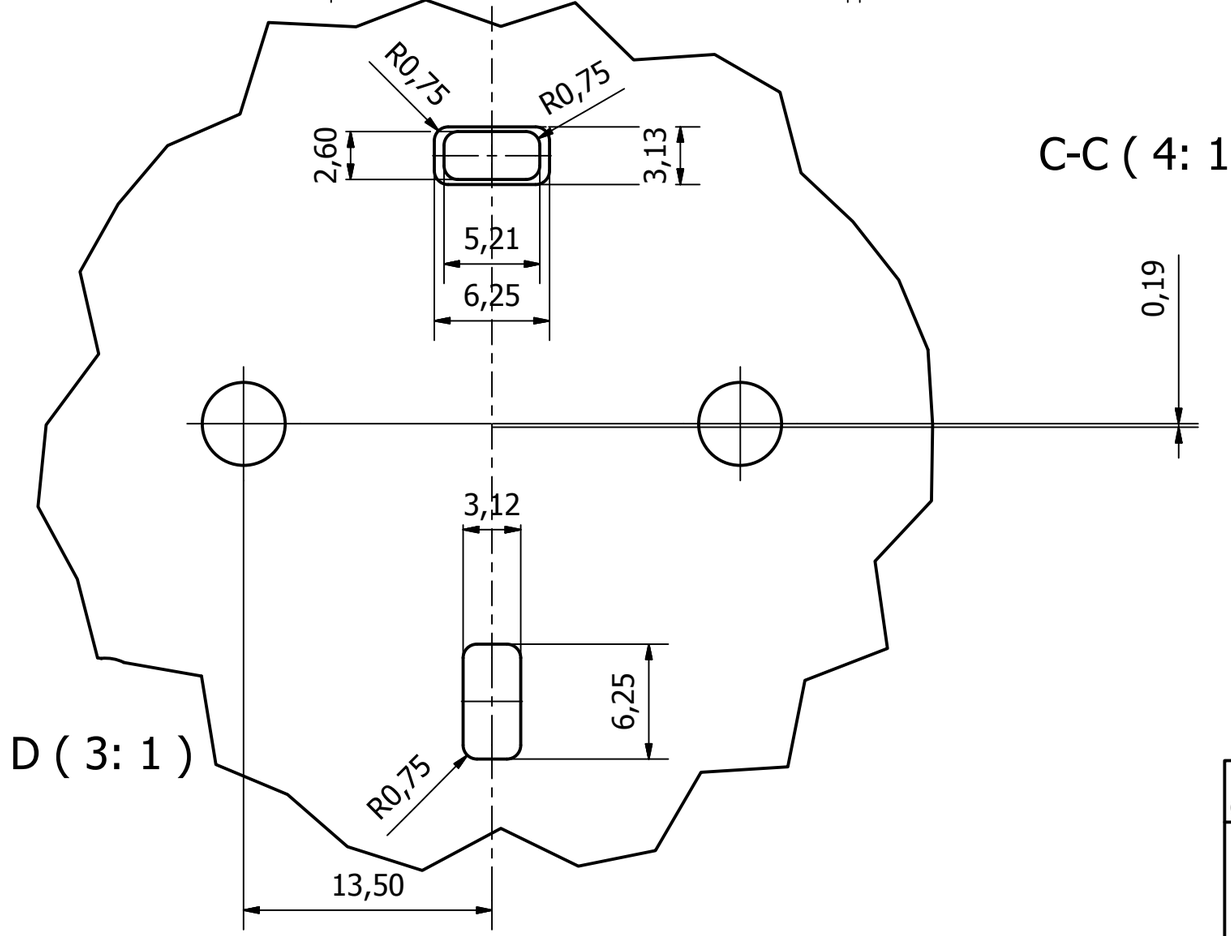

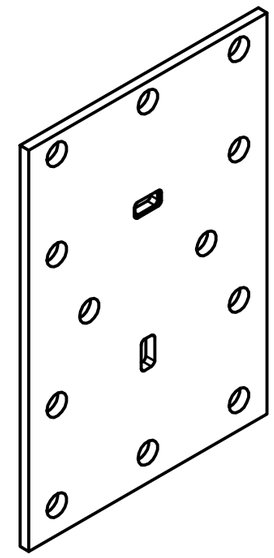

Progettato da	Controllato da	Approvato da	Data		Data	
Giacomo Trevisan					23/02/2012	

Lmina5	Edizione	Foglio 1 / 1

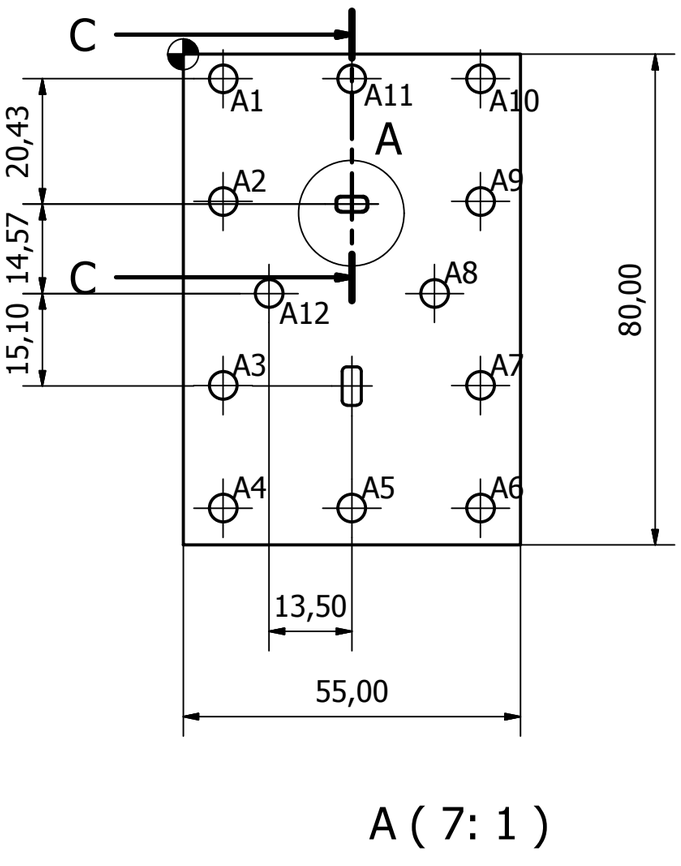

A (7: 1)

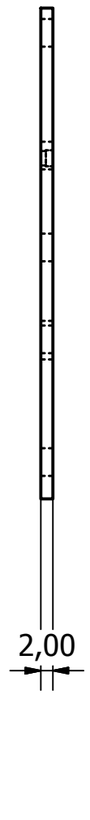

C-C (3: 1)

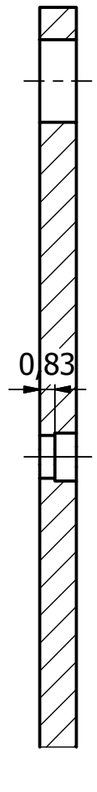

TABELLA FORO			
FORO	Quota X	Quota Y	DESCRIZIONE
A1	6,50	-4,00	Ø4,50 PASS.
A2	6,50	-24,00	
A3	6,50	-54,00	
A4	6,50	-74,00	
A5	27,50	-74,00	
A6	48,50	-74,00	
A7	48,50	-54,00	
A8	41,00	-39,00	
A9	48,50	-24,00	
A10	48,50	-4,00	
A11	27,50	-4,00	
A12	14,00	-39,00	

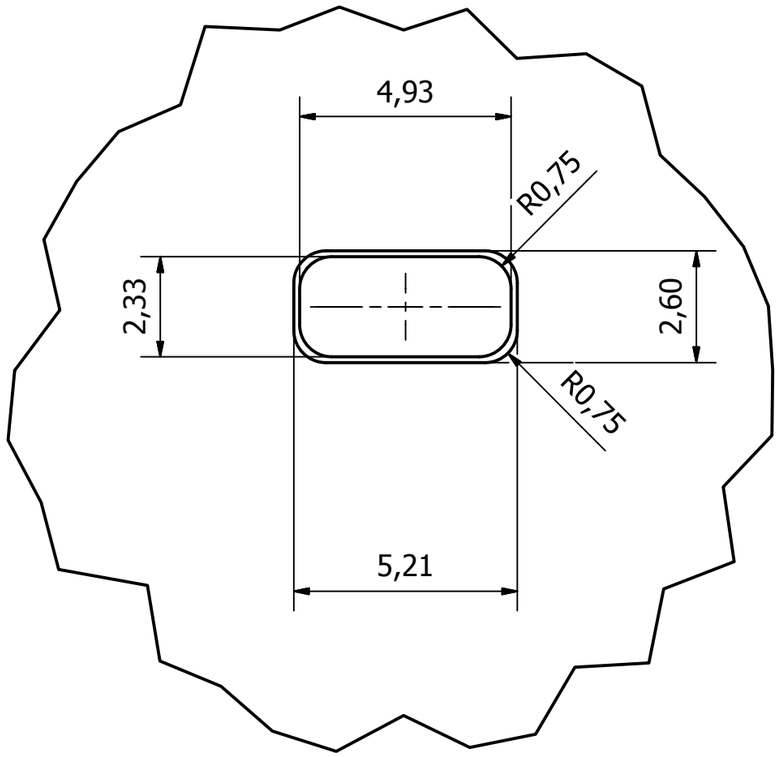

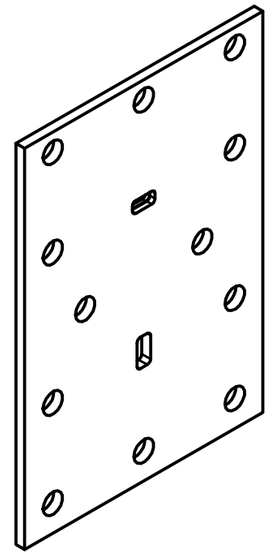

Progettato da	Controllato da	Approvato da	Data		Data	
Giacomo Trevisan					23/02/2012	

Lamina6	Edizione	Foglio 1 / 1

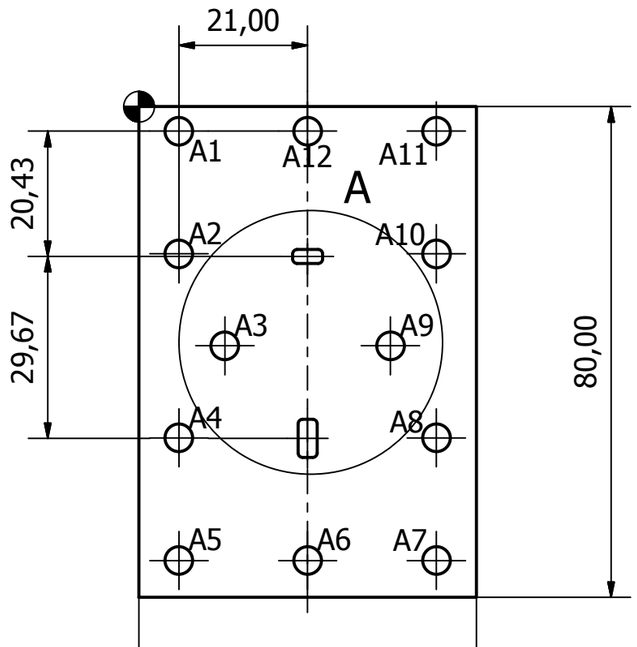

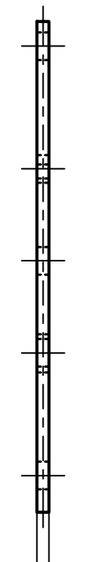

TABELLA FORO			
FORO	Quota X	Quota Y	DESCRIZIONE
A1	6,50	-4,00	Ø4,50 PASS.
A2	6,50	-24,00	
A3	14,00	-39,00	
A4	6,50	-54,00	
A5	6,50	-74,00	
A6	27,50	-74,00	
A7	48,50	-74,00	
A8	48,50	-54,00	
A9	41,00	-39,00	
A10	48,50	-24,00	
A11	48,50	-4,00	
A12	27,50	-4,00	

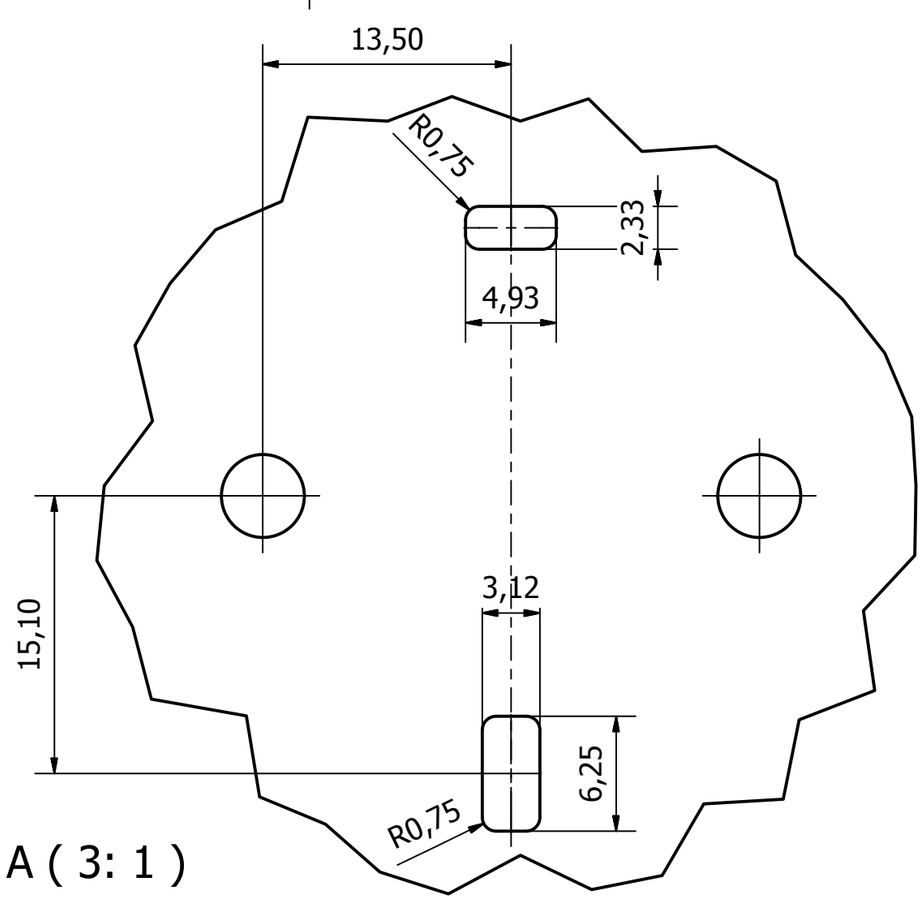

A (3: 1)

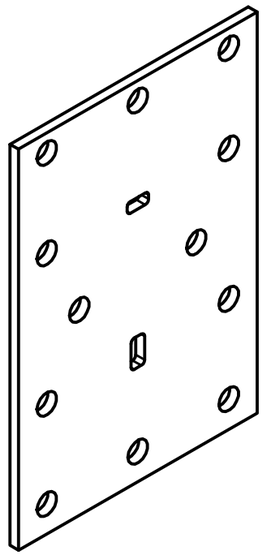

Progettato da	Controllato da	Approvato da	Data		Data	
Giacomo Trevisan					23/02/2012	

Lamina7	Edizione	Foglio 1 / 1

CREATO CON LA VERSIONE DIDATTICA DI UN PRODOTTO AUTODESK

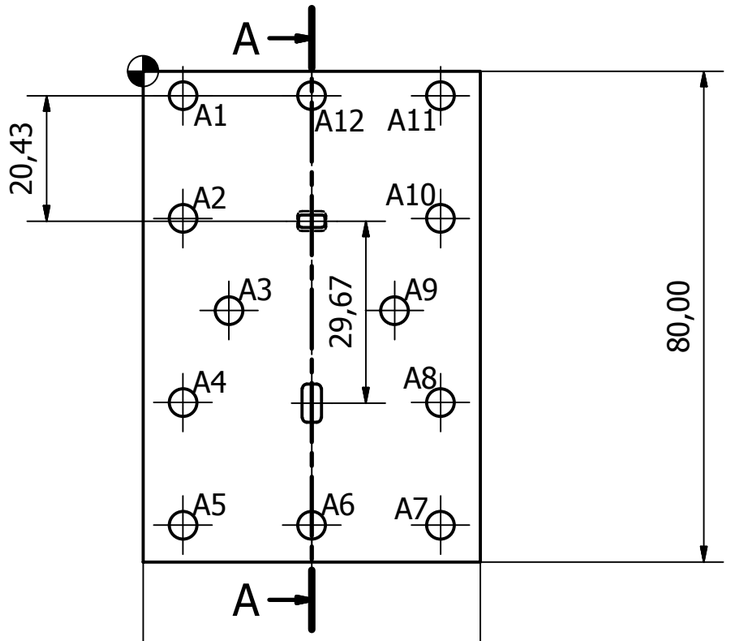

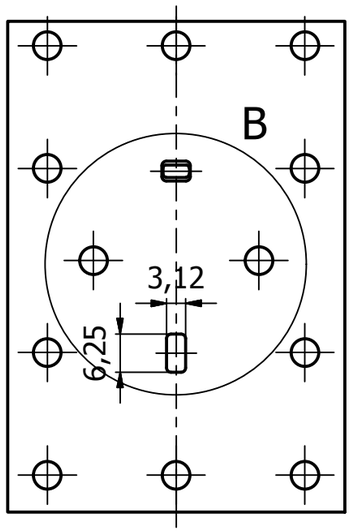

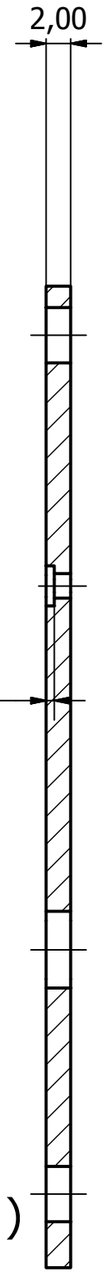

A-A (2: 1)

TABELLA FORO			
FORO	Quota X	Quota Y	DESCRIZIONE
A1	6,50	-4,00	Ø4,50 PASS.
A2	6,50	-24,00	
A3	14,00	-39,00	
A4	6,50	-54,00	
A5	6,50	-74,00	
A6	27,50	-74,00	
A7	48,50	-74,00	
A8	48,50	-54,00	
A9	41,00	-39,00	
A10	48,50	-24,00	
A11	48,50	-4,00	
A12	27,50	-4,00	

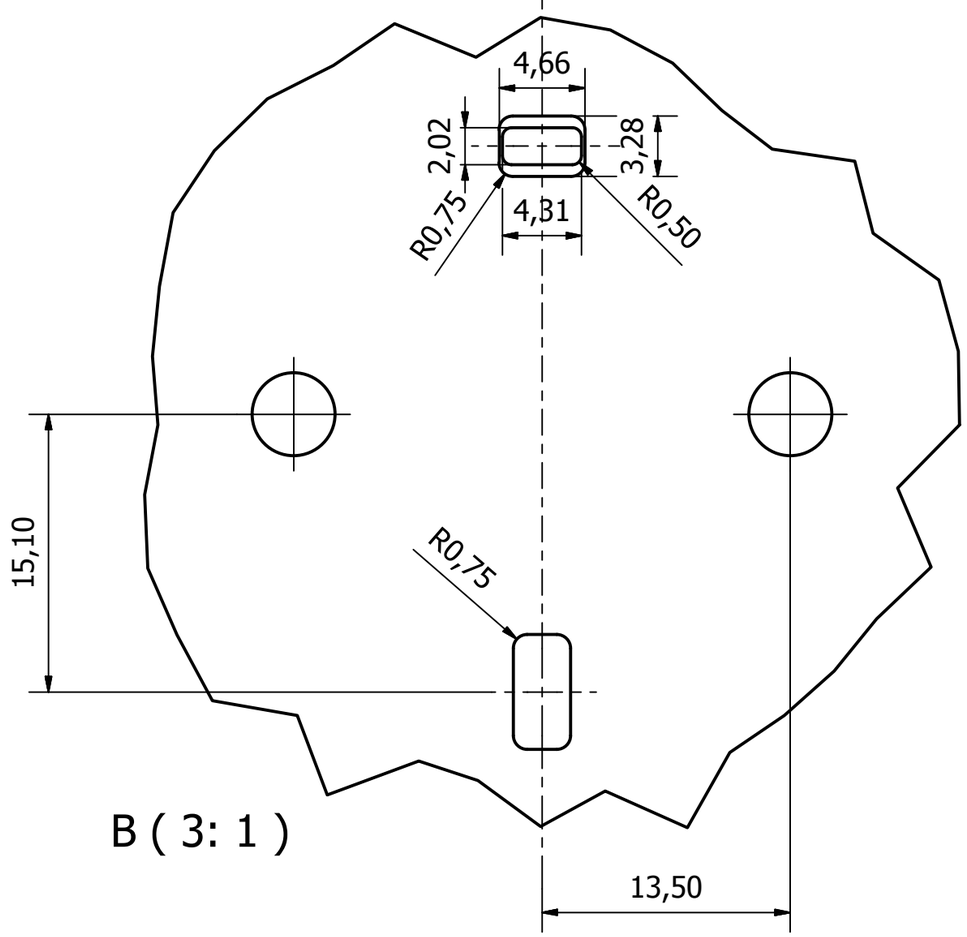

B (3: 1)

Progettato da	Controllato da	Approvato da	Data		Data	
Giacomo Trevisan					23/02/2012	

Lamina8	Edizione	Foglio 1 / 1

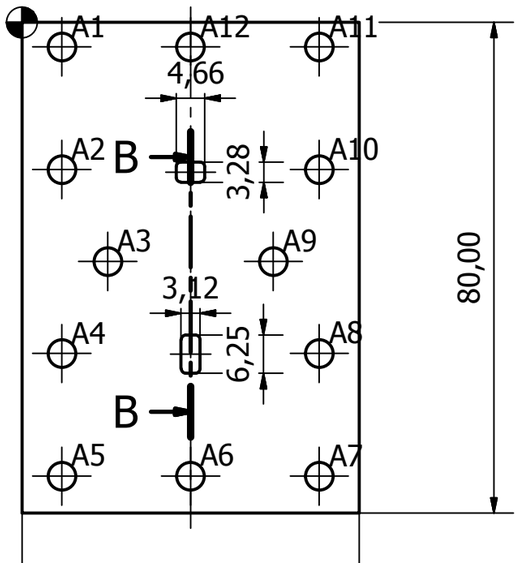

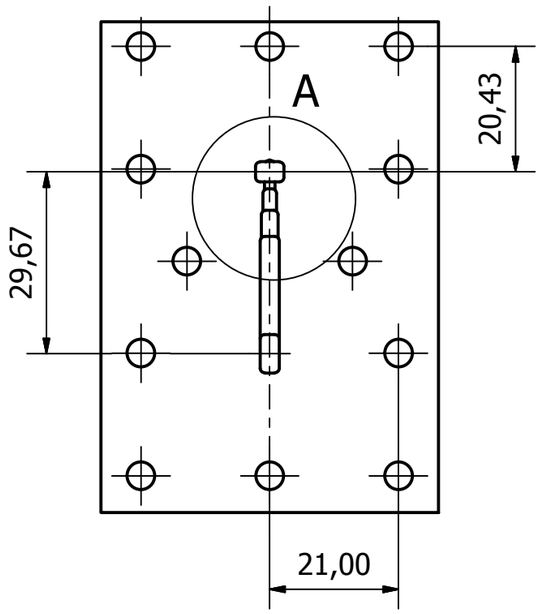

B-B (3: 1)

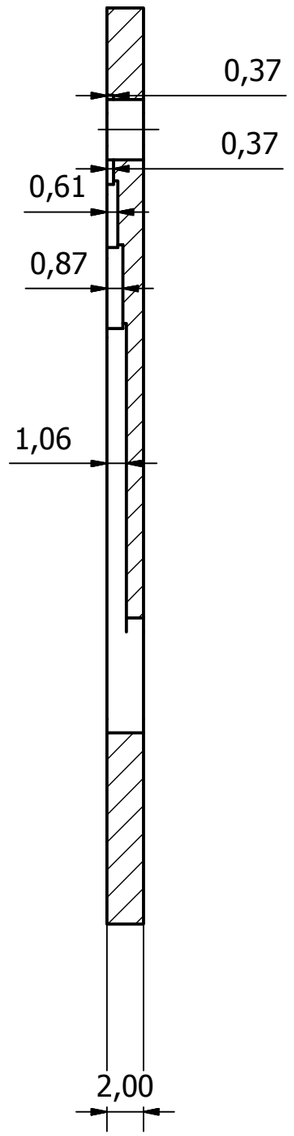

TABELLA FORO			
FORO	Quota X	Quota Y	DESCRIZIONE
A1	6,50	-4,00	Ø4,50 PASS.
A2	6,50	-24,00	
A3	14,00	-39,00	
A4	6,50	-54,00	
A5	6,50	-74,00	
A6	27,50	-74,00	
A7	48,50	-74,00	
A8	48,50	-54,00	
A9	41,00	-39,00	
A10	48,50	-24,00	
A11	48,50	-4,00	
A12	27,50	-4,00	

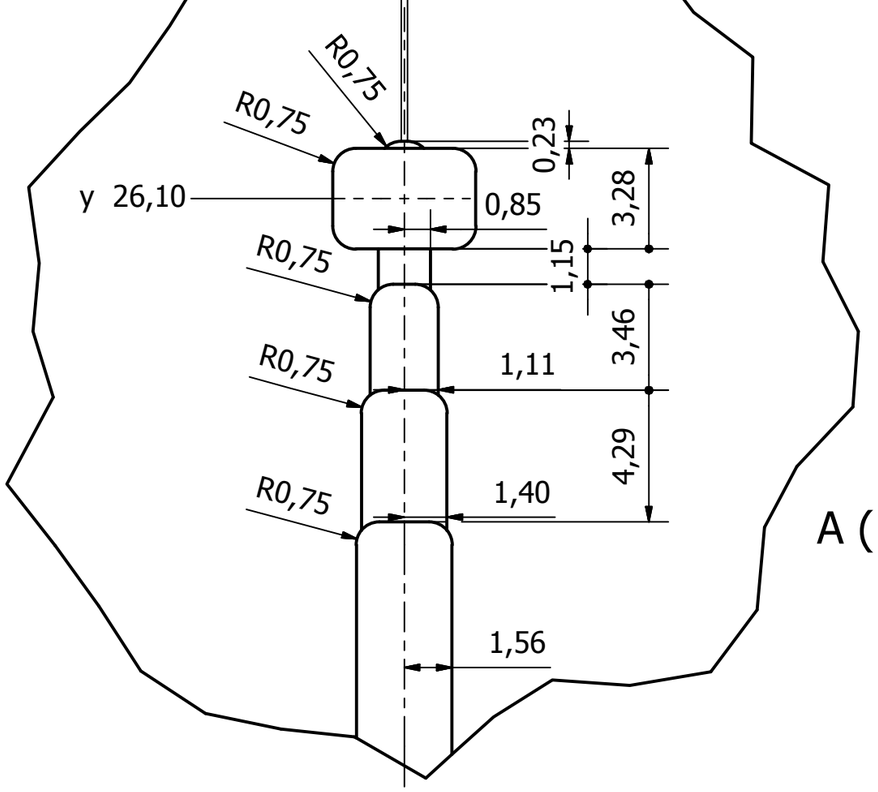

A (5: 1)

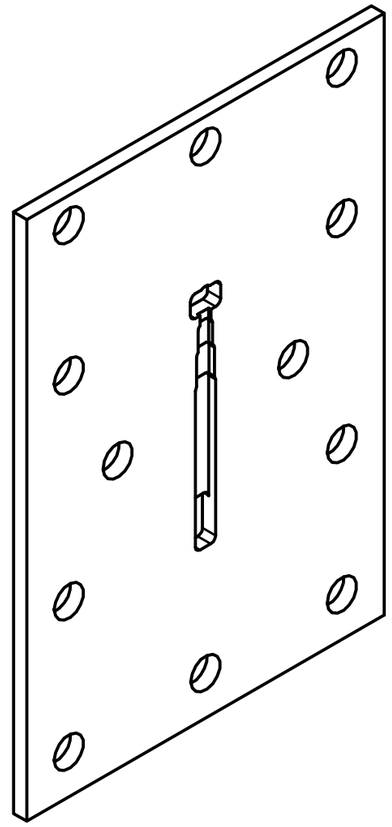

Progettato da	Controllato da	Approvato da	Data		Data	
Giacomo Trevisan					23/02/2012	

Lamina9	Edizione	Foglio 1 / 1

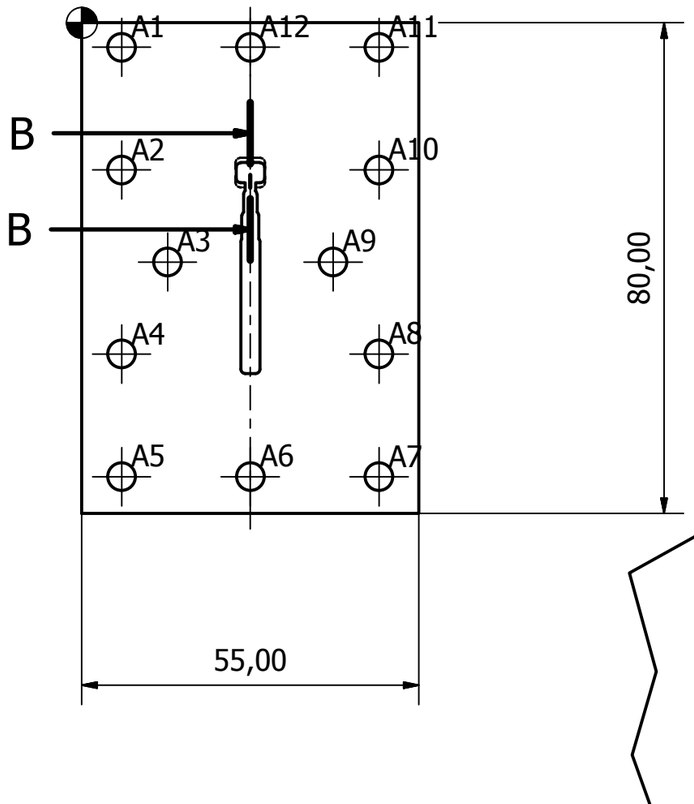

TABELLA FORO			
FORO	Quota X	Quota Y	DESCRIZIONE
A1	6,50	-4,00	Ø4,50 PASS.
A2	6,50	-24,00	
A3	14,00	-39,00	
A4	6,50	-54,00	
A5	6,50	-74,00	
A6	27,50	-74,00	
A7	48,50	-74,00	
A8	48,50	-54,00	
A9	41,00	-39,00	
A10	48,50	-24,00	
A11	48,50	-4,00	
A12	27,50	-4,00	

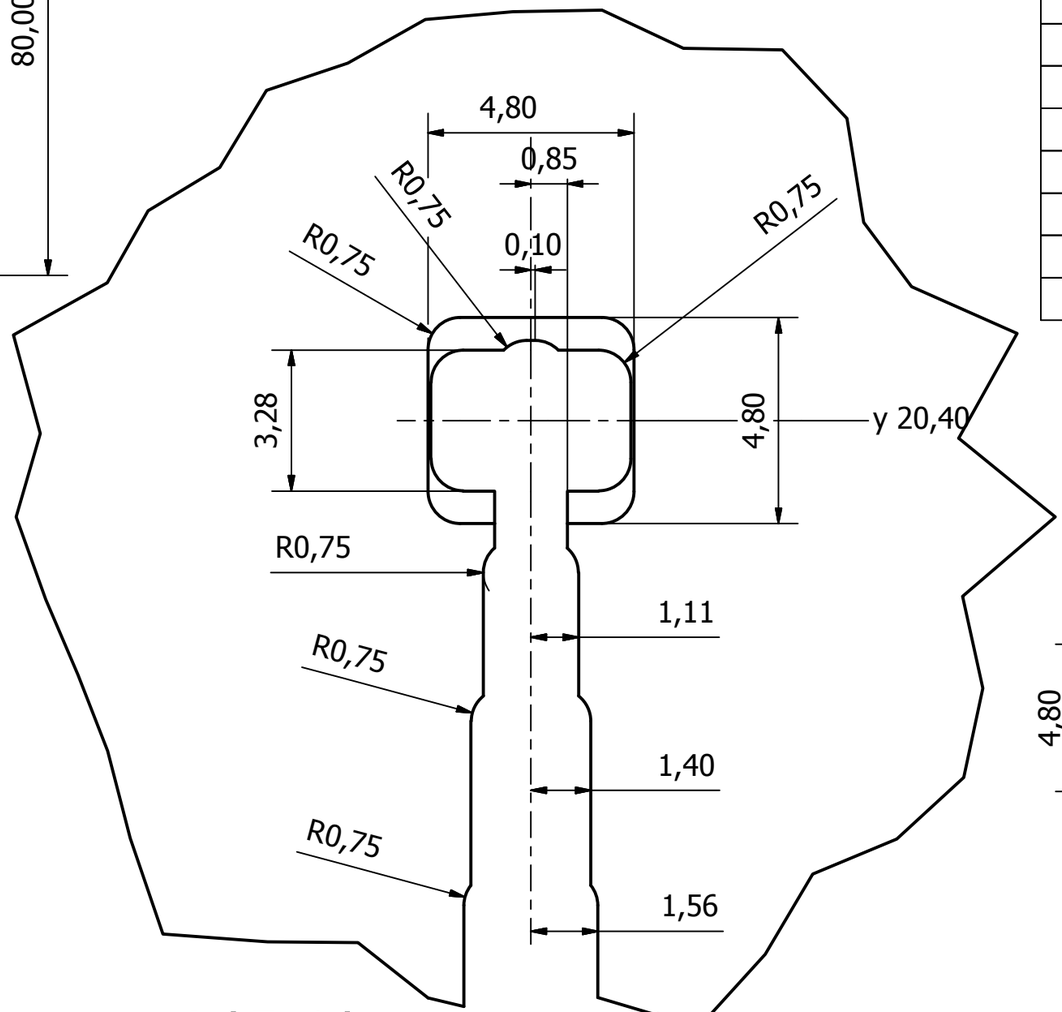

A (7: 1)

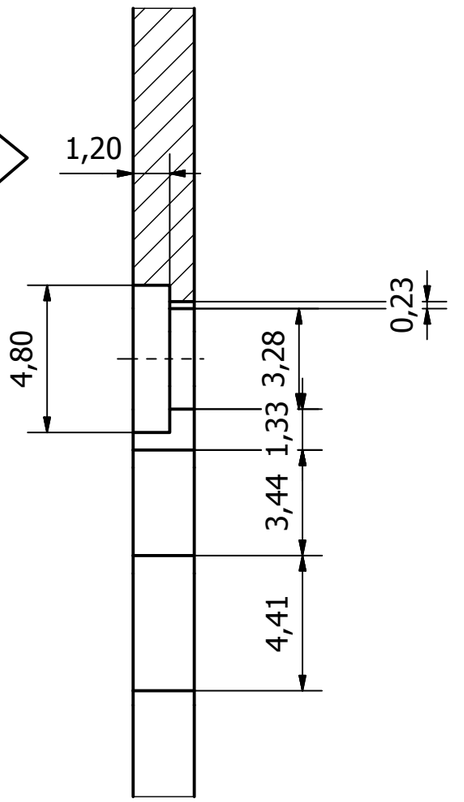

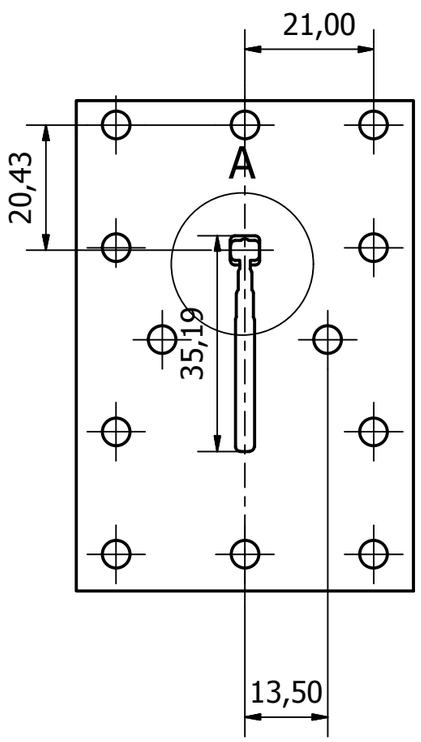

Progettato da	Controllato da	Approvato da	Data		Data	
Giacomo Trevisan					23/02/2012	

Lamina10	Edizione	Foglio 1 / 1

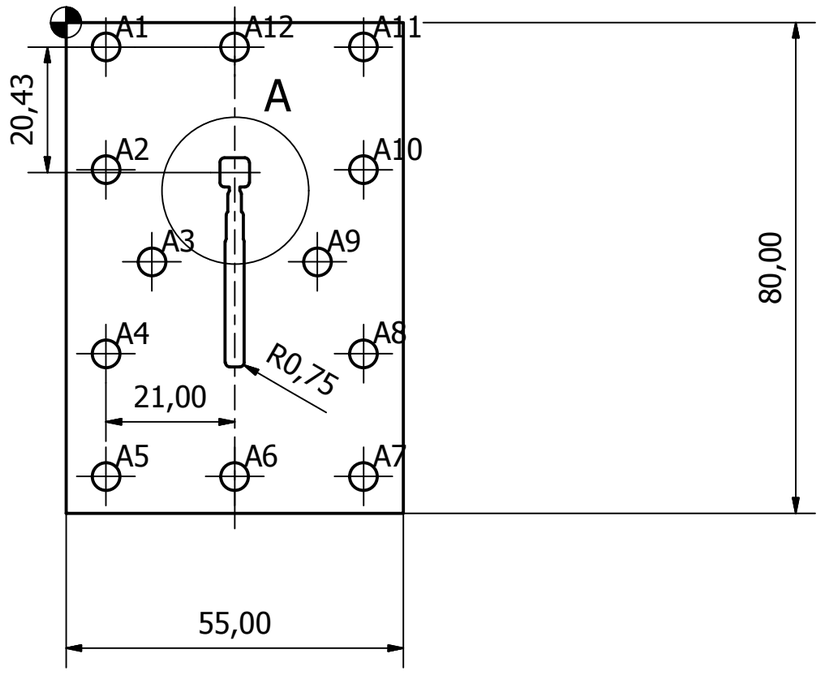

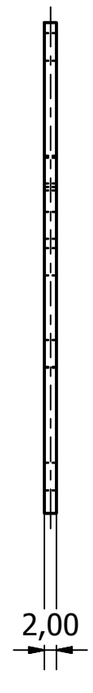

TABELLA FORO			
FORO	Quota X	Quota Y	DESCRIZIONE
A1	6,50	-4,00	Ø4,50 PASS.
A2	6,50	-24,00	
A3	14,00	-39,00	
A4	6,50	-54,00	
A5	6,50	-74,00	
A6	27,50	-74,00	
A7	48,50	-74,00	
A8	48,50	-54,00	
A9	41,00	-39,00	
A10	48,50	-24,00	
A11	48,50	-4,00	
A12	27,50	-4,00	

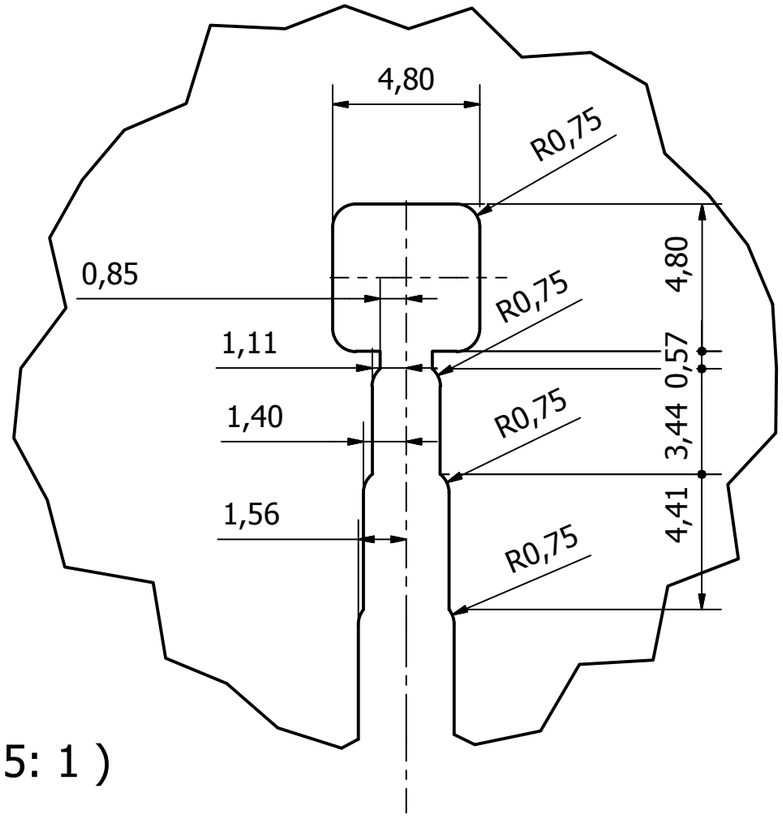

A (5: 1)

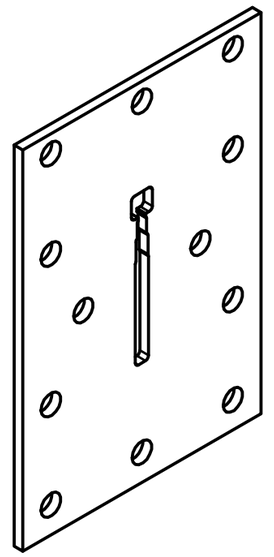

Progettato da	Controllato da	Approvato da	Data		Data	
Giacomo Trevisan					23/02/2012	

Lamina11	Edizione	Foglio 1 / 1

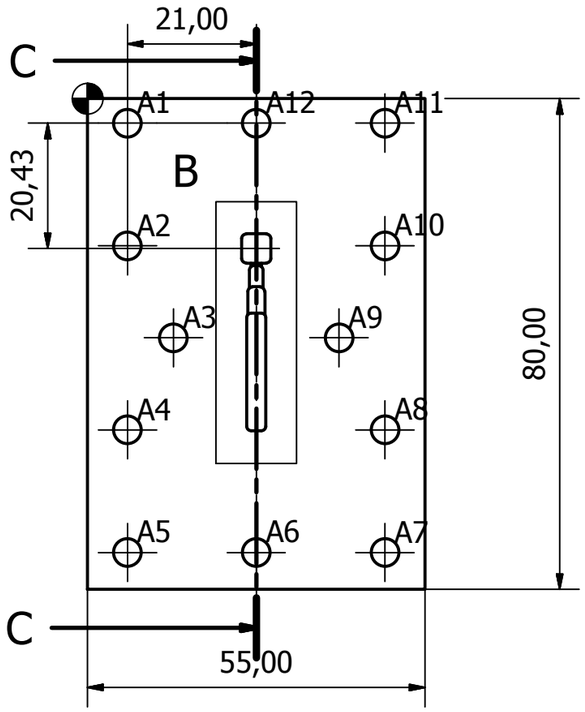

TABELLA FORO			
FORO	Quota X	Quota Y	DESCRIZIONE
A1	6,50	-4,00	Ø4,50 PASS.
A2	6,50	-24,00	
A3	14,00	-39,00	
A4	6,50	-54,00	
A5	6,50	-74,00	
A6	27,50	-74,00	
A7	48,50	-74,00	
A8	48,50	-54,00	
A9	41,00	-39,00	
A10	48,50	-24,00	
A11	48,50	-4,00	
A12	27,50	-4,00	

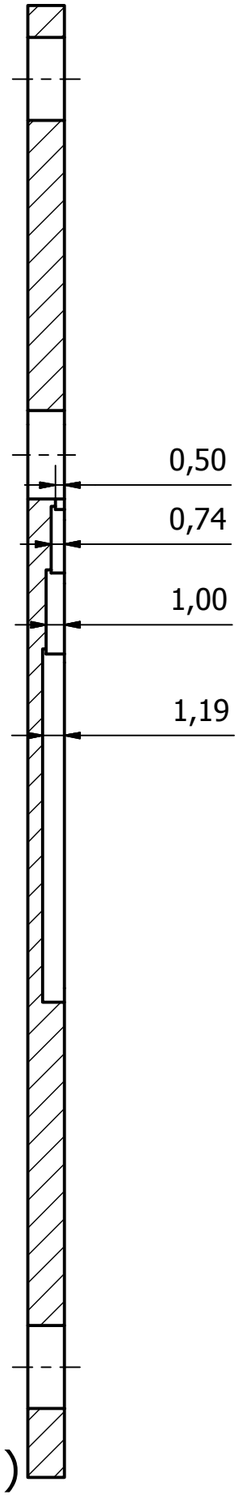

C-C (3: 1)

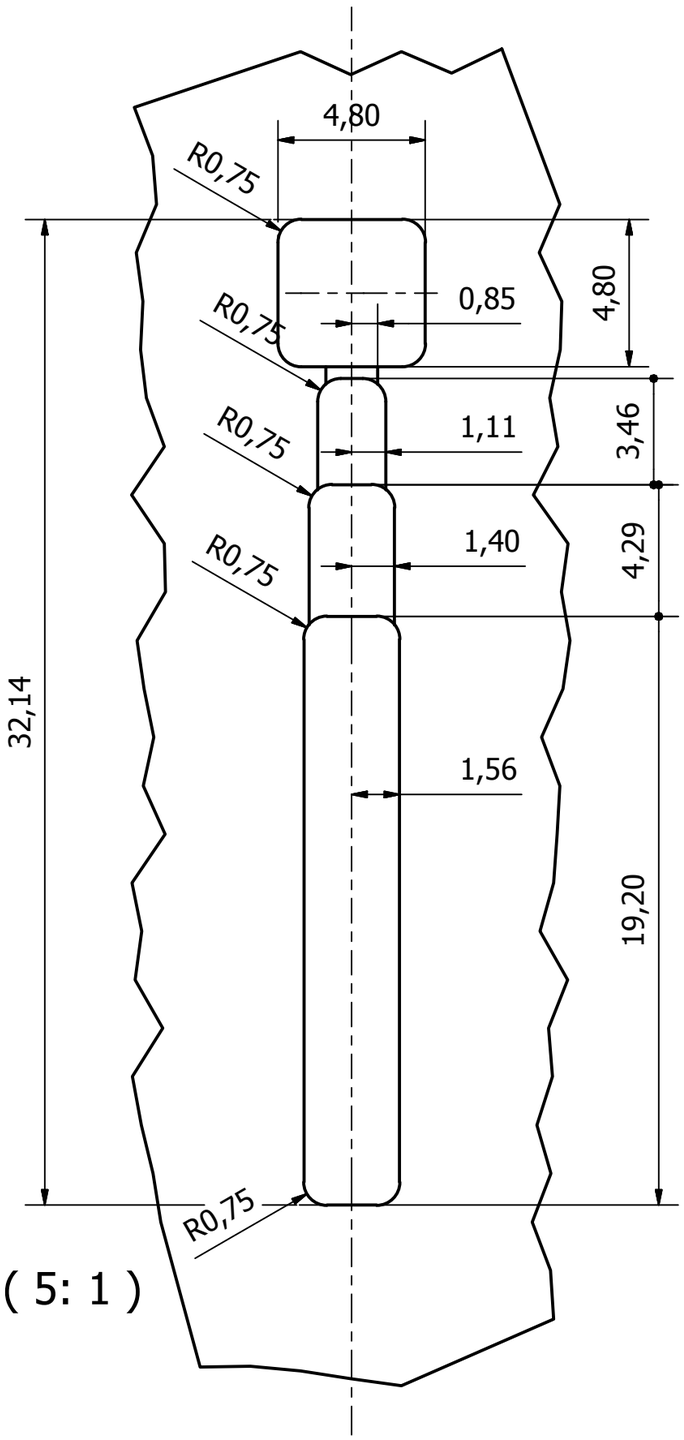

B (5: 1)

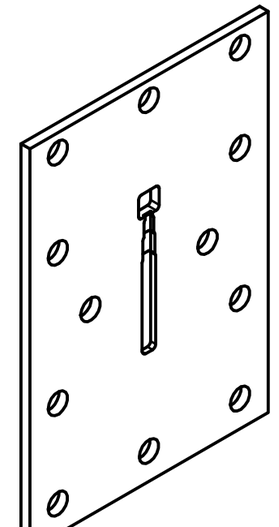

Progettato da	Controllato da	Approvato da	Data		Data	
Giacomo Trevisan					23/02/2012	

Lamina12	Edizione	Foglio 1 / 1

TABELLA FORO			
FORO	Quota X	Quota Y	DESCRIZIONE
A1	6,50	-4,00	Ø4,50 PASS.
A2	6,50	-24,00	
A3	14,00	-39,00	
A4	6,50	-54,00	
A5	6,50	-74,00	
A6	27,50	-74,00	
A7	48,50	-74,00	
A8	48,50	-54,00	
A9	41,00	-39,00	
A10	48,50	-24,00	
A11	48,50	-4,00	
A12	27,50	-4,00	

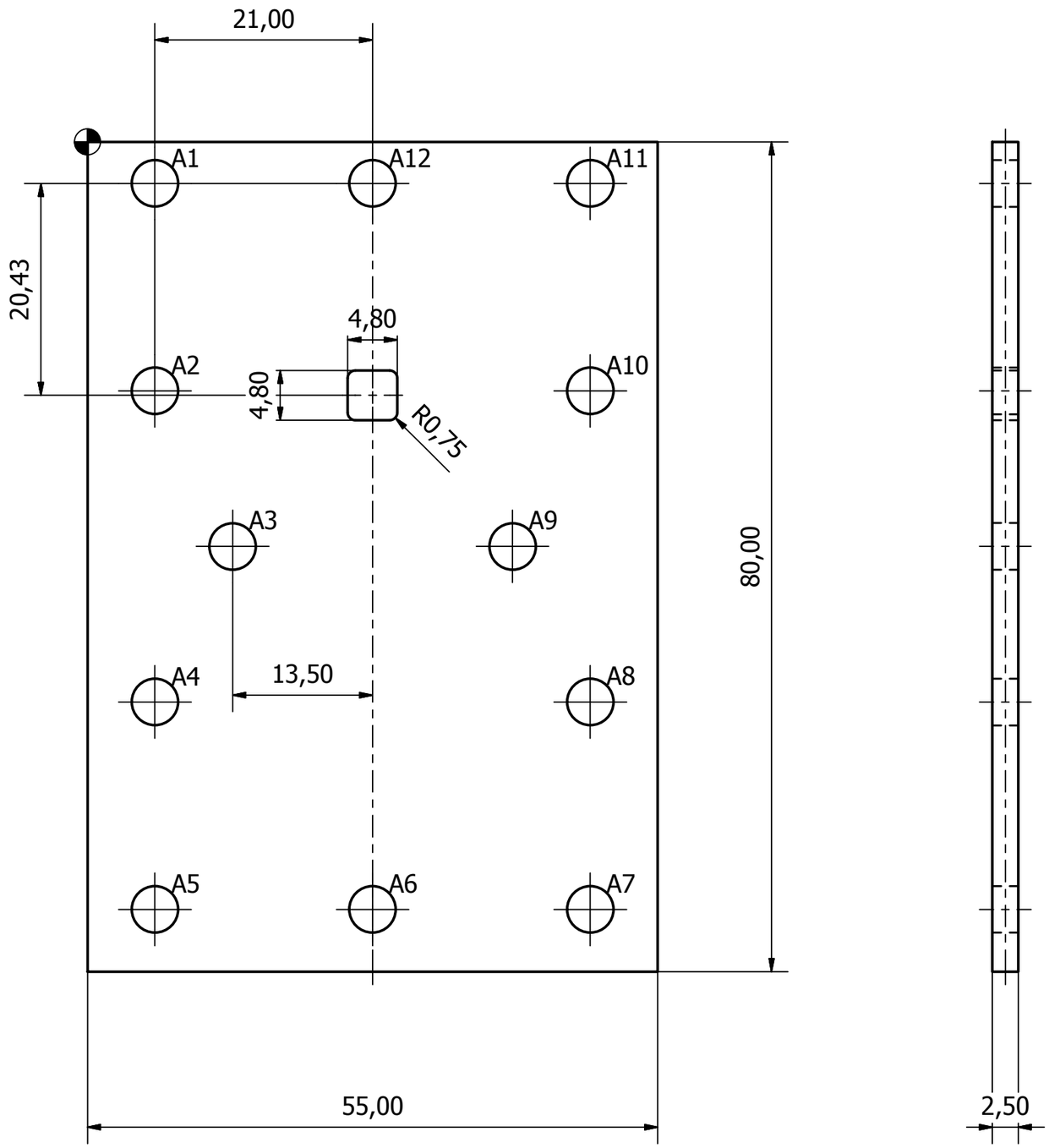

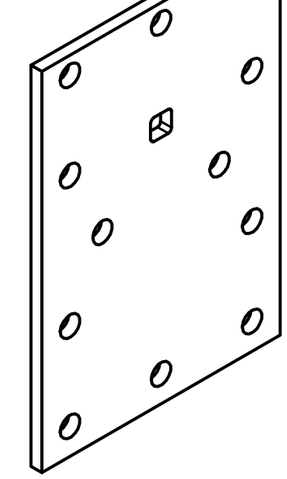

Progettato da	Controllato da	Approvato da	Data		Data	
Giacomo Trevisan					23/02/2012	

	Lamina13	Edizione	Foglio 1 / 1

TABELLA FORO			
FORO	Quota X	Quota Y	DESCRIZIONE
A1	6,50	-4,00	Ø4,50 PASS.
A2	6,50	-24,00	
A3	14,00	-39,00	
A4	6,50	-54,00	
A5	6,50	-74,00	
A6	27,50	-74,00	
A7	48,50	-74,00	
A8	48,50	-54,00	
A9	41,00	-39,00	
A10	48,50	-24,00	
A11	48,50	-4,00	
A12	27,50	-4,00	

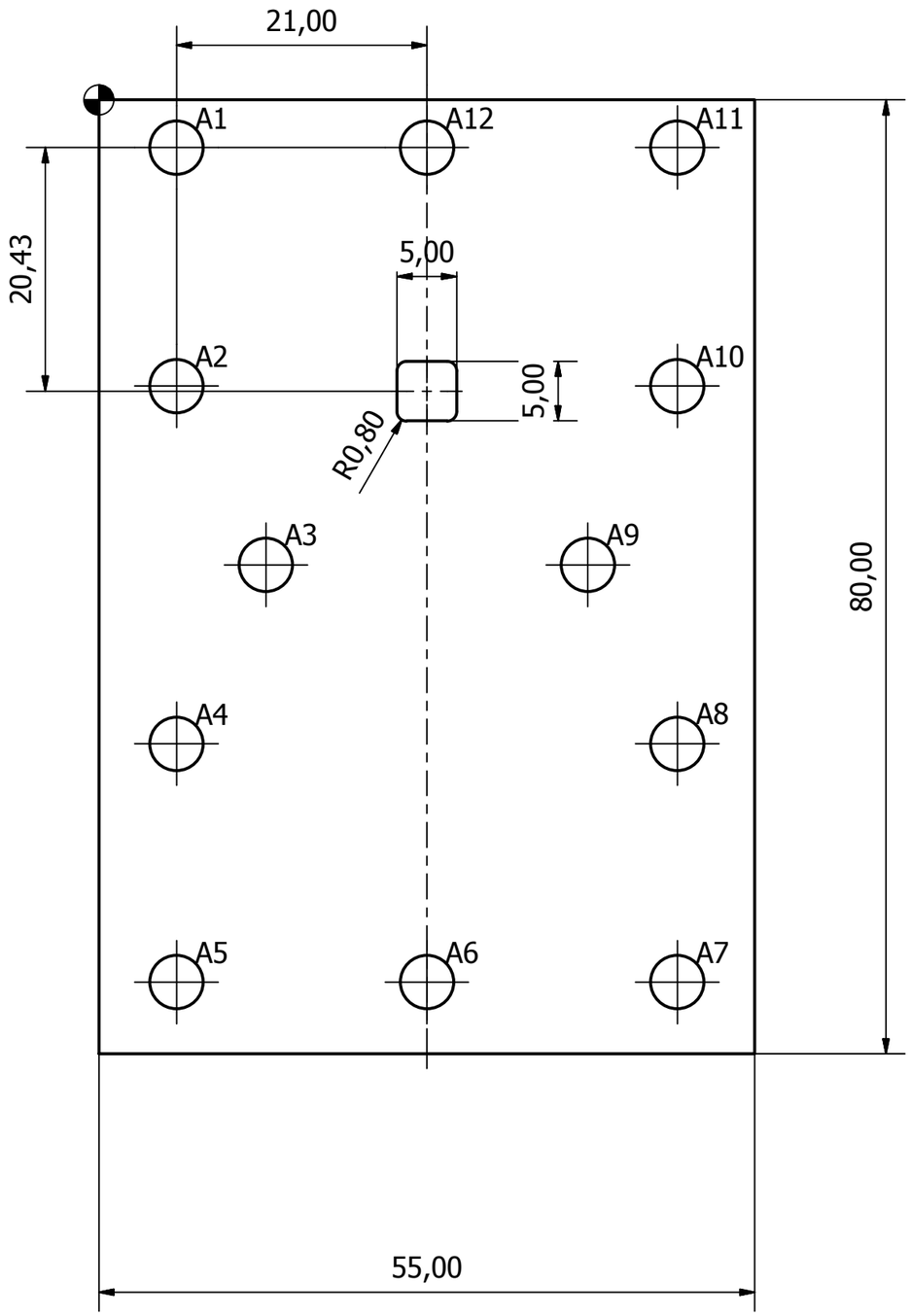

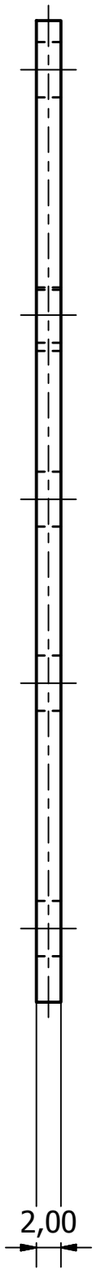

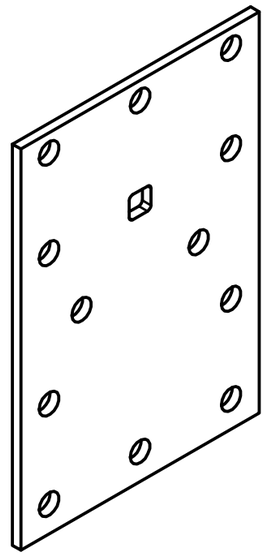

Progettato da	Controllato da	Approvato da	Data		Data	
Giacomo Trevisan					23/02/2012	

Lamina14	Edizione	Foglio 1 / 1

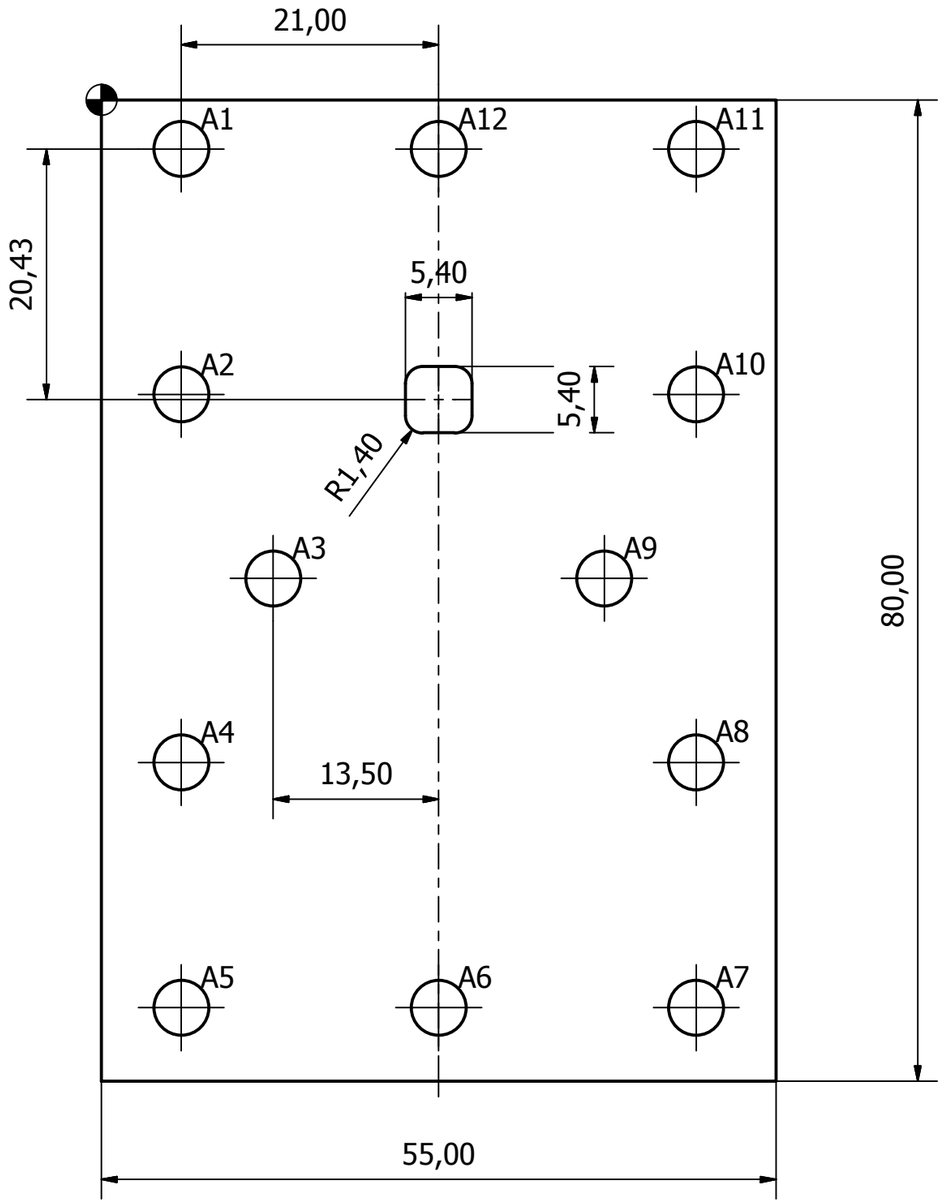

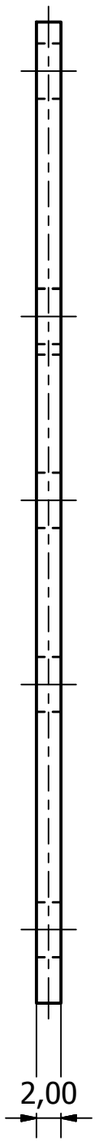

TABELLA FORO			
FORO	Quota X	Quota Y	DESCRIZIONE
A1	6,50	-4,00	Ø4,50 PASS.
A2	6,50	-24,00	
A3	14,00	-39,00	
A4	6,50	-54,00	
A5	6,50	-74,00	
A6	27,50	-74,00	
A7	48,50	-74,00	
A8	48,50	-54,00	
A9	41,00	-39,00	
A10	48,50	-24,00	
A11	48,50	-4,00	
A12	27,50	-4,00	

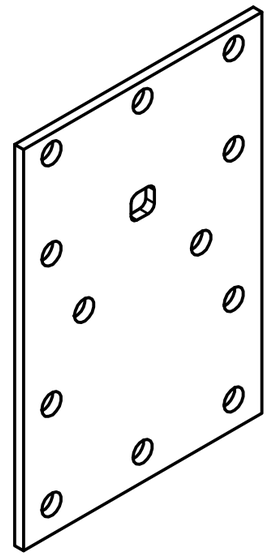

Progettato da	Controllato da	Approvato da	Data		Data	
Giacomo Trevisan					23/02/2012	

	lamina15	Edizione	Foglio 1 / 1

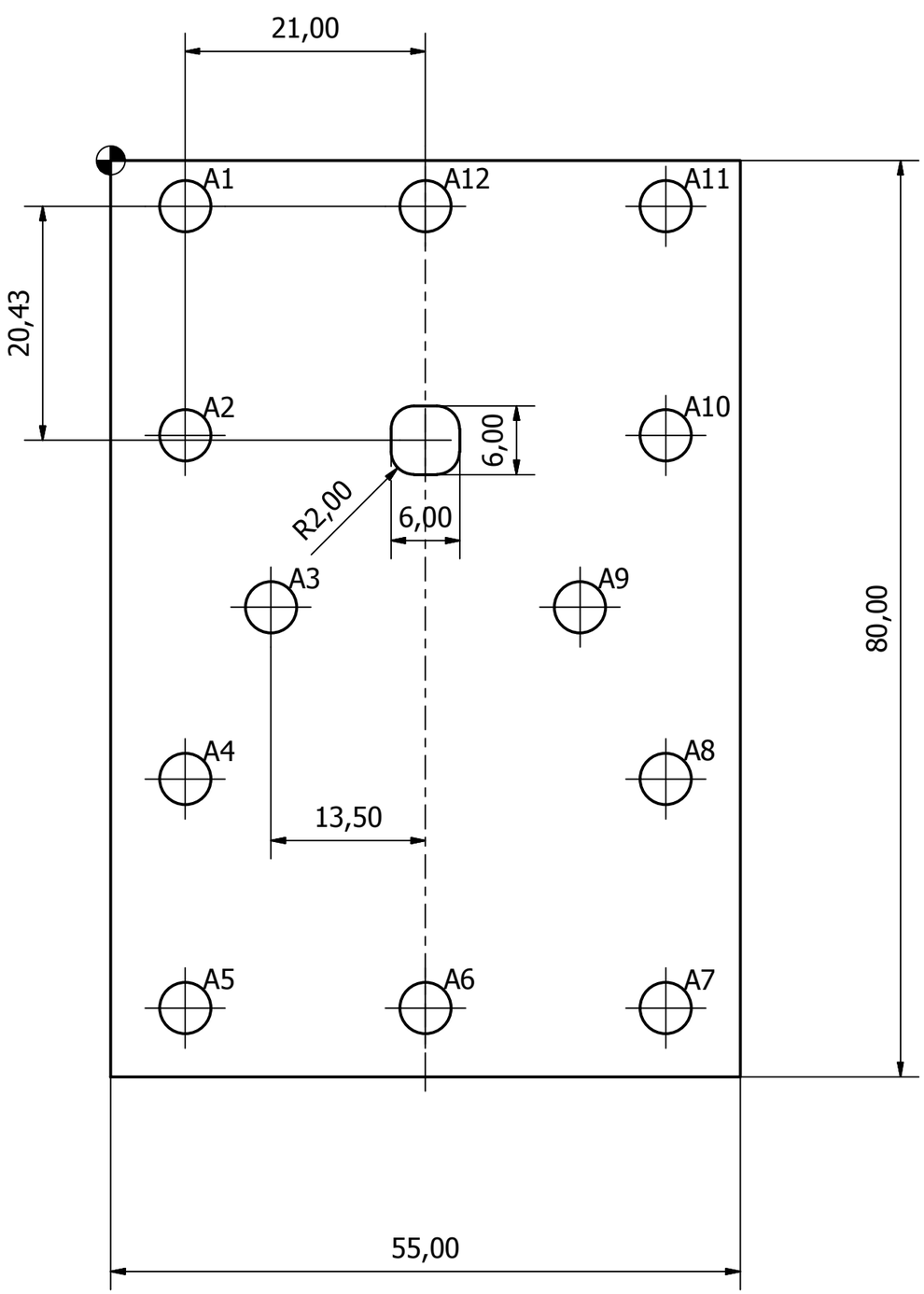

TABELLA FORO			
FORO	Quota X	Quota Y	DESCRIZIONE
A1	6,50	-4,00	Ø4,50 PASS.
A2	6,50	-24,00	
A3	14,00	-39,00	
A4	6,50	-54,00	
A5	6,50	-74,00	
A6	27,50	-74,00	
A7	48,50	-74,00	
A8	48,50	-54,00	
A9	41,00	-39,00	
A10	48,50	-24,00	
A11	48,50	-4,00	
A12	27,50	-4,00	

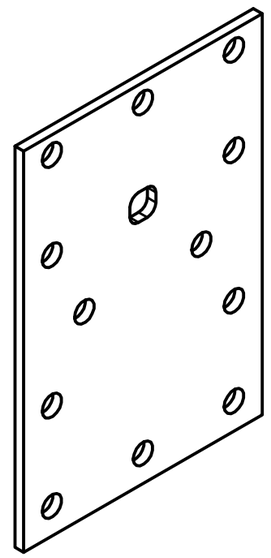

Progettato da	Controllato da	Approvato da	Data		Data	
Giacomo Trevisan					23/02/2012	

Lamina16	Edizione	Foglio 1 / 1

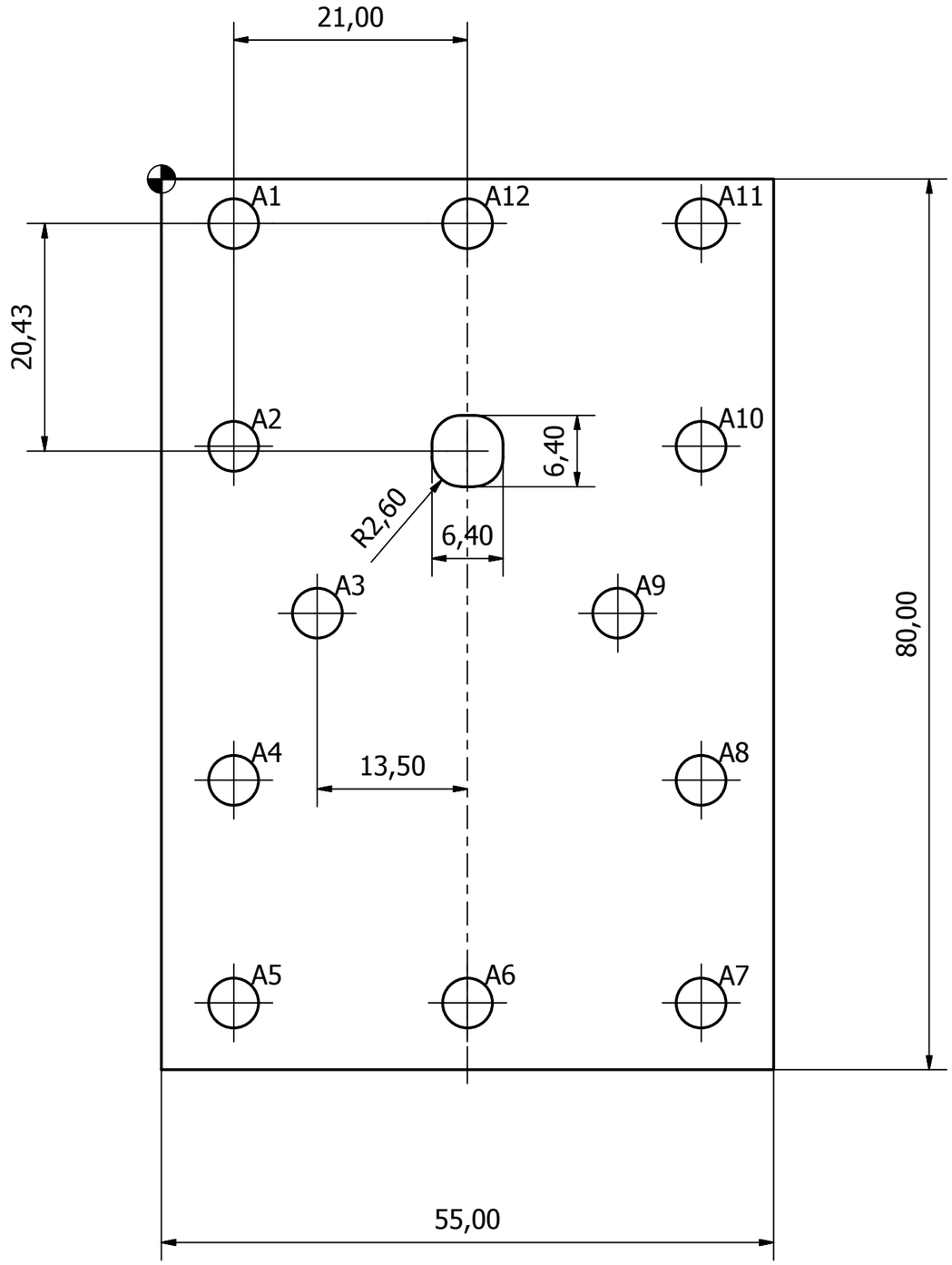

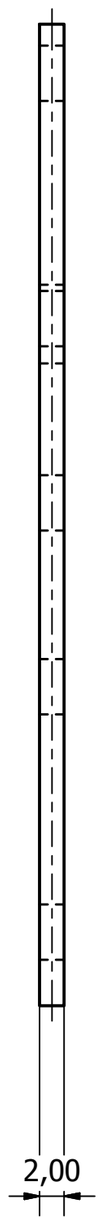

TABELLA FORO			
FORO	Quota X	Quota Y	DESCRIZIONE
A1	6,50	-4,00	Ø4,50 PASS.
A2	6,50	-24,00	
A3	14,00	-39,00	
A4	6,50	-54,00	
A5	6,50	-74,00	
A6	27,50	-74,00	
A7	48,50	-74,00	
A8	48,50	-54,00	
A9	41,00	-39,00	
A10	48,50	-24,00	
A11	48,50	-4,00	
A12	27,50	-4,00	

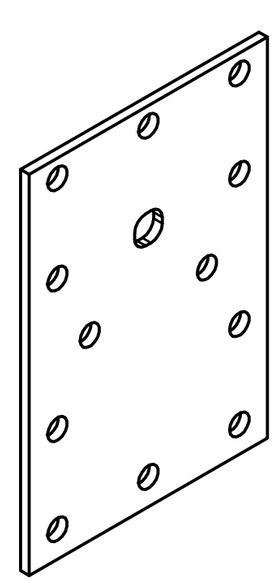

Progettato da	Controllato da	Approvato da	Data		Data	
Giacomo Trevisan					23/02/2012	

Lamina17	Edizione	Foglio 1 / 1

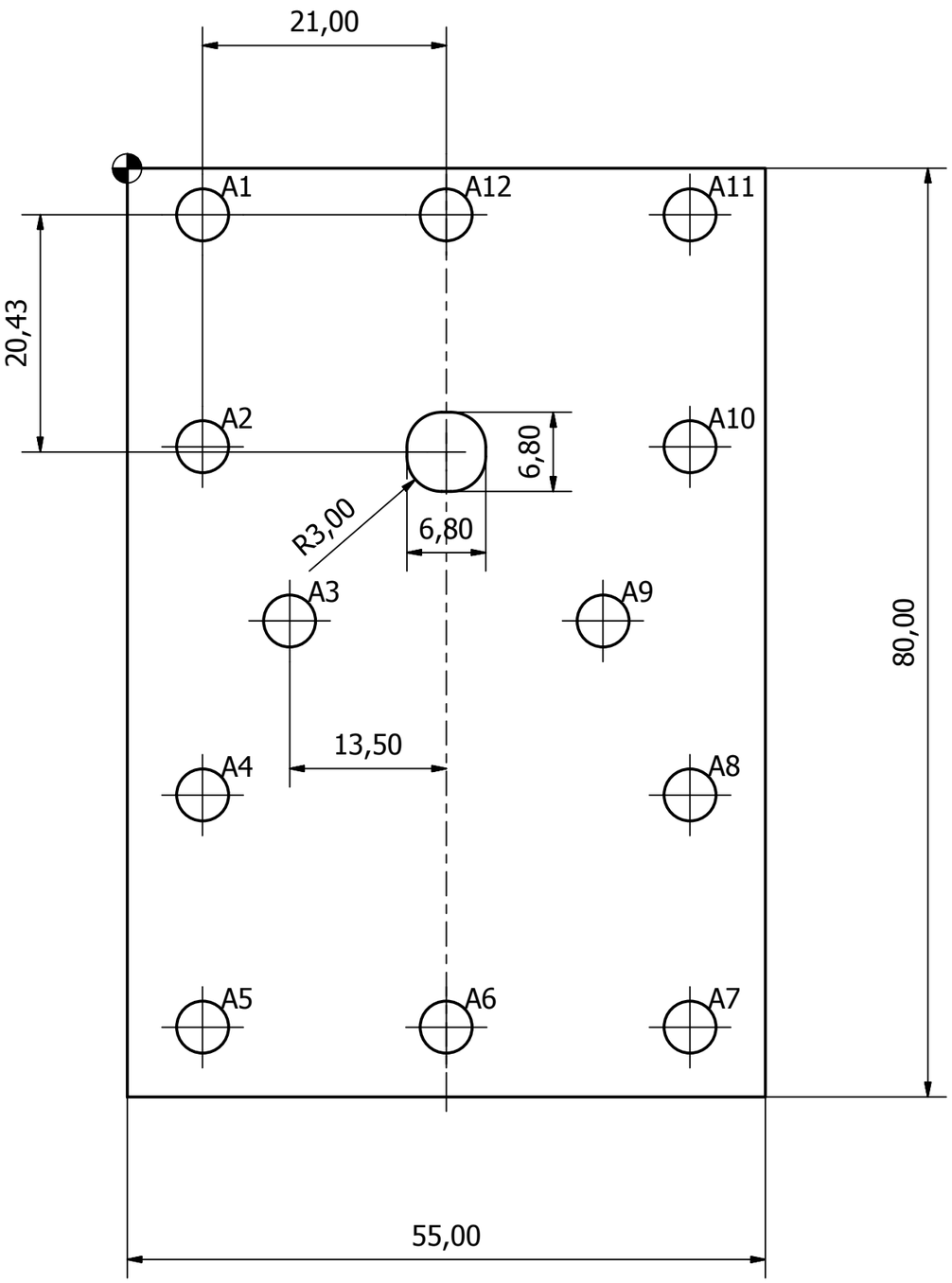

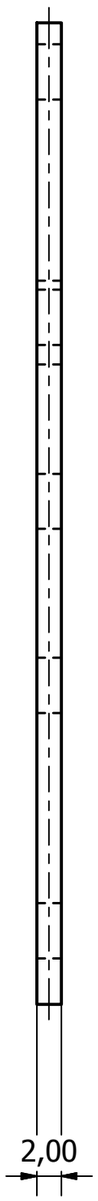

TABELLA FORO			
FORO	Quota X	Quota Y	DESCRIZIONE
A1	6,50	-4,00	Ø4,50 PASS.
A2	6,50	-24,00	
A3	14,00	-39,00	
A4	6,50	-54,00	
A5	6,50	-74,00	
A6	27,50	-74,00	
A7	48,50	-74,00	
A8	48,50	-54,00	
A9	41,00	-39,00	
A10	48,50	-24,00	
A11	48,50	-4,00	
A12	27,50	-4,00	

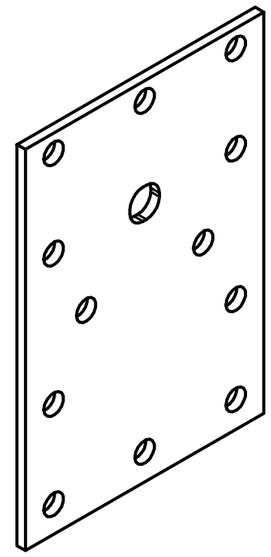

Progettato da	Controllato da	Approvato da	Data		Data	
Giacomo Trevisan					23/02/2012	

Lamina18

Edizione

Foglio 1 / 1

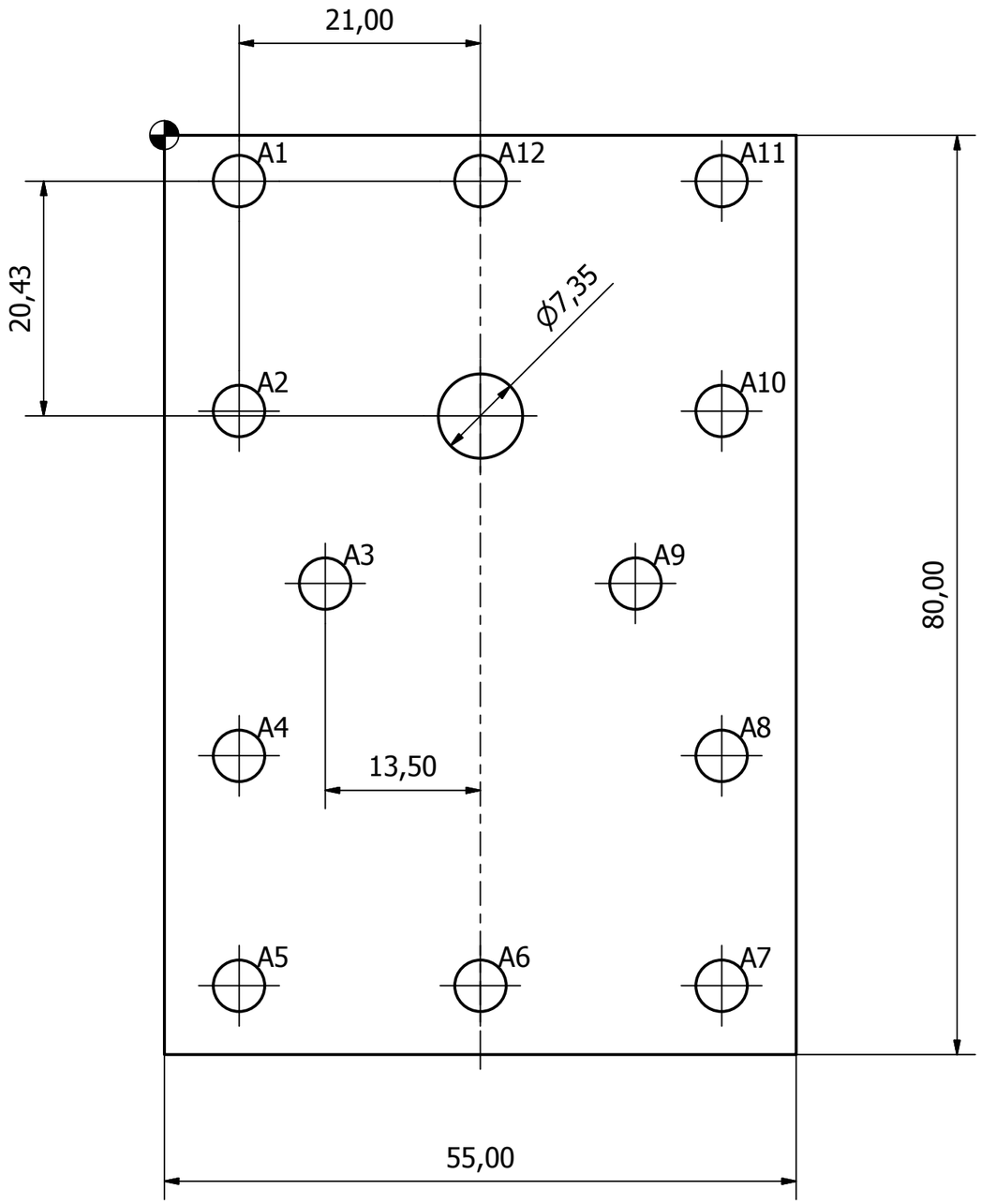

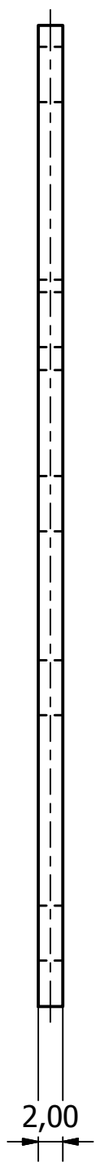

TABELLA FORO			
FORO	Quota X	Quota Y	DESCRIZIONE
A1	6,50	-4,00	Ø4,50 PASS.
A2	6,50	-24,00	
A3	14,00	-39,00	
A4	6,50	-54,00	
A5	6,50	-74,00	
A6	27,50	-74,00	
A7	48,50	-74,00	
A8	48,50	-54,00	
A9	41,00	-39,00	
A10	48,50	-24,00	
A11	48,50	-4,00	
A12	27,50	-4,00	

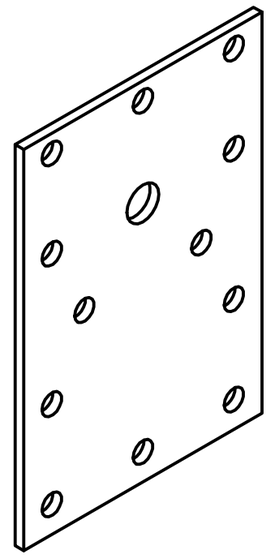

Progettato da	Controllato da	Approvato da	Data		Data	
Giacomo Trevisan					23/02/2012	

Lamina19	Edizione	Foglio 1 / 1

Bibliography

[1] D.Pozar, Microwave Engineering 2nd Ed.,1998

[2] Conciauro, Introduzione alle onde elettromagnetiche, 1993

[3] Markuvitz, Waveguide Handbook, 1985

[4] K.W.Yoon, J.W.Appel,J.E.Austermann et al., Feedhorn-coupled TES polarimeters for next-generation CMB instruments , 2009

[5] http://map.gsfc.nasa.gov/media/060917/index.html

[6] http://lambda.gsfc.nasa.gov

[7] Huan T.Tran, Polarization comparison between on-axis and off-axis dual reflector telescopes: Zemax and Grasp8 simulations, New Astronomy reviews 47 (2003).

[8] A.Navarrini, R.L.Plambeck , Orthomode Transducers (OMTs) for millimetric wavelenghts, Ottawa URSI meeting,26 Luglio 2007.

[9] Engargiola, R.L.Plambeck, 2003.

[10] P.Mauskopf,P.Ade,J.Zhang,P.Grime, Clover Polarimetric Detector - A novel design of an Ortho-mode transducer at 150 and 225 GHz, Progress in Electromagnetics research symposium, Hangzhou,China, Marzo 2008.

[11] S.Srikanth, M.Solatka, M.Meek , Turnstile Junction Orthomode Transducer An option for EVLA X-Band Receiver , 2009.

[12] Y. Aramaki, N. Yoneda, M. Miyazaki and T. Horie, Ultra-thin Broad-band OMT with Turnstile Junction, 2003 ,IEEE MTT-S International Microwave Symposium Digest, vol. 1, pp 47-50, June 2003.

[13] M. Bersanelli, N. Mandolesi, R. C. Butler, A. Mennella et al. , Planck pre-launch status: Design and description of the Low Frequency Instrument, AA 520 A4, 2010.

[14] F. Villa, L. Terenzi, P. Meinhold, C. Franceschet et al. ,Planck pre-launch status: Calibration of the Low Frequency Instrument flight model radiometers, AA 520 A6, 2010

[15] P.De Bernardis, Tecniche sperimentali in astrofisica, dispense 2010.

[16] Polarization Modulators for CMBPol, David T Chuss, Shaul Hanany, B.Keating et al. Journal of Physics Conference Series 155, 2009.

[17] Jamie Bock , Space-Borne Measurements of CMB Polarization , The Path to CMBPOL: Upcoming Measurements of CMB Polarization University of Chicago, July 2009.

[18] M.Stennes, A Planar OMT for the EVLA ,NRAO , October 2009.

[19] G.Narayan, N.Erickson, A novel full waveguide band orthomode transducer, XIII international symposium on space therahertz technology, March 2002.

[20] G. Chattopadhyay, Dual Polarized And Balanced Receivers At Millimeter And Submillimeter Wavelengths, 2000.

[21] P.K.Grimes et al., Compact broadband planar orthomode transducer, September 2007

[22] R.Nesti, Orthomode Transducer at 43GHz, INAF.

[23] G. Chattopadhyay, A 96-GHz Ortho-Mode Transducer for the Polatron,1998

[24] Electroforming, E. N. Castellano and H. Woellmer ,GAR Electroforming Div.MITE Corp.Danbury, Conn

[25] F.del Torto, Realizzazione e testing di un array di feed horn corrugati per la misura della polarizzazione della radiazione di fondo cosmico, Thesis, 2007.

[26] J. Gundersen, E.J. Wollac, Millimeter Wave Corrugated Platelet Feeds, 2009.

[27] A.Navarrini, R.Nesti, Symmetric Reverse-Coupling Waveguide Orthomode Transducer for the 3-mm Band, IEEE Transactions on Microwave Theory and Techniques, VOL. 57, NO. 1, January 2009.

[28] Jeng, S.L., L.G. Chen and W.H. Chieng. Analysis of Minimum Clamping Force. Int. J. Mach. Tools Manufact., 35(9), pp. 1213-1224.1995.

[29] Chou, Y.C. Geometric Reasoning for Layout Design of Machining Fixtures. Int. J. Computer Integrated Manufacturing, Vo1.7, No.3, pp175-185. 1994.

[30] L. Perregrini, Guide d'onda, Dipartimento di Elettronica, Università di Pavia.

[31] Carstensen, Funken, Hackbusch, Hoppe, Monk, Computational Electromagnetic, Kiel, January 2001.